# Nonlinear Dielectric Effects and Modification of Supramolecular Structures in Monohydroxy Alcohols

by

Amanda R. Young-Gonzales

A Dissertation Presented in Partial Fulfillment
of the Requirements for the Degree
Doctor of Philosophy

Approved April 2019 by the
Graduate Supervisory Committee:

Ranko Richert, Chair
C. Austen Angell
George H. Wolf

ARIZONA STATE UNIVERSITY

May 2019

# ABSTRACT

A driving force for studies of water, alcohols, and amides is the determination of the role of hydrogen bonding. Hydrogen bonds can break and reform, consequently creating supramolecular structures. Understanding the role supramolecular structures play in the dynamics of monohydroxyl alcohols is important to understanding hydrogen bonding in more complex systems such as proteins. Since many monohydroxyl alcohols are good glass formers, dielectric spectroscopy in the supercooled regime is used to gather information about the dynamics of these liquids. Application of high external fields will reversibly alter the polarization responses of the material from the linear response. This results in nonlinear dielectric effects (NDE) such as field induced suppression (saturation) and enhancement of amplitudes (chemical effects) as well as shifts in the time constants toward slower (entropy) and faster (energy absorption) dynamics.

The first part of this thesis describes the nonlinear dielectric experiments on monohydroxyl alcohols, with an emphasis on the time dependence of NDEs. For the first time, time-dependent experiments on monoalcohols were done, the results showed that NDEs occur on the Debye time scale. Furthermore, physical vapor deposition (PVD) is used to modify the supramolecular structure of 4-methyl-3-heptanol. Upon deposition the film cannot form the ring like structures, which are preferred in the bulk material. The as deposited film shows an enhancement of the dielectric peak by a factor of approximately

11 when compared to the bulk material. The conversion from the as deposited material back to the near bulk material was found to occur on the Debye timescale.

The second part of this thesis focuses on the question of what is governing the field induced changes seen in the liquids studied. Here a complete set of high field experiments on highly polar propylene carbonate derivatives were performed. It was demonstrated that these materials exhibit a Debye-like peak and using a combination of Adam-Gibbs and Fröhlich's definition of entropy, proposed by Johari [G.P. Johari, J. Chem. Phys 138, 154503 (2013)], cannot solely be used to describe a frustration of dynamics. It is important to note that although these material exhibit a Debye like peak, the behavior is much different than monoalcohols.

To my family and friends, your support means the world to me.

“Can you believe?”

– Jonathan Van Ness

ACKNOWLEDGMENTS

To my advisor, Ranko Richert, thank you for your mentorship, never ending patience, and support throughout my graduate career. To my supervisory committee members, C. Austen Angell and George Wolf, thank you for your support and guidance. This dissertation would not have been possible without your input and guidance.

To the friends that have become family during graduate school, I cannot express how grateful I am that you can into my life when you did. To Claire Crowther, thank you for always being the ear I needed, my coffee date when the days were long, the random adventures, and the stories I will never forget. To Birte Riechers, I am so glad that we got to work together, not once, but twice. Thank you for the laughter, endless coffee dates, random dinner adventures, and for being my concert date. It was truly a pleasure to work with you. To Rafael Alcala-Torano, I am eternally grateful for your friendship. Thank you for the laughter always, judgment when I need it, and your level headedness when I get too crazy.

To my husband Andrew, your support throughout this journey has been unfailing. Thank you for always being the person to encourage me, being the anchor that keeps me grounded, and always cheering me on, even when I didn't think I could keep going. Your unending faith in me gives me confidence I forget I have. You truly make everyday better.

To my family, thank you for always being just a call away. Your support has been incredible. I would not be here without all of my parents.

TABLE OF CONTENTS

Page

LIST OF TABLES

LIST OF FIGURES

Figure Page

Figure Page

Figure Page

Figure Page

Figure Page

# CHAPTER 1

## INTRODUCTION

A driving force for studies of water, alcohols, and amides is the determination of the role of hydrogen bonding. Hydrogen bonds have the ability to break and reform, consequently creating supramolecular structures. Understanding the microscopic role these supramolecular structures play in the dynamics of monohydroxyl alcohols is important to understanding the importance of hydrogen bonding in more complex systems such as proteins.

Monohydroxy alcohols have been a subject of interest since the late 19$^{th}$ century. In this time there have been many studies done on these materials and a clear microscopic understanding of the structure and dynamics is still yet to be determined. In 1913, Peter Debye devised a model to apply to the dielectric properties of liquids.[1] He found that his model described the main dielectric absorption peak of 1-propanol.[2] Later Davidson and Cole found that though Debye's model was able to describe monoalcohols, but found it failed for polyols.[3] In this study they stated that the narrow shape of the peak was due to the existence of a single relaxation process rather that a variety of modes of reorientation. It wasn't until 1970's that it was proposed that Debye's model may not truly be applicable to monohydroxy alcohols.[4] Another feature found for monohydroxyl alcohols was that the overall dielectric strength is highly dependent on the position of the hydroxyl group and the molecular branching.[5-9]

If these findings didn't make monohydroxyl alcohols interesting then Kauzmann's calorimetric study[10] where he suggested a different microscopic origin for

the Debye type peak than structural relaxation like for typical liquids, did. It was not until later experiments by Litovitz[11,12] suggested that the Debye process may not be governed by microscopic changes in flow, did the idea that many techniques would be unable to probe this peak really take off. Many techniques from NMR[13, 14], to Light scattering experiments[15] show no signature of the Debye peak. From the light scattering experiments it was concluded that unlike typical alpha relaxations, the Debye type peaks were not related to structural relaxation.[15] Now, the Debye peak is generally associated with hydrogen bonding, and is a non-dispersive, single exponential peak.

Since many pure monohydroxy alcohols are known to be good glass formers, they can easily be supercooled far below their melting point and can be studied over a broad spectral range. In their supercooled state, monohydroxy alcohols display a prominent Debye type peak in dielectric spectroscopy. This technique seems to be a good way to further probe the microscopic origins of the Debye peak. I

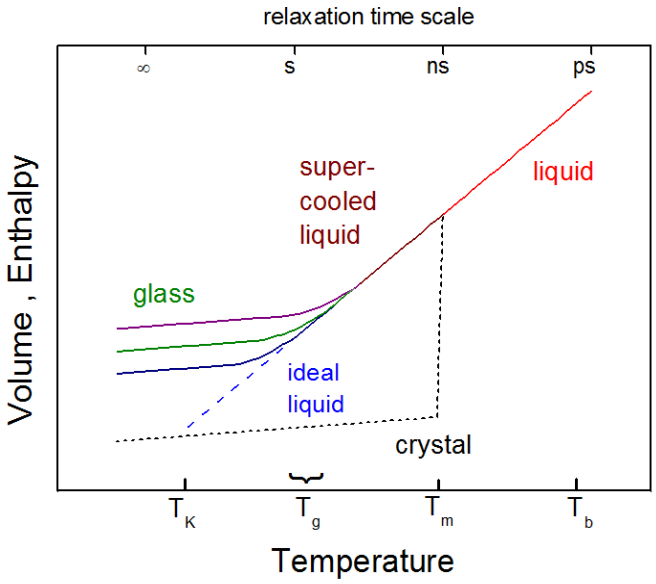


Fig. 1.1 Volume/Enthalpy vs. Temperature plot showing three regions of a glass forming liquid upon cooling to a glassy state. Depending on the cooling rate, the glass transition

will occur within a range of temperatures. The equilibrium supercooled line can be extrapolated to the Kauzmann temperature $T_K$. (adapted from ref.16)

When a liquid is cooled sufficiently fast below its melting point ($T_m$) crystallization can be suppressed, and glass transition can occur. Glass transition, in a true sense, is not a thermodynamic phase transition because it is dependent on cooling rate. The relaxation times gradually increase upon cooling to the glass transition temperature ($T_g$). Near $T_g$ relaxation timescales exceed experimental time scales (~ 100 s), and the material becomes an amorphous solid (glass, Fig. 1.1).[16] The typical timescale associated with the structural relaxation range from seconds to minutes. Broadband dielectric spectroscopy (BDS) is generally used to obtain relaxation timescale from the linear response of disordered materials over a large frequency range ($10^{-6}$ Hz – $10^{12}$ Hz).

**1.1 Typical Glass Forming Liquids**

A characteristic of typical molecular glass formers is a non-exponential primary relaxation process. This primary or α relaxation process is typically the main structural relaxation process. Although the liquid relaxation appears to be exponential above $T_m$, as it approaches $T_g$ the relaxation deviates further from exponentiality. The structural relaxation peak (α-peak) of a disordered material can be characterized by a nonexponential, Kohlrausch-Williams-Watts (KWW)[17] (Fig 1.2), type decay in the time domain. where $\beta_{KWW}$ gauges the deviation from exponentiality

$$\phi(t) = \phi_0 \exp\left[-\left(\frac{t}{\tau_{KWW}}\right)^{\beta_{KWW}}\right] \qquad (1.1)$$

For a typical viscous liquid $0 < \beta_{KWW} < 1$, usually the value is well below the Debye limit $\beta_{KWW} = 1$. The smaller the value of $\beta_{KWW}$, the larger the deviation from exponentiality. In the frequency domain, this stretched exponential appears as an asymmetrical loss

peak (Fig. 1.2). In this case Cole-Davidson, and Havriliak-Negami functions can be used to describe the peak. For the symmetric β relaxation a Cole-Cole function will be added to the HN fit. Havriliak – Negami fitting functions will be described later in this section

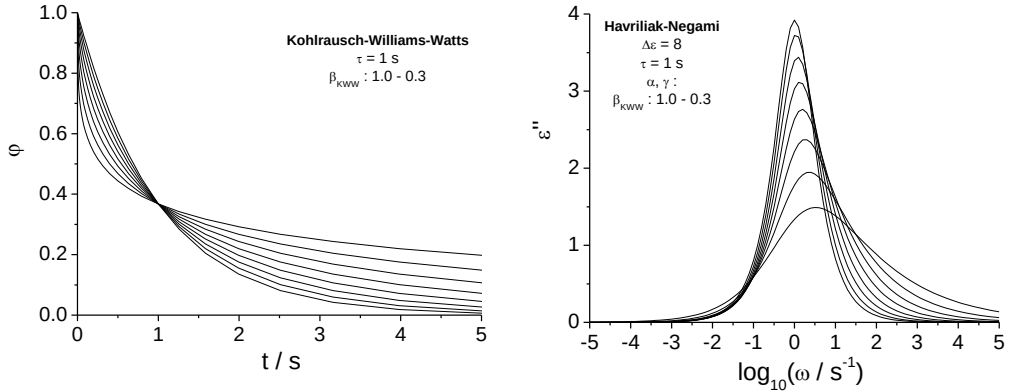


Fig. 1.12 correlation factor. vs time curve for βKWW values ranging from 1.0 - 0.3 at τ = 1 s. (Left) ε'' vs log frequency of HN fit curves describing the same systems as the KWW plot. (Right)

Furthermore, the relaxation times that correspond to the α-relaxation process typically follow Vogel-Fulcher-Tammann (VFT) temperature dependence over a wide range of temperatures.[18] This temperature dependence can be described using Eq. 1.2.

$$\tau(T) = \tau_\infty \exp\left(\frac{B}{T - T_0}\right) \qquad (1.2)$$

Where τ(T) is the relaxation time at temperature T, $\tau_\infty$ is the high temperature limit of the relaxation time, B is a constant activation parameter, and $T_0$ is the temperature at which the dynamics of the system tend to diverge (VFT temperature), suggesting an underlying phase transition.

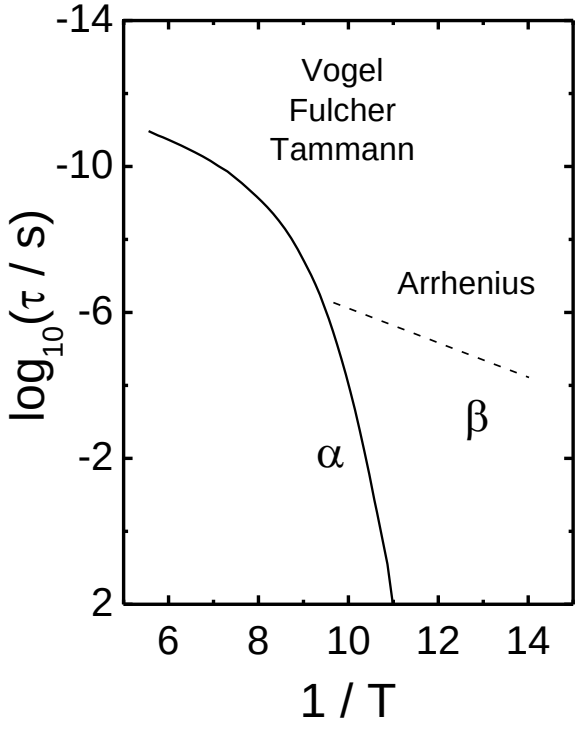


Fig. 1.13 Temperature dependence of structural relaxation timescale for a typical glass forming liquid.

In the frequency domain, these non-exponential decays can be described by a Havriliak- Negami (HN) empirical function

$$\hat{\varepsilon}(\omega) = \varepsilon_\infty + \frac{\Delta\varepsilon_k}{[1+(i\omega\tau_k)^{\alpha_k}]^{\gamma_k}} \qquad (1.3)$$

$\alpha_k$ and $\gamma_k$ represent the symmetric and asymmetric stretching of the loss spectra with the constraint $0 < \alpha_k, \alpha_k\gamma_k < 1$. When both $\alpha$ and $\gamma$ are equal to 1, the Debye expression is obtained. Fig. 1.4 shows supercooled glycerol fit with both a Debye fit (blue) and an HN (red) fit. The Debye fit does not accurately capture the broadness of the relaxation peak, while the HN fit does.

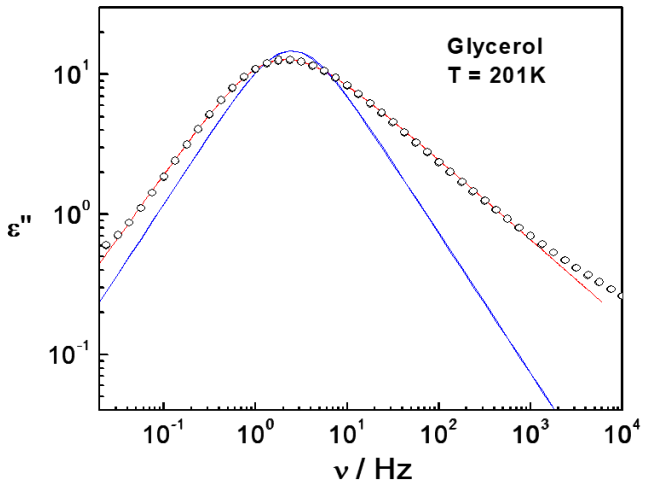


Fig. 1.4 Experimental dielectric loss curve for glycerol at T = 210 K. Experimental data points have been fit with both Debye (blue) and Havriliak-Negami (red) fitting functions.

## 1.2 Monohydroxy Alcohols

Unlike typical molecular liquids, monohydroxy alcohols exhibit a prominent Debye type relaxation process as the most prominent and lowest frequency peak in their dielectric spectra. In contrast to typical liquids, this dominant signature is not a signature of structural relaxation. This can be seen by comparing the dielectric features with mechanical[12], calorimetric[19-21], etc. measurements. These measurements show very little contribution in the frequency range of the Debye signal. The Debye type peak has been attributed to hydrogen bonding, but not all liquids with hydrogen bonding show a Debye type peak. For instance, most polyalcohols and diols do not exhibit a Debye type peak, nor do more sterically hindered monohydroxy alcohols (e.g., 1-phenyl-1-propanol[22], 2-phenyl-1-ethanol[23], and 3-methyl-3-heptanol[24]). One way the difference between monohydroxyl alcohols and typical molecular liquids is seen is the dielectric constants deviation from Onsager's relation. In Onsager's theory as link between dipole density

and dielectric constant is made, but it does not account for short range orientational correlations that materials with intermolecular interactions (such as hydrogen bonding) have. This deviation can be accounted for numerically by the Kirkwood correlation factor which will be discussed in the following sections.

### 1.2.1 Kirkwood Correlation Factor

In 1968, Dannhauser reported a study of molecular structure of a series of octyl alcohols on the static dielectric constant.[5] This study showed that by varying the position of the methyl group relative to a fixed hydroxyl group position, the value of the static dielectric constant dramatically increases as the distance between the methyl and hydroxyl group increases. Since the molecular dipole moment (and thus the dipole density) of the octyl alcohols is independent of the position of the methyl group, the difference in the static permittivity must reflect a difference in the structure of the liquids and the Kirkwood correlation factor, $g_k$.

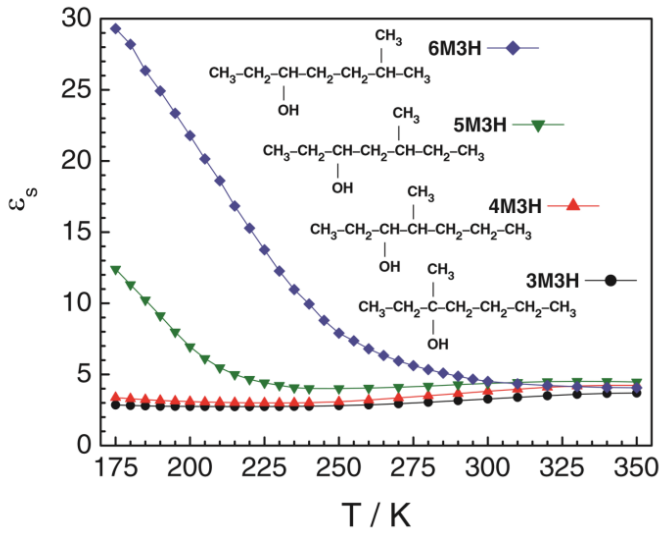


Fig. 1.5 Temperature dependence of the static dielectric constant, $\varepsilon_s(T)$, for four isomeric octyl alcohols identified in the legend: 3M3H, 4M3H, 5M3H, and 6M3H. The structures of the isomers are included on the graph. [ adapted from Ref. **24**]

Kirkwood-Fröhlich's equation is a generalization of Onsager's relation (eq.1.4) between the molecular dipole μ and permittivity[25]. The instantaneous effect of polarizability is expressed in terms of the high frequency limit of the dielectric constant, $\varepsilon_\infty \approx n^2$, where n is the optical refractive index.

$$\frac{(\varepsilon_s-\varepsilon_\infty)(2\varepsilon_s+\varepsilon_\infty)}{\varepsilon_s(\varepsilon_\infty+2)^2} = \frac{\rho N_A}{9k_bT\varepsilon_0 M}\mu^2 \qquad (1.4)$$

In this equation, $N_A$ is Avogadro's number, ρ is density, M is molar mass, $k_B$ is Boltzmann's constant, and $\varepsilon_0$ is the permittivity of vacuum. Onsager's equation ignores short range orientational correlations, to account for these the Kirkwood correlation factor is added to eq. 1.4

$$\frac{(\varepsilon_s-\varepsilon_\infty)(2\varepsilon_s+\varepsilon_\infty)}{\varepsilon_s(\varepsilon_\infty+2)^2} = \frac{\rho N_A}{9k_bT\varepsilon_0 M} g_k\mu^2 \qquad (1.5a)$$

$$g_k = \frac{\mu_{eff}^2}{\mu^2} = 1 + z\langle cos\,\theta\rangle \qquad (1.5b)$$

Where $\langle cos\,\theta\rangle$ is the average cosine of the angle, and z is the number of correlated neighboring dipoles. While many molecular liquids have a $g_k \approx 1$, monohydroxy alcohols have been shown to deviate from this value. Numerous alcohols have been shown to have a $g_k > 1$, and series studied by Dannhauser show $g_k$ values ranging from $g_k < 1$ to $g_k > 4$.

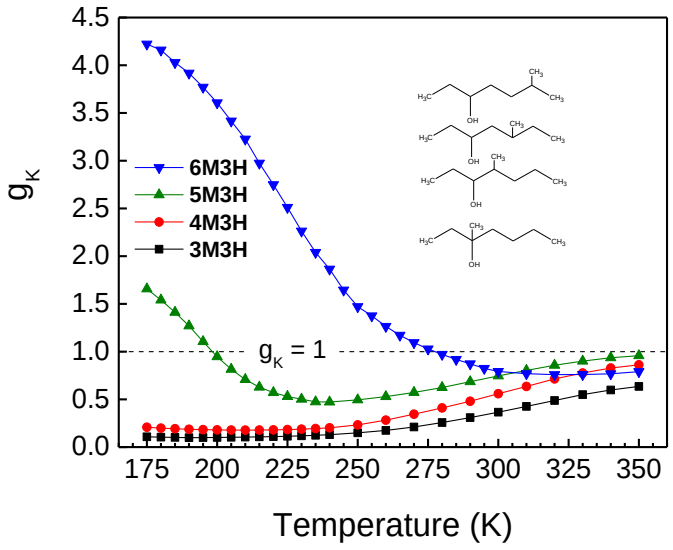


Fig. 1.6: Kirkwood correlation factor, $g_k$ versus temperature for four isomeric octyl alcohols, 3M3H, 4M3H, 5M3H, and 6M3H. The structures of the isomers are included on the graph to show the changing methyl position along the chain. [Ref. 25]

The situation $g_k > 1$ along with the high static dielectric constant is reflective of a preference to have a parallel alignment of neighboring dipoles, while those with a $g_k < 1$ are indicative of an antiparallel alignment.[5, 26]

This work will discuss alcohols with a varying range of $g_k$ values from far below 1 to above 4. In chapter 3, all the alcohols discussed have $g_k$ values above one. In chapter 4, 5-methyl-3-hepanol was studied. This material is shown to have a $g_k$ near 1 in the temperature range studied.[24] Finally, in chapter 5, 4-methyl-3-hepantol is studied and is shown to have a $g_k$ value near 0.1, but upon vapor deposition the deposited film has a $g_k$ of 1.

### 1.2.2 End to End Dipole Fluctuation

In the previous section the Kirkwood correlation factor was discussed in terms of the parallel or antiparallel alignment of neighboring dipoles, but another way to think of

this is the material having chain like (parallel) or ring like (anti parallel) supramolecular structures (Fig 1.7).

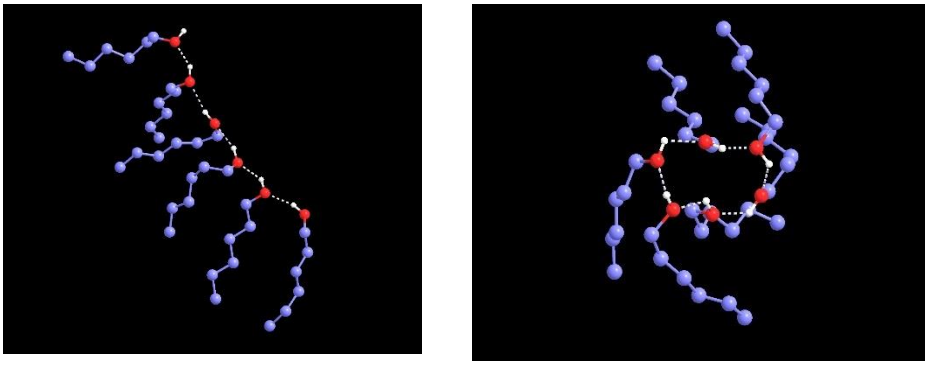

Fig. 1.7. (Left) Simulated chain like supramolecular structure of n-hexanol. (Right) Simulated ring like supramolecular structure of n-hexanol. [provided by Rafael Alcala-Torano]

These supramolecular structures are held together by relatively weak intramolecular interactions. In monoalcohols, the supramolecular structures formed are dependent on the steric hinderance of the hydroxyl group. For example, as the position of the methyl group in the octyl alcohol series (Fig 1.6) is shifted from the 6- position to the 3- position, the hydroxyl group become more sterically hindered. The difference in the methyl position changes the preference of which supramolecular structures are formed, more chain like or ring like. The alignment of a chain like structure will yield a more polar material and a higher Kirkwood correlation factor than a material with a more ring like structure. With this knowledge, an alcohol having a $g_k < 1$ would be characterized as having ring dominated structures, while $g_k > 1$ would be chain dominated. Field induced changes of these hydrogen bonded structures from a more ring like state to a more chain like state can help to show that the fluctuation is occurring, and when used with time resolved measurements, show that these changes occur on the Debye timescale.

The Debye peak can be understood as a signature of end to end vector chain fluctuations that are equivalent to fluctuations in the net $g_k$.[27] There have been several models involving end to end vector fluctuations analogous to polymer chains.[28, 29] The model proposed by Singh and Richert[27] describes the change in the chain structures as going from an extended chain to a more curled, ring like formation. This is similar to the model proposed by Levin and Feldman[28] to describe n-alcohols, but the contribution to the end to end fluctuation by the chain cleavage and reconnection to other fragment and the bond rotation are relevant in monohydroxy alcohols.

In high ac field experiments[27], it was shown that field induced changes in the supramolecular structure can be seen in the permittivity when the ring to chain equilibrium (independent dipoles) or $g_k \approx 1$. These changes in the end to end distances in the structure have been observed to occur on the Debye time scale. Although field induced changes using realistic fields can only be seen in alcohols with a $g_k \approx 1$ (i.e., 5M3H), the end to end distances in alcohols with a $g_k > 1$ (i.e. 2E1H, nPOH, etc.) still fluctuate under the field. The chains will fluctuate between more compact or more extended in length, but do not have significant ring structures.

**1.3 Linear Response from Dielectric Spectroscopy**

In our lab, dielectric spectroscopy is used to look at the dynamics and structure of super cooled liquids. The premise of this technique is that the orientation of dipoles within a material can be polarized by applying an external electric field. The polarization (macroscopic) is heavily dependent upon the material and temperature, and the time it takes for the polarization to reach a steady state value reveals the relaxation time of the

material. The overall polarization can be divided into two parts: electronic polarization and polarization originating from the dipoles orientating (orientational polarization). Orientational polarization is defined as $P_0 = \frac{N}{V}\langle\mu\rangle_z$, where N is the number of dipoles in a macroscopic sample of volume V, and $\langle\mu\rangle_z$ is the average of all the projected dipole moments on the z-axis. In the linear regime, polarization is proportional to the applied field.

$$P^*(\omega) = \varepsilon_0\chi^*(\omega)E^*(\omega) \qquad (1.6)$$

$\chi^*$, is the complex dielectric susceptibility. This is related to the complex permittivity by $\chi^* = (\varepsilon^*(\omega) - 1)$, with $\varepsilon^*(\omega) = \varepsilon'(\omega) - i\varepsilon''(\omega)$. The storage component, $\varepsilon'(\omega)$, relates to the amount of energy the material stores from the applied field, and the loss component, $\varepsilon''(\omega)$, corresponds to the dielectric loss of the material, or the dissipation of the energy from the applied field. A schematic representation of both the real and imaginary parts of permittivity are shown in Fig. 1.2.

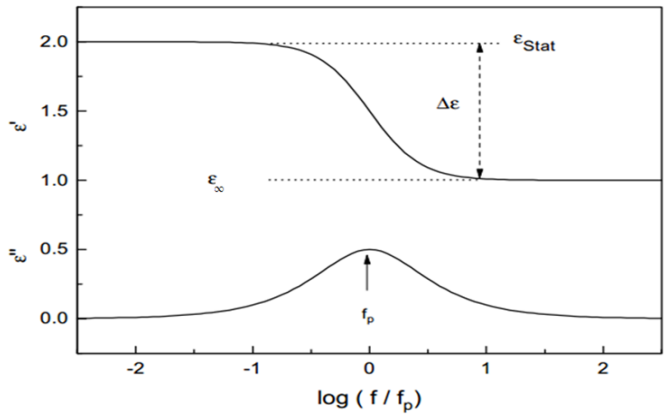


FIG 1.8: Schematic representation of both the real and imaginary part of permittivity.

At the high frequency side, dipoles cannot keep up with the rate at which the field is changing, so its value. On the low frequency end of the spectrum, the field changes are

slow, and the dipoles have the opportunity to align with the changing field. The plateau on the low frequency side of the 'real' part of permittivity is the static dielectric constant , $\varepsilon_s$, and the high frequency plateau is $\varepsilon_\infty$, which is approximately equal to the refractive index squared. The difference between the high and low frequency sides of the real component of the permittivity is called relaxation strength $\Delta\varepsilon = \varepsilon_s - \varepsilon_\infty$. In the loss component, relaxation peaks are observed when the frequency of the applied field is equal to the relaxation rate of the material. The timescale of the relaxation process is related to the frequency of the maximum of the dielectric loss peak by $\tau \approx 1/2\pi f_p$ Since both the storage and the loss components are derived from the same complex function, they are related to each other by the Kramers-Kronig relation.

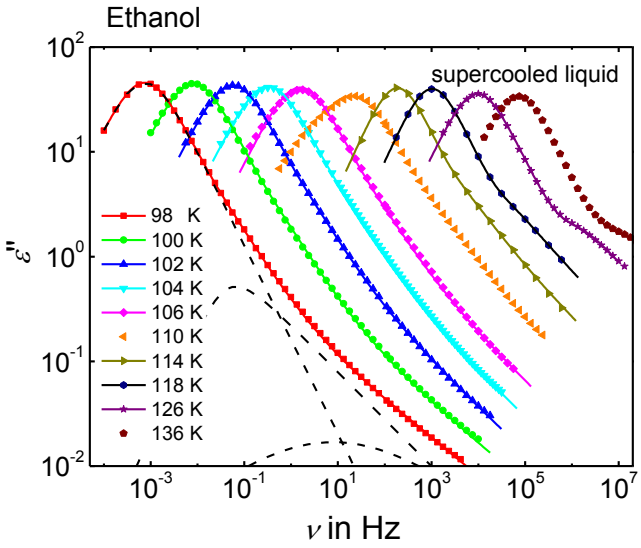


Fig. 1.9: Re-evaluation of the experimental dielectric loss spectra of ethanol from Brand et al. (symbols, Ref.30) in the supercooled liquid state for temperatures between 98 K to 136 K. The solid lines represent fits based on Equation 1.3. The dashed lines indicate the three distinct contributions to the 98 K curve: Debye, structural α-relaxation, and JG secondary process in the order of increasing peak frequency. [Figure adapted from Ref 31]

As previously mentioned, typical supercooled liquids show a broadened peak in the dielectric spectra and are fit using a Havriliak- Negami fitting function (eq. 1.3).

However, monohydroxy alcohols contain a large Debye type peak, as well as underlying primary and secondary relaxation signatures. (Fig. 1.9) The loss curves for monohydroxy alcohols are evaluated using the sum of a Debye-like, a HN, and a Cole-Cole (CC) type dielectric process using equation (1.7)

$$\hat{\varepsilon}(\omega) = \varepsilon_\infty + \frac{\Delta\varepsilon_D}{1+(i\omega\tau_D)} + \frac{\Delta\varepsilon_\alpha}{[1+(i\omega\tau_\alpha)^\alpha]^\gamma} + \frac{\Delta\varepsilon_\beta}{1+(i\omega\tau_\beta)^\beta} \qquad (1.7)$$

**1.4 Nonlinear Dielectric Spectroscopy**

In the linear response, the relationship between polarization (P) and electric field (E) at equilibrium is $P=\varepsilon_o\chi E$ where $\chi$ is the susceptibility ($\varepsilon_s - 1$). In a nonlinear approach, higher order terms will contribute to the overall polarization

$$\frac{P}{\varepsilon_0} = \chi E + \chi^{(3)}E^3 + \cdots \qquad (1.8)$$

The superscript associated with the susceptibility $\chi^{(n)}$ refers to the power of the electric field (i.e., $\chi^{(3)}E^3$). For an electric field, $E(t) = E_o\cos(\omega t)$, the resulting polarization will generate Fourier components at the first and third harmonics ($\omega$ and $3\omega$). Although not typically valid for frequency dependent susceptibilities, the $\chi^{(n)}(\omega)$ can be calculated for a DC bias field ($E(t) = E_B + E_o\cos(\omega t)$ with $E_B$ representing the bias field. The nonlinear behavior with applied bias fields are depicted in fig. 1.3, where the slope of P vs. E depends not only on the field $E_B$ and $E_0$, but on the frequency and time the field is applied as well.

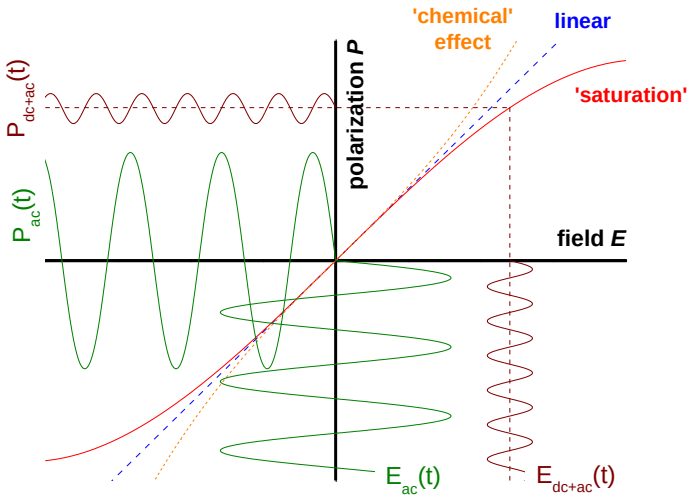


Fig. 1.10: Polarization against field strength showing the chemical effect (orange) and saturation(red) indicate a deviation from the linear response (blue). Two different ways of achieving nonlinearity are shown, high AC amplitude (green)and high amplitude DC bias field superimposed with a low amplitude AC field (dark red).

Deviations from linearity also give rise to higher order Fourier components in the polarization response to a harmonic field. These components can be indiviaually expressed where the odd harmonics can be normalized to the peak value of the AC field. Higher order terms may be required at high field amplitudes, and the even Fourier components will appear in the presence of a DC bias field.

$$\frac{\hat{P}_1(\omega)}{\varepsilon_0 E_0} = \hat{\chi}_1(\omega) + \hat{\chi}_1^{(3)}(\omega)E_0^2 + \cdots \quad (1.9)$$

$$\frac{\hat{P}_3(\omega)}{\varepsilon_0 E_0} = \hat{\chi}_3^{(3)}(\omega)E_0^2 + \cdots \quad (1.10)$$

A qualitative link between the non linear features of equation (1.9) and (1.10) will be discussed in later chapters.

Early studies of nonlinear dielectric effects (NDE) of alcohols were done by Malecki[32,33] and Piekara.[34] In these studies, reduction of permittivity or polarization were

described as “negative saturation” while a field induced increases were coined “ positive saturation”. These terms were later renamed as ‘ Langevin saturation’ and ‘chemical’ effects.[35] High ac field experiments[24,27] on monohydroxyl alcohols have shown a field induced increase in the dielectric constant similar to the ‘chemical effect’ seen in the earlier studies. In the high ac measurements, accelerated dynamics, or a shift of the spectral peak toward higher frequencies, due to energy absorption from the time dependent field. Over time, the energy is that is transferred from the field to the sample will be converted to heat.[36,37, 38]. For cleaner experiments, high dc fields can be applied to the sample and both ‘chemical’ effects and ‘saturation’ can still be seen. Another NDE seen with high dc experiments is a frustraion of dynamics, this can be seen as a shift in the spectral peak toward lower frequencies.[39] In later chapters, further studies exploring the chemical effect and looking more indepth into the frustration of dynamics will be discussed.

**1.5 References**


1 P. Debije, Verh. Dtsch. Phys. Ges. **15** 777 (1913).

2 P. Debye, *Polar Molecules*, Chemical Catalog Company, New York, 1929.

3 D.W. Davidson, R.H. Cole, J. Chem Phys. **19**, 1484 (1951).

4 W. Dannhauser, A. F. Flueckinger, Phys. Chem. Liq. **2**, 37 (1970).

5 W. Dannhauser, J. Chem. Phys. **48**, 1911 (1968).

6 G. P. Johari, W. Dannhauser, J. Chem. Phys. **48**, 3407 (1968) .

7 G. P. Johari, W. Dannhauser, J. Phys. Chem. **72**, 3273 (1968).

8 J.K. Vij, W.G. Scaife, J.H. Calderwood, J. Phys. D: Appl. Phys. **11**, 545 (1978).

9 J.K. Vij, W.G. Scaife, J.H. Calderwood, J. Phys. D: Appl. Phys. **14**, 733 (1981).

[10] W. Kauzmann, Chem. Rev. **43**, 219 (1948).

[11] T. Lyon, T. A. Litovitz, J. Appl. Phys. **27**, 179 (1956).

[12] T. A. Litovitz, G. E. McDuffie, J. Chem. Phys. **39**, 729 (1963).

[13] B.M. Fung, T.W. McGaughy, J. Chem. Phys. **65**, 2970 (1976).

[14] H. Versmold, Ber. Bunsenges. Phys.Chem. **78**, 1318 (1974).

[15] C. Hansen, F. Stickel, T. Berger, R. Richert, E.W. Fischer, J. Chem. Phys. **107**, 1086 (1997).

[16] P. G. Debenedetti, F. H. Stillinger; *Nature* **410**, 259 (2001).

[17] R. Kohlrausch, Ann. Phys. **167**, 179 (1854); G. Williams and D.C. Watts, Trans. Faraday Soc. **66**, 80 (1970).

[18] H. Vogel, Phys. Z. 22, 645 (1921); G.S. Fulcher, J. Am. Ceram. Soc. **8**, 339 (1925); G. Tammann, W. Hesse, Z. Anorg. Allgem. Chem. **156**, 245 (1926)

[19] H. Huth, L.-M. Wang, C. Schick, and R. Richert, J. Chem. Phys. **126**, 104503 (2007).

[20] S. S. N. Murthy and M. Tyagi, J. Chem. Phys. **117**, 3837 (2002).

[21] L.-M. Wang, Y. Tian, R. Liu, and R. Richert, J. Chem. Phys. **128**, 084503 (2008).

[22] G. P. Johari, O. E. Kalinovskaya, and J. K. Vij, J. Chem. Phys. **114**, 4634 (2001).

[23] O. E. Kalinovskaya, J. K. Vij, and G. P. Johari, J. Phys. Chem. A **105**, 5061 (2001).

[24] L. P. Singh, C. Alba-Simionesco, and R. Richert, J. Chem. Phys. **139**, 144503 (2013).

[25] J. G. Kirkwood, J. Chem. Phys. **7**, 911 (1939)

[26] C. J. F. Bötcher, *Theory of Electric Polarization* (Elsevier, Amsterdam, 1973), Vol. 1.

[27] L. P. Singh and R. Richert, Phys. Rev. Lett. **109**, 167802 (2012).

[28] V. V. Levin and Y. D. Feldman, Chem. Phys. Lett. 87, 162 (1982

[29] C. Gainaru, R. Meier, S. Schildmann, C. Lederle, W. Hiller, E. A. Rössler, and R. Böhmer, Phys. Rev. Lett. 105, 258303 (2010).).

[30] R. Brand, P. Lunkenheimer, U. Schneider, and A. Loidl, J. Phys. Rev. B **62**, 8878 (2000).

[31] Y. Z. Chua, A. R. Young-Gonzales, R. Richert, M. D. Ediger, C. Schick, J. Chem. Phys. **147**, 014502.1 (2017).

[32] J. Malecki, J. Chem. Phys. **36,** 2144 (1962).

[33] J. Malecki, J.Chem. Phys. **43**, 1351 (1965).

[34] A. Piekara, J. Chem. Phys. **36**, 2145 (1962)

[35] J. Malecki, J. Mol. Struct. **436,** 595 (1997).

[36] T. Matsuo, H. Suga, and S. Seki, Bull. Chem. Soc. Japan, **39**, 1827 (1996)

[37] A. Khalife, U. Pathak, and R. Richert, Eur. Phys. J. B **83**, 429 (2011).

[38] S. Galema, Chem. Soc. Rev. **26**, 233 (1997)

[39] R. Richert, J. Phys.: Condens. Matter **29**, 363001 (2017).

# CHAPTER 2

# EXPERIMENTAL SETUPS

In this chapter, experimental setups for different techniques that have been employed in our lab will be described. Setups from linear dielectric measurements to nonlinear dielectric experiments along with their time resolved versions and physical vapor deposition.

## 2.1 Linear Dielectric Measurements:

In this set up an electric field, E (ω) =$E_o$exp ($i$ωt) where ω is the angular frequency (2πυ) and $i = \sqrt{-1}$, is used to perturb the system. The complex dielectric permittivity ε*(ω) equation 1 is obtained from the linear response.

$$\varepsilon^*(\omega) = \varepsilon'(\omega) - i\varepsilon''(\omega) \qquad (2.1)$$

ε' (ω) is the storage (real) component of the complex equation, and ε" (ω) is the loss (imaginary) component. ε' (ω) is a measure of the energy the material stores from the external field where as ε" (ω) accounts for the dissipation part of the energy.

For a capacitor C filled with a material, $\varepsilon*(\omega) = \frac{C(\omega)}{C_o}$ where $C_o$ is the vacuum capacitance[2]. Using the sinusoidal electric field E (ω), the complex dielectric can be derived by measuring the complex impedance Z*(ω).

$$\varepsilon^*(\omega) = \frac{1}{i\omega Z^*(\omega)C_o} \qquad (2.2)$$

When a sinusoidal voltage $U_1$ (t) is applied to the sample, a resistor converts the sample current I (t) into a voltage $U_2$ (t). These voltages are analyzed based on amplitude and

phase of the waves $U^*(\omega)$ and $I^*(\omega)$.[1] $Z^*(\omega)$ can be calculated from the sample voltage ($U_s^*$) and current ($I_s^*$) from the equation

$$Z_S^* = \frac{U_S^*}{I_S^*(\omega)} \tag{2.3}$$

The response to the signal $U_1$ (t) is two components, in phase (real) and out of phase (imaginary). The two signals are subject to Fourier analysis by

$$\frac{1}{NT}\int_0^{NT} S(t)\sin(\omega t)\,dt = A\cos(\varphi) = R \tag{2.4}$$

$$\frac{1}{NT}\int_0^{NT} S(t)\cos(\omega t)\,dt = A\sin(\varphi) = I \tag{2.5}$$

$$S(t) = \begin{cases} U(t) \\ I(t) \end{cases} \tag{2.6}$$

Where the amplitude is obtained by $A=\sqrt{R^2 + I^2}$ and the phase by φ=arc tan (I/R). If S(t) = $U_1$(t) then the amplitude and phase would be denoted as voltage data (equation 5); similarly, if S(t) =I(t) A and φ would be current data[2]

$$U_1(t) = U_o\sin(\omega t + \varphi) \tag{2.7}$$

When equation 2.4 and 2.5 are integrated over a number of periods (N) for a certain time (T=N2π/ω), the result of the sample yields $S_o$(t) sin (ϕ) and $S_o$(t) cos (ϕ) respectively. Instead of representing the Fourier components as sums of sinusoidal functions, they are represented as complex forms of voltage and current. The actual voltage and current can be obtained from the complex representation by multiplying the complex number representation by $e^{i\omega t}$.[3]

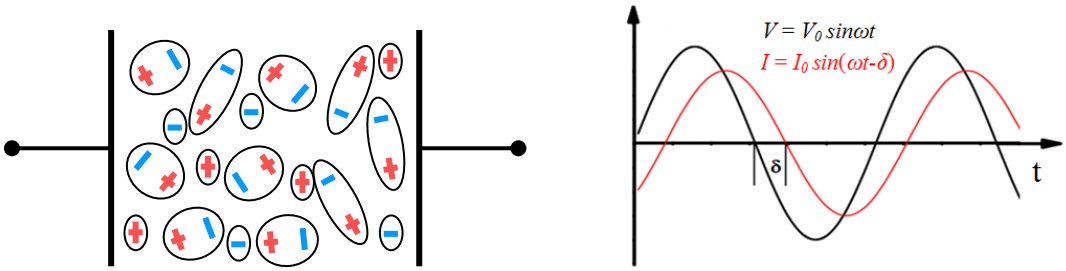


Fig. 2.1: Liquid molecules between two electrodes having a separation of distance d and an area A (Left) Schematic representation of the Voltage signal, V(t), applied to the sample, and the corresponding current signal from the sample, I(t). The difference in the phase angle is represented as δ.

Samples are generally prepared between two spring loaded polished electrodes (stainless steel/titanium with separations varying from 8μm to 100μm using a Teflon or Kapton polyimide ring spacer depending on the material or experiment. The spacing ring covers the circumference of the lower electrode.

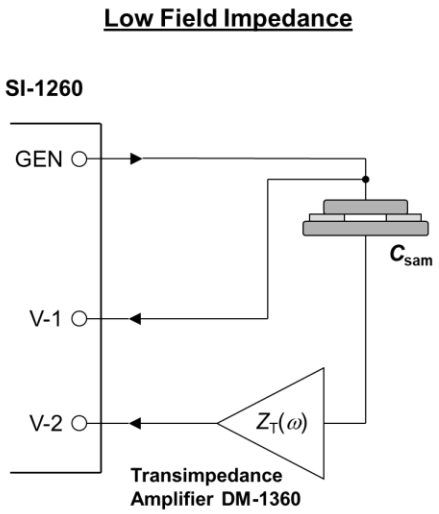


Fig. 2.2: Schematic of the linear dielectric measurement set up.

A Solartron SI-1260 gain/phase analyzer in combination with a homebuilt DM-1360 transimpedance amplifier is used for measurements in the frequency range of 10 mHz- 10MHz. The SI-1260 produces the desired voltage. The DM-1360 converts low

amplitude currents to measurable voltages over the entire frequency range. The voltage of the sample is recorded at the V1 input of the SI-1260. The current is recorded via the V2 input. The amplitude and phase relation of the complex current I*(ω) and voltage V*(ω) are determined, and the complex dielectric ε*(ω) can be determined from Eq. 2.1.

**2.2 Standard High DC field impedance setup:**

For high field measurements, thin samples (8 µm- 10µm) and high electric fields (≥100kV/cm) are required. High bias experiments are performed with the Solartron SI-1260 gain/phase analyzer, with either a Trek PZD 350A or 700 amplifier (Fig. 2.3), near steady state conditions. The voltage at the sample is measured at the V1 input of theSI-1260 using the voltage monitor of the high voltage amplifier which is internally attenuated by a factor o

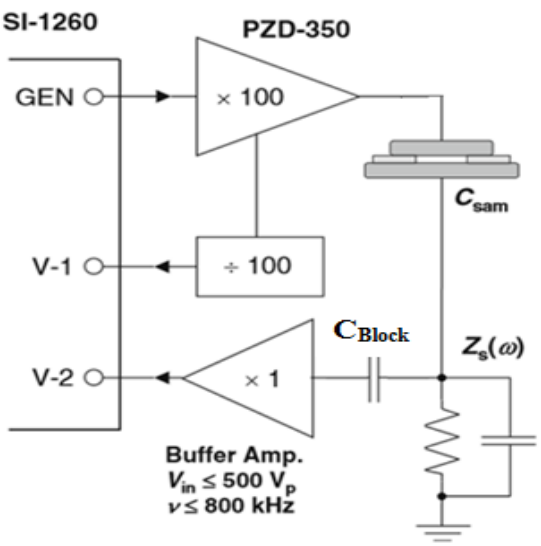


Fig. 2.3: Schematic of the high DC field impedance setup. The various components are described in text

The low potential side of the capacitor is ground via a shunt with the impedance $Z_s(\omega)$. The value of $Z_s(\omega)$ is determined by a parallel circuit with a combination of resistors and

capacitors set in a way that the frequency dependent change in the shunt impedance can counteract the reduction of current toward low frequencies (Fig. 2.4) The current is measured as a voltage drop over an RC shunt network via the V2 input. The voltage is ac-coupled to a home built linear buffer amplifier. This buffer amplifier protects the V2 input against high voltages in case of sample failure (dielectric breakdown).

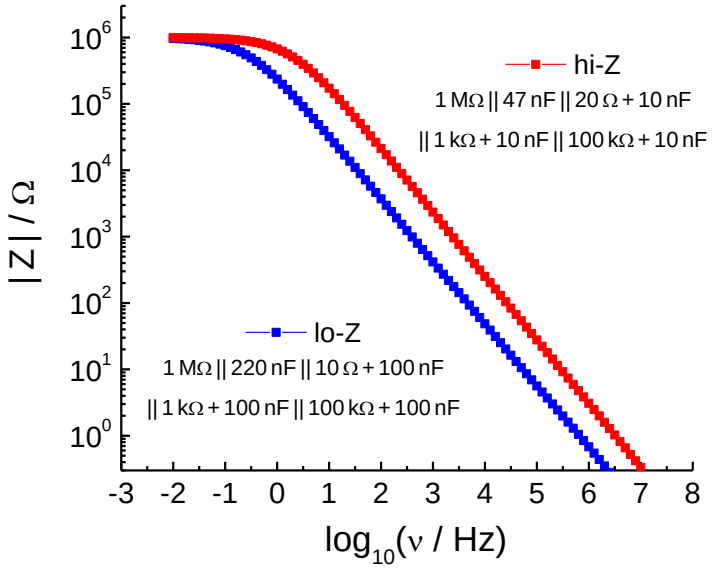


Fig. 2.4: Frequency dependent impedance values for two different types of shunts used in high field experiments.

For each frequency, the system is programmed to perform a set number of measurements with a bias field, immediately followed by a set number of measurements with a zero bias. The number of measurements chosen are dependent on the material and is typically set to between 3 and 6 per bias.

**2.3 Time Resolved Technique**

Samples for the time resolved measurements are prepared similarly to typical high field measurements. The cell is mounted to a cold stage of a closed cycle He-refrigerator

cryostat Leybold RDK 6-320 with Leybold Coolpack-6200 compressor. Temperature is stabilized within several mK using a Lakeshore Model 340 temperature controller equipped with DT-470-CU sensor diodes.

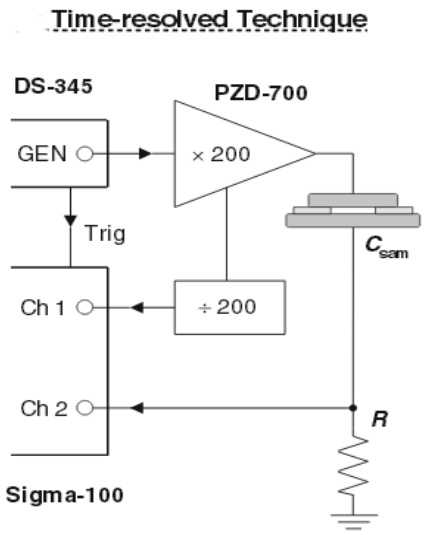


Fig. 2.5: Schematic of the time resolved high DC field impedance setup. The various components are described in text

For observing the rise and decay of nonlinear effects, the voltage applied to the sample is generated using a programmable function generator (Stanford Research Systems DS-345) and amplified by a factor of 100 or 200 using either a Trek PZD-350A or PZD 700 high voltage amplifier. The programmed voltage waveforms (16300 points, 12bit) consist of an integer number of periods of a sinusoidal signal, $V(t) = V_0\sin(\omega t)$, with a bias voltage amplitude $V_B$ superimposed over an underlying AC voltage (10% - 20% $E_B$). Measurements are takes with both a positive and negative bias to account for the spike in current upon application of the field. The two biases are then averaged and period by period Fourier analysis is done at the fundamental frequency which yields the

amplitude (A) and phase (φ) of both the current and voltage. The "permittivity" can then be calculated using eq. 2.9

$$e'' = \left|\frac{A_I \cos(\varphi_I - \varphi v)}{\omega A_v C_0}\right| \qquad (2.9)$$

The notation $e''$ is used instead of $\varepsilon''$ because $e''$ changes with time in this nonequilibrium situation, and ε is not defined. $C_0$ is the geometric capacitance, $C_0 = \varepsilon_0 A/d$.

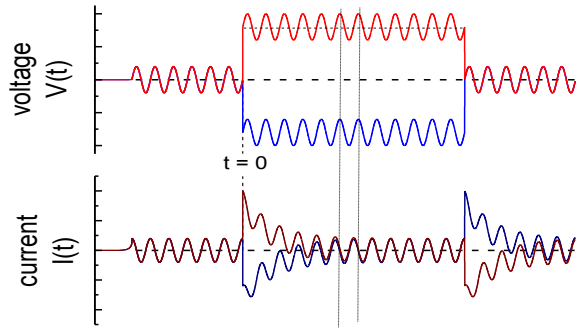


Fig. 2.6: Schematic representation of the voltage protocol used for time resolved high DC field experiments.

**2.4 Physical Vapor Deposition**

Molecular glasses made using physical vapor deposition (PVD) can display higher kinetic stability, higher density, and lower density relative to glasses prepared by cooling the liquid to below $T_g$. These results are seen because the surface mobility is high enough to allow substantial equilibration, even below $T_g$, but the same is not true of monohydroxyl alcohols. For glasses of monoalcohols and other hydrogen bonded liquids prepared by PVD little to no enhancement to kinetic stability is seen.[5,6] Work done by Wübbenhorst *et al.* with glycerol showed that when heated above $T_g$, vapor deposited

glycerol forms a liquid with a $g_k$ substantially higher than the ordinary supercooled liquid.[7,8] The results for glycerol imply that vapor deposition of hydrogen bonded systems at low temperatures, will yield structures that are trapped far from equilibrium. Thus, making PVD and ideal technique for looking at low $g_k$ alcohols.

A small amount of sample is held in a reservoir which can be evacuated. The reservoir is connected via a pressure regulator, a shut off valve, a regulating needle valve, and a second shut off valve to an opening in the vacuum enclosure of a closed cycle helium cryostat (Leybold RDK 10-320) to facilitate vapor deposition onto a cold substrate. The cryostat is then evacuated to a pressure lower than $10^{-3}$ Pa using a turbo pump supported by the cryo-pump action of the cold finger within the vacuum system. The substrate holder temperature can be adjusted between 30 K and 300 K using a Lakeshore model 340 temperature controller equipped with DT-470 diode sensor. The substrate holder is surrounded by a radiation shield held near 100 K with an aperture that is aligned with the molecular beam.

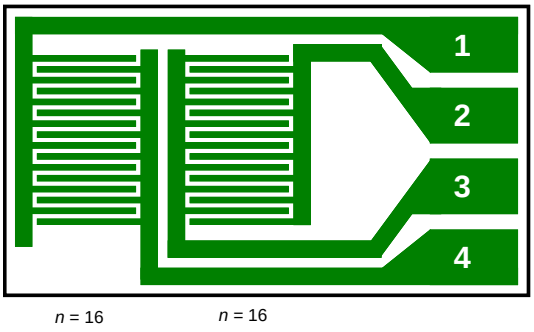


Fig. 2.7: Schematic of IDE cell.

The vapor is deposited onto an interdigitated electrode (IDE) cell, IME 1050.50-FD-Au from ABTECH scientific, on a borosilicate substrate. [4,5] The electrode has a

geometric capacitance of, $C_{geo}$, 2pF[9] and the effective height of the electric field is estimated to be d = 5μm. The film thickness is determined using a change in capacitance. The capacitance is measured with an Andeen-Hagerling ultra precision capacitance bridge (AH-2700A) for frequencies ranging from ν = 100 Hz – 20 kHz.

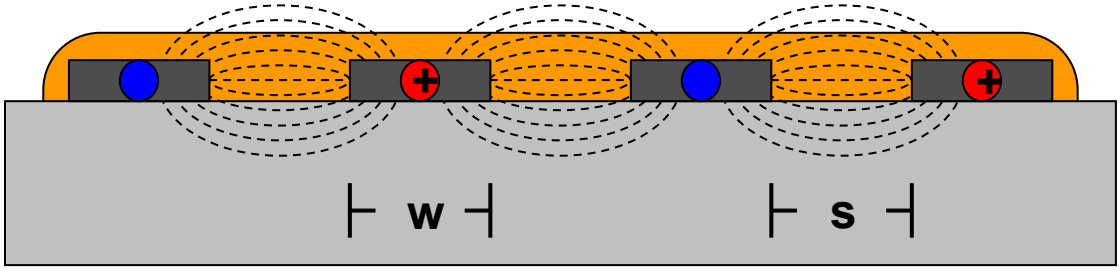


Fig. 2.8: Schematic of the effective field lines through a sample (orange) from the IDE cell.

During the deposition process, the capacitance and temperature are recorded as a function of time where the initial rate and total capacitance change are evaluated to yield the deposition rate $\nu_{Dep}$ and film thickness, h. After the deposition the sample is cooled to a set point well below $T_g$ and three subsequent scans are taken during which the temperature and permittivity are recorded. To account for the permittivity of the borosilicate glass, baseline measurements of the IDE cell are taken under measurement conditions and subtracted.

**2.5 References**


1 F. Kremer, A. Schönhals (Eds.), Broadband Dielectric Spectroscopy ( Springer, 2003)

2 W. Huang and R. Richert, J. Chem. Phys.130, 194509 (2009).

3 P. Horowitz, The Art of Electronics 2nd ed. (Winfield Hill, 1989)

4 L. Yang, A. Guiseppi-Wilson, and A. Guiseppi-Elie, Biomed. Microdevices **13**, 279 (2011).

[5] M. Tylinski, M. S. Beasley, Y. Z. Chua, C. Schick, and M. D. Ediger, J. Chem. Phys. **146**, 203317 (2017).

[6] M. Tylinski, Y. Z. Chua, M. S. Beasley, C. Schick, and M. D. Ediger, J. Chem. Phys. **145**, 174506 (2016).

[7] S. Capponi, S. Napolitano, and M. Wübbenhorst, Nat. Commun. **3**, 1233 (2012)

[8] A. Kasina, T. Putzeys, and M. Wübbenhorst, J. Chem. Phys. **143**, 244504 (2015)

[9] B. Reichers, A. Guiseppi-Ellie, M.D. Ediger, and R. Richert, J. Chem. Phys. (Submitted)

# CHAPTER 3

## RISE AND DECAY OF ANISOTROPY IN THE NONLINEAR REGIME

This chapter focuses on the effects of applying a dc bias field to polar super cooled liquids. Then using time resolved measurements to characterize the origin of the effects seen. The results of these experiments can be used to obtain thermodynamic data, but is not calculated in this thesis. I conducted all high field experiments on the monohydroxy alcohols.

### 3.1 Introduction

In the context of dielectric relaxation, non-linearity refers to a deviation from the linear relation between polarization *P* and field *E*, where linearity is observed only at sufficiently low field amplitudes. The recent literature documents an increasing interest in non-linear dielectric effects (NDE's), mainly motivated by the prospect of gaining more detailed insight into the structure and dynamics of liquids and glasses relative to what can be learned from experiments restricted to the linear regime.[1] The common expression of non-linearity involves higher order susceptibilities, $\chi^{(n)}$, that are associated with higher powers of the field, $E^n$,

$$\frac{P}{\varepsilon_0} = \chi E + \chi^{(2)}E^2 + \chi^{(3)}E^3 + \dots \quad (3.1)$$

Due to its limitation to steady state situations, this approach is far from being capable of describing the diversity of non-linear effects that have been observed by dielectric techniques. There are numerous sources and signatures of non-linear dielectric behavior: dielectric saturation,[2,3,4] chemical changes,[5,6] field induced changes in barrier height,[7,8] in

dielectric constants of mixtures,[9,10] and in configurational entropy,[11,12] field dependent charge densities,[13,14] electrocaloric effects,[15] and elevations of effective temperatures,[16,17,18,19] analogous to microwave heating.[20] Non-linear dielectric features have also been related to the number of dynamically correlated particles or non-trivial length scales in supercooled liquids.[21,22,23]

To fully exploit the potential of non-linear dielectric experiments, both experimental and theoretical progress is highly desirable. The present work is concerned with the effects of applying a dc bias field to a polar supercooled liquid, using glycerol and several mono-hydroxy alcohols as examples. Time resolved techniques are employed to characterize the origin of the non-linear effects and to be able to distinguish between the alternatives shown in Fig. 3.1: (a) a deviation from linear $P(E)$ behavior limited to the regime of high fields, or (b) a field induced change of the $P$ versus $E$ slope that includes the low field regime. The former case would involve a non-zero value of $\chi^{(3)}$ in eq. (3.1), whereas the latter is dominated by a field induced change in $\chi$, i.e., in the linear term. To rationalize the observed time dependence of the NDE's at constant temperature, the energy absorbed from the time dependent field (when switching the bias on or off) as well as the impact of entropy reduction, $\Delta_E S$, need to be considered. The rise and decay patterns associated with the field induced anisotropy are asymmetric in the sense that the NDE rises slowly upon applying the dc field relative to its subsequent decay when the field is removed. This feature has been observed also for the birefringence, $\Delta_E n$, in experiments on electro-optical Kerr effects, which are much related to the present non-linear dielectric features.[24] The time dependence of the NDE's including the rise/decay

asymmetry can be rationalized on the basis of the low field permittivity, $\varepsilon(t)$, if the quadratic field dependence of $\Delta S(E)$ is accounted for. The effects observed for the present glass-forming liquids are consistent only with the Fig. 3.1b scenario. Observing the analogous NDE pattern in monohydroxy alcohols on the time scale of their prominent Debye type dielectric polarization clearly links these NDE's to polarization anisotropy, rather than features associated with mechanical or enthalpy relaxation.

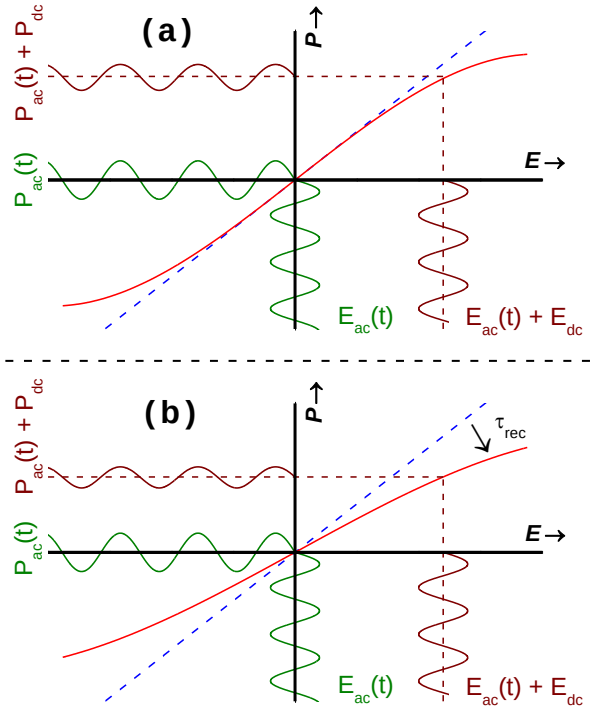


FIG. 3.1: Non-linear $P(E)$ behavior is represented by the red solid curve, which deviates symmetrically from the blue dashed linear line. Brown and green sinusoidal curves are for the field and polarization versus time with and without bias field, respectively. **(a)** In the absence of a large dc-field, $E_{dc}$, the small amplitude sine, $E_{ac}(t)$, will always probe only the original linear $P(E)$ dependence. **(b)** On a structural recovery time scale ($\tau_{rec}$), the large dc-field leads to a deviation from linearity and to a change in the slope $dP/dE$, even near $E = 0$.

### 3.2 Experiments

The materials used for this study are glycerol (GLY, 99.5+%, spectrophotometric grade), 2-ethyl-1-hexanol (2E1H, 99+%), 2-ethyl-1-butanol (2E1B, 98%), and 6-methyl-3-heptanol (6M3H, purity not specified), all purchased from Sigma-Aldrich and used as received. Regular low field impedance experiments are performed using a system based upon a Solartron SI-1260 gain/phase analyzer and a Mestec DM-1360 transimpedance amplifier, applying fields not exceeding 1 $kV_{rms}$/cm. For all measurements, the instrumentation is calibrated using low loss capacitors with $\tan\delta < 10^{-4}$, with the capacitances determined by an Andeen-Hagerling AH-2700 ultra-precision capacitance bridge.

The high field capacitor cell consists of two spring-loaded polished stainless-steel disks (16 and 20 mm ∅), separated by a Teflon ring of $d$ = 10 μm thickness (Kapton ring, $d$ = 13 μm, for 6M3H) that leaves an inner area of 14 mm diameter for the sample. For time resolved measurements, the cell is mounted onto the cold stage of a closed-cycle He-refrigerator cryostat Leybold RDK 6-320 with Leybold Coolpak-6200 compressor. Temperature stability within several mK is achieved using a Lakeshore Model 340 temperature controller equipped with DT-470-CU sensor diodes.

For observing the rise and decay of the non-linear effects, the voltage applied to the sample is generated by a programmable function generator (Stanford Research Systems DS-345) and amplified by a factor of 100 or 200 using a Trek PZD-350 or PZD-700 high-voltage amplifier, respectively. The programmed voltage waveforms (16300 points, 12 bit) consist of an integer number of periods of a sinusoidal signal, $V(t) = V_0\sin(\omega t)$,

with a bias voltage of amplitude $V_B$ superposed for some of the periods, where a voltage ratio of $V_B/V_0 = 4$ is used. In order to avoid excessive current spikes, changes in the bias level are realized through linear voltage ramps that use 10% of the duration of a period. The waveform is repeated once every five seconds, ensuring that the electric field remains zero for a long time relative to the duration of the waveform signal. With the phase of the harmonic signal unchanged, each experiment is performed for both positive and negative bias patterns.

Voltage and current ($R$ = 3 kΩ shunt) signals are recorded with a digitizing oscilloscope (Nicolet Sigma 100) with $10^6$ points along the time axis and 12 or 14 bit vertical resolution, averaging over 3000 waveform repetitions. All signal traces shown refer to the average of two measurements, one with positive and one with negative bias, in order to eliminate the direct polarization response to the bias field steps. The resulting two averaged signals, voltage $V(t)$ and current $I(t)$, are subject to period-by-period Fourier analysis at the fundamental frequency. This analysis yields amplitude ($A$) and phase ($\varphi$) of the voltage ($A_V$, $\varphi_V$) and of the current ($A_I$, $\varphi_I$). The effect of the high bias field is quantified by means of the out-of-phase 'permittivity' evaluated for each period of the measurement, using

$$e'' = \left| \frac{A_I \cos(\varphi_I - \varphi_V)}{\omega A_V C_0} \right| . \qquad (3.2)$$

The notation $e''$ instead of $\varepsilon''$ is used because $e''$ changes with time in this non-equilibrium situation, where permittivity $\varepsilon$ is not properly defined.

High field spectra (without time resolution) are obtained with the cell outlined above, but in a *l*-$N_2$ cryostat with a Novocontrol Quatro temperature controller. High bias-field experiments near steady-state conditions are performed with the SI-1260 analyzer, with the voltage amplified using a Trek PZD 350 or 700 amplifier. The voltage at the sample is recorded via input V1 of the SI-1260 using the voltage monitor output of the high-voltage amplifier. The current is recorded via the input V2 as the voltage drop across an *RC* network shunt, the impedance of which increases from 50 Ω at $10^4$ Hz to 180 kΩ at 1 Hz with a limiting slope of 6dB/octave, and its dc impedance reaches 340 kΩ. This voltage is ac coupled to a home-built linear buffer amplifier ($f_T$ = 800 kHz) which protects the V2 input against high voltages in case of sample failures. For each frequency, the system is programmed to perform 3 measurements with the bias field $E_B$ on, followed by 3 measurements with zero bias. The rms amplitude of the harmonic field is set to 20% of $E_B$. Due to the lack of time resolution in this mode, the results may not reflect true steady state levels.

### 3.3 Model Considerations

In this section we develop the relations necessary to rationalize the time dependence of the NDE's observed in this work. We consider a dielectric between planar electrodes with surface area *A* and uniform separation *d*, leading to a sample volume $\upsilon = Ad$. The initial condition is characterized by zero voltage across the capacitor, $V(t < 0) = 0$, resulting in the depolarized state of the dielectric, with polarization $P(t < 0) = 0$ and thus displacement $D(t < 0) = 0$. The dielectric has a frequency dependent permittivity,

expressed here as superposition of Debye type contributions following the probability density $g(\tau_D)$ regarding its dielectric time constant,

$$\hat{\varepsilon}(\omega) = \varepsilon'(\omega) - i\varepsilon''(\omega) = \varepsilon_\infty + \Delta\varepsilon \int_0^\infty \frac{1}{1 + i\omega\tau_D} g(\tau_D) d\tau_D \ . \tag{3.3}$$

The relaxation amplitude is defined as $\Delta\varepsilon = \varepsilon_s - \varepsilon_\infty$, with $\varepsilon_s$ and $\varepsilon_\infty$ being the low and high frequency limits of the permittivity, respectively. The function $g(\tau)$ can be determined from a Havriliak-Negami (HN) fit to permittivity.[25] For times $0 \le t \le t_{off}$, the voltage is set to a value of $V_B$, leading to a field of magnitude $E_B = V_B/d$, whereas $E_B = 0$ at all other times. The time $t_{off}$ is sufficiently long so that steady state is reached prior to the end of the high field time segment. The field transitions are considered to be fast compared with all retardation times of the dielectric, but slow enough to ensure reversibility of the processes involved. The temperature of the dielectric is uniform and held constant at $T_0$ by thermal contact to a large heat bath.

### 3.3.1 Effects of Field Switching

Due to the inevitable presence of dc-conductivity in polar liquids, experiments involving bias fields require that the time duration of the field application be limited, so that switching on/off effects have to be considered. The work involved in generating steady state polarization following $t = 0$ is the sum of $U_\infty$ and $\Delta U(t)$, respectively associated with the instantaneous ($\varepsilon_\infty$) and slow ($\Delta\varepsilon$) contributions to permittivity. For the former contribution, displacement follows the field without lag, $D_\infty = \varepsilon_0\varepsilon_\infty E_B$, and

$$U_\infty = \upsilon \int_0^{D_\infty} E' dD' = \varepsilon_0\varepsilon_\infty \upsilon \int_0^{E_B} E' dE' = \tfrac{1}{2}\varepsilon_0\varepsilon_\infty \upsilon E_B^2 \ . \tag{3.4}$$

For the latter contribution that involves slower degrees of freedom, the displacement follows the field in a retarded fashion, $D(t) - D_\infty = \varepsilon_0[\varepsilon(t) - \varepsilon_\infty]E_B$, where $\varepsilon(t)$ is given by

$$\varepsilon(t) = \varepsilon_\infty + \Delta\varepsilon\int_0^\infty \left(1 - e^{-t/\tau_D}\right) g(\tau_D) d\tau_D \ , \qquad (3.5)$$

i.e., $-d\left(\varepsilon(t) - \varepsilon_\infty\right)/dt$ and $\hat{\varepsilon}(\omega) - \varepsilon_\infty$ are related by the Fourier-Laplace transform. The result for $\Delta U(t)$ is given by[26]

$$\Delta U(t) = \upsilon \int_{D_\infty}^{D(t)} E' dD'(t) = \varepsilon_0 E_B^2 \upsilon \int_{0^+}^{t} \frac{d\varepsilon(t')}{dt'} dt' = \upsilon E_B \int_{0^+}^{t} j(t') dt' \ . \qquad (3.6)$$

In the steady state limit, we obtain $\Delta U(t \to \infty) = \Delta U_s = V_B \Delta Q = \Delta C V_B^2$, where $\Delta Q$ is the total charge transferred to the capacitance $\Delta C = \varepsilon_0 \Delta\varepsilon A/d$. Since no work in excess of $U_\infty$ is regained when the field is removed, the entire amount of $\Delta U_s$ is transferred irreversibly from the field to the sample. Following the previous success of applying these ideas to the effects of high ac fields,[16, 27] we assume heterogeneous dynamics in the sense that the overall dispersive polarization response is the superposition of independent domains or modes.[28,29] Each mode has its individual retardation time constant $\tau_D$, and the volume fraction of modes with time constants in the range between $\tau_D$ and $\tau_D + d\tau_D$ is $g(\tau_D)d\tau_D$, see eq. (3.3) and eq. (3.5). As a result of domain specific $\tau_D$ values, different modes absorb different amounts of energy from the field. For modes with $\tau_D \pm d\tau_D/2$, the rate of energy increase following each field step (i.e., at $t = 0$ and $t = t_{off}$) is given by the 'power' term $p(t)$, determined analogous to a previous approach,[30]

$$p(t) = \varepsilon_0 \upsilon E_B^2 \Delta\varepsilon \frac{1}{\tau_D} \exp\left(-\frac{2t}{\tau_D}\right) g(\tau_D) d\tau_D \ . \qquad (3.7)$$

The total energy absorbed is obtained by integration over all $\tau_D$ and over time, which amounts to $\varepsilon_0 \upsilon E_B^2 \Delta\varepsilon$, half of which is transferred at each of the two field transitions (at $t$ = 0 and $t = t_{off}$). Domains are also considered independent regarding their effective temperature, $T_{eff}$, that is determined on the basis of the energy absorbed by that mode, $p(t)dt$, and its heat capacity, $\Delta C_{cfg} g(\tau_D)\, d\tau$, where $\Delta C_{cfg}$ is the configurational contribution to the glass-to-liquid heat capacity step of the sample at constant pressure. Since calorimetry will yield excess heat capacities, a correction according to $\Delta C_{cfg} = f_C \Delta C_{exc}$ is applied,[31] provided that $f_C$ is known and temperature invariant. For each domain, the equation governing the balance of effective temperature has a gain term involving $p(t)$, and a loss term originating from the relaxation of the excess effective temperature to the real temperature at a rate given by the inverse enthalpy relaxation time ($\tau_T$) of that domain,

$$\frac{dT_{eff}(t)}{dt} = \frac{p(t)}{\Delta C_{cfg} g(\tau_D) d\tau_D} - \frac{T_{eff}(t) - T_0}{\tau_T} \ . \qquad (3.8)$$

For isothermal conditions (constant $T_0$), the solution to eq. (3.8) with $p(t)$ from eq. (3.7) is

$$\Delta_E T_{eff}(t) = T_{eff}(t) - T_0 = \frac{E_B^2 \varepsilon_0 \upsilon \Delta\varepsilon}{\Delta C_{cfg}} \times \frac{\tau_T}{\tau_D - 2\tau_T} \times \left[e^{-2t/\tau_D} - e^{-t/\tau_T}\right] . \qquad (3.9)$$

The time constants associated with dielectric and enthalpy dynamics would be considered identical for many simple molecular liquids, i.e., $\tau_T = \tau_D$, but not in the case of

monohydroxy alcohols.[32] The impact of this field induced change in effective temperature, $\Delta_E T_{eff}$, is mainly that of altering the relaxation time constant, $\tau_D$, while the effect on the relaxation amplitude is relatively small. Therefore, small changes of $T_{eff}$ modify the permittivity via

$$\Delta_E \ln \tau_D = \frac{d \ln \tau}{dT} \Delta_E T_{eff}(t) \,, \tag{3.10}$$

where the slope, $d\ln\tau/dT$, is taken from the overall activation behavior of the dielectric retardation times. The assumption that the energy absorbed by a mode has the same effect as an equivalent temperature increase but remains localized in that domain for the time $\tau_T$ is clearly non-trivial. However, this phenomenological model (a 'box' model analogue for field steps) has been demonstrated to yield quantitative agreement with the effect of energy absorbed from time-dependent fields of high amplitudes.[16,20,26,32,33,34] For the case of dispersive (non-Debye) dynamics, a final integration over all $\tau_D$ according to eq. (3.3) is required.

### 3.3.2 Effects of Bias Field

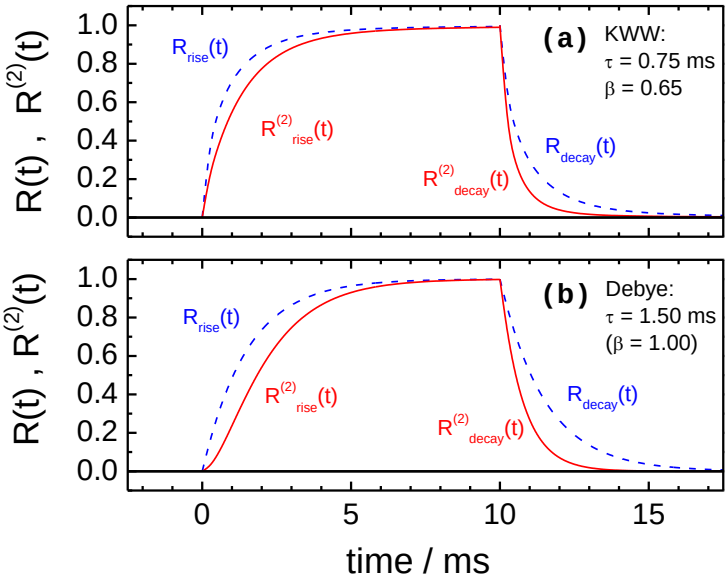


FIG. 3.2.: Comparison of symmetric rise and decay behavior, $R_{\text{rise}}(t) = 1 - \phi(t)$ and $R_{\text{decay}}(t) = \phi(t - t_{\text{off}})$ with $\phi(t) = \exp[-(t/\tau_D)^{\beta}]$, and their squared counterparts, $R^{(2)}(t)$, obtained by applying the power of two separately to each Debye contribution: **(a)** for the stretched exponential (KWW) case with $\tau = 0.75$ ms and $\beta = 0.65$, and **(b)** for the single exponential (Debye) case, , with $\tau = 1.50$ ms and $\beta = 1.00$. In both cases, the rise behavior of $R^{(2)}(t)$ is slower than the corresponding decay.

The consequences of a steady state polarization on the dynamics are determined following the idea of Johari,[11] proposing that slower dynamics result from the field induced reduction in entropy[25] if the Adam-Gibbs[36] relation is employed for connecting configurational entropy with relaxation time or viscosity. The steady state change in configurational entropy due to isothermal polarization induced by the dc-field can be obtained from the Maxwell relation,[15]

$$\left(\frac{\partial S}{\partial E}\right)_T = \left(\frac{\partial P}{\partial T}\right)_E = \varepsilon_0 \left(\frac{\partial \varepsilon_s}{\partial T} E\right)_E . \qquad (3.11)$$

Integration with respect to field yields the steady state change in configurational entropy, $\Delta_E S$, as a result of applying a field of magnitude $E$. The sign of $\Delta_E S$ is governed by the slope $\partial\varepsilon_s/\partial T$, which is negative and approximated by $-\Delta\varepsilon/T$ for the case of simple liquids (see Appendix A). For including a time dependence, it has to be realized that $\Delta_E S$ depends quadratically on field, while polarization $P$ is approximately linear in the field, even at relatively high electric fields. A consequence of $\Delta_E S \propto P^2$ is that the time dependence of $\Delta_E S$ should reflect that of the dielectric retardation squared. This yields for each domain

$$\Delta_E S(t) = \frac{E_B^2 \varepsilon_0 M}{2\rho} \frac{\partial \varepsilon_s}{\partial T} \times R^2(t) \ , \tag{3.12a}$$

$$R^2(t) = \begin{cases} \left(1 - e^{-t/\tau_D}\right)^2 & , \quad 0 \le t \le t_{off} \\ \left(e^{-(t-t_{off})/\tau_D}\right)^2 & , \quad t \ge t_{off} \end{cases} \ , \tag{3.12b}$$

where $M$ is the molar mass and $\rho$ the density. The top and bottom exponential terms in eq. (3.12b) are associated with applying ($t$ = 0) and removing ($t$ = $t_{off}$) the field, $E_B$, respectively. Fig. 3.2 demonstrates an important feature of the quadratic dependence on polarization: If $R(t)$ as defined in eq. (3.12b) represents the normalized time dependent contribution to polarization, then $R_{rise}(t) = 1 - \exp(-t/\tau_D)$ and $R_{decay}(t) = \exp(-(t-t_{off})/\tau_D)$ display symmetric rise and decay behavior, as shown as dashed lines in Fig. 3.2. By contrast, the rise of $R^{(2)}(t)$ is always slower that its decay counterpart, see solid lines in Fig. 3.2.

To capture the effect of the change in entropy on the dielectric properties, the dynamics of each domain are considered to be altered via the Adam-Gibbs approach[34]

$$\log(\tau/s) = A_{AG} + \frac{C_{AG}}{TS_{exc}(T)} \ , \tag{3.13}$$

while the dependence of the relaxation amplitude ($\Delta\varepsilon$) on the configurational entropies is presently disregarded. Although the Adam-Gibbs relation is meant to relate $\tau$ or $\eta$ to configurational entropy, the parameter $C_{AG}$ is usually determined on the basis of experimentally accessible excess entropy values ($S_{exc}$) obtained from calorimetry.[37] Therefore, we use $d\log\tau/dS_{exc} = -C_{AG}/(TS_{exc}^2)$, and then transition to configurational values by the term $f_S = S_{cfg}/S_{exc}$, which should be equal to $f_C = C_{p,cfg}/C_{p,exc}$,[31] and both $f_S$ and $f_C$ are assumed to be temperature invariant. The overall change in time constant, $\tau_D$, with field induced (configurational) entropy, $\Delta_E S$, then reads,

$$\Delta_E \ln\tau_D = -\frac{\ln(10)C_{AG}}{T\times S_{exc}^2(T)}\frac{1}{f_S}\Delta_E S(t) \ . \tag{3.14}$$

For the case of dispersive (non-Debye) dynamics, the resulting changes of $\tau_D$ with time can be entered into eq. (3.3) to assess the effect of the time dependent field on the overall $\varepsilon'(\omega)$ and $\varepsilon''(\omega)$. Note that both field induced time constant modifications, $\Delta_E\ln\tau_D$ from eq. (3.10) and from eq. (3.14), will impact permittivity and that they generally have opposite signs.

saturation and to susceptibilities of even order, e.g., $\chi^{(2)}$.[12] All these consequences of significant polarization anisotropy are expected to follow the same time dependence observed for the present NDE.

### 3.4. Results and Discussion

Glycerol and monohydroxy alcohols differ qualitatively regarding their dielectric dynamics. While glycerol is subject to hydrogen bonding, the dynamics of this glass-former are very much like those of simple molecular liquids without hydrogen bonding capability. By contrast, the prominent dielectric loss peak of the alcohols studied here is a Debye type process that occurs on a time scale that is slow relative to shear mechanical and enthalpy relaxation times.[38] As a result, the field effects on these different liquid classes are discussed separately.

#### 3.4.1 Glycerol

Several predictions of electric field dependent dynamics in polar liquids have been advanced, either in terms of a field dependent elevation of the glass transition temperature $T_g$,[39] or, similarly, as a field induced increase of relaxation times or viscosities.[11] More recently, such field effects have been verified experimentally for the case of glycerol[12, 40] In the preceding paper of the present series,[12] a quantitative test of the steady state case of configurational entropy effects via the Adam-Gibbs relation, eq. (3.13), has been performed, motivated by the prediction put forward by Johari[11] Using eq. (3.12) and eq. (3.14) in the $t \to \infty$ limit, the predicted field effect amounted to $\Delta_E \ln \tau_\alpha$ = 3.0%, somewhat higher than the experimentally observed value of $\Delta_E \ln \tau_\alpha$ = 2.7%. The calculation leading to the 3.0% result was subject to two errors that nearly cancelled each

other: the actual field was $E_B$ = 174 kV/cm rather than 225 kV/cm, and the configurational fraction factor, $f_S = S_{cfg}/S_{exc}$, see eq. (3.14), was applied erroneously. The corrected prediction reads $\Delta_E \ln \tau_\alpha$ = 2.8%, and is thus within a few percent of the experimental value of 2.7%. The field correction also restores better agreement with the field induced $T_g$ shifts reported by L'Hôte *et al.*,[39] which extrapolates to $\Delta T_g$ = +114 mK at $E_B$ = 174 kV/cm, 35% higher than our value of $\Delta T_g$ = +84 mK at that field. The experimental data leading to the $\Delta_E \ln \tau_\alpha$ = 2.7% result are reproduced as circles (yellow) in Fig. 3.3, where the increase in the time constants leads to a reduction of $\varepsilon''$ by 1.38% at $T$ = 213 K and $\nu$ = 4 kHz. That this change of the dielectric loss is due to field dependent time constants rather than amplitudes has been verified recently[12]

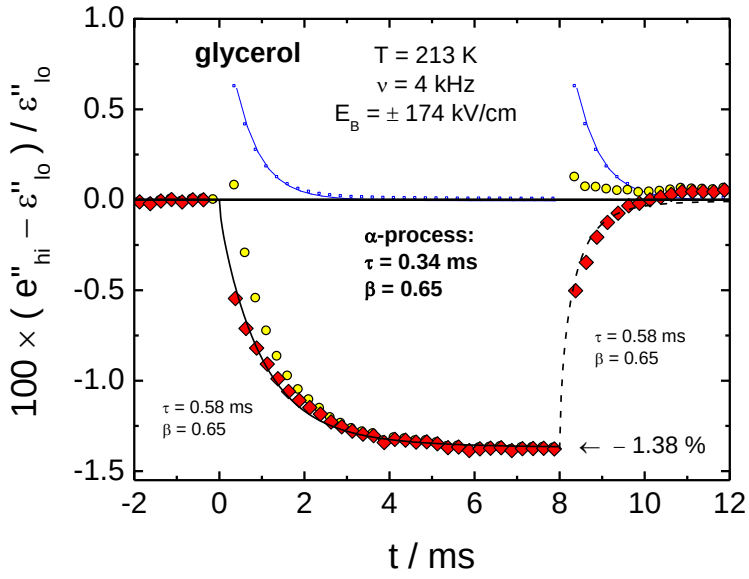


FIG. 3.3: Field induced relative change of the 'dielectric loss' component, $e''(t)$, probed at $\nu$ = 4 kHz for glycerol at a temperature of $T$ = 213 K. The bias field $E_B$ is applied in the time range $0 \le t \le 8$ ms. Circles (yellow) are from ref. 12 and represent the results from the average of the two signals with $E_B$ = +174 kV/cm and $E_B$ = –174 kV/cm, where the

direct response to the bias step is cancelled. The diamonds (red) represent the experimental data after subtracting the heating effect shown as squares (blue). The solid and dashed curves are respective fits to the rise and decay of the NDE with the common parameters indicated.

The above coincidence of experimental and calculated field effect on the relaxation time suggests that the effect of the field induced entropy change on dynamics is captured by the Adam-Gibbs relation, at least for glycerol. However, the original data (yellow dots) appear inconsistent with the expectation of a more symmetric and gradual time dependence of the field effect, since the observed NDE rises slowly and decays back almost instantaneously when the field is removed. The remedy to this situation is the recognition that switching the field on or off transfers energy from the field to the sample, as detailed in Section 3.3.1. Analogous to heating, this effect counteracts that of the entropy reduction by leading to temporarily smaller time constants, resulting in the positive transients in terms of $(e''_{hi} - \varepsilon''_{lo})/\varepsilon''_{lo}$ at a frequency $\nu > \nu_{max}$, which are determined using eq. (3.9) and shown in Fig.3.3 as open squares (blue). The parameters are: $\Delta\varepsilon = 66.4$, $\tau_{HN} = 0.61$ ms, $\alpha_{HN} = 0.96$, $\gamma_{HN} = 0.63$, $\tau_T = \tau_D$, $E_B = 174$ kV/cm, $\partial \ln \tau / \partial T = -0.345$ K$^{-1}$, $\Delta C_{exc} = 1.245$ J K$^{-1}$ cm$^{-3}$,[12] and using $f_C = 0.8$ which is consistent with results for glycerol based upon high ac fields.[41] Subtracting these from the observed values (circles) leads to the 'heating' corrected (red) diamonds in Fig. 3.3, which now represent the impact of the presence of a high bias field but without the transient effects of switching the bias on or off. The steady state amplitude of the remaining NDE is unchanged and amounts to –1.38% regarding $(e''_{hi} - \varepsilon''_{lo})/\varepsilon''_{lo}$ or +2.7% regarding $\Delta_E \ln \tau_\alpha$,

i.e., after subtracting the 'heating' effect still consistent with the +2.8% result from eq. (3.12) and eq. (3.14).

Supported by the analysis discussed above, the time-resolved NDE results obtained after correcting for the switching effects are now understood to reflect the consequences of the field induced entropy reduction, $\Delta_E S$. The diamonds in Fig. 3.3 reveal transitions between the zero field and high field levels that are now gradual in time, but not symmetric, i.e., the rise of the NDE following $t = 0$ is still slower that the decay initiated at $t = 8$ ms. This complex time dependence is well approximated by the quadratic exponentials in eq. (3.12) that originate from the quadratic dependence of the NDE on field and thus on polarization, see Section 3.3.2. Both rise and decay of the NDE are respectively approximated by the solid and dashed line, which are based on eq. (3.12) using the same $g(\tau_D)$ that represents the dielectric retardation in the linear response regime ($\beta_{KWW} = 0.65$ in terms of a stretched exponential[42,43] representation), but with time constants that are a factor of 1.7 larger ($\tau_{KWW} = 0.58$ ms) than the linear response value of $\tau_\alpha = 0.34$ ms.

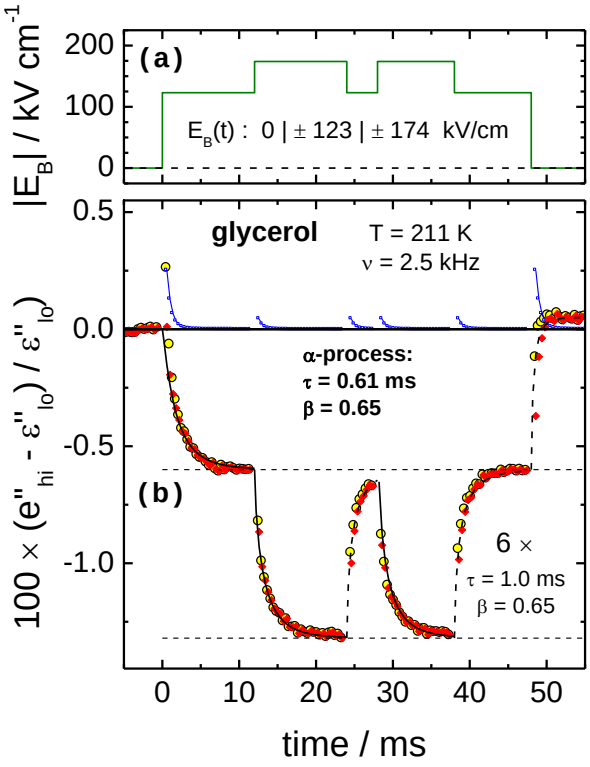


FIG. 3.4. **(a)** The bias field pattern, $E_B(t)$, used to measure the data in this plot. **(b)** Field induced relative change of the 'dielectric loss' component, $e''(t)$, probed at $\nu = 2.5$ kHz for glycerol at a temperature of $T = 211$ K. Circles (yellow) represent the results from the average of the two signals with positive and negative $E_B(t)$ pattern, where the direct response to the bias step is cancelled. The diamonds (red) represent the experimental data after subtracting the heating effect shown as squares (blue). The solid and dashed curves are respective fits to the rise and decay of the NDE with the common parameters indicated.

Additional justification of the above analysis of the time evolution of the NDE comes from an experiment similar to that leading to the data of Fig. 3.3, but with a more complex field pattern outlined in Fig. 3.4a. Here, the field transitions between three levels, zero, $E_B/\sqrt{2}$, and $E_B$, and the resulting levels of the NDE are –0.60% and about twice that value, –1.32%, as expected from the quadratic field dependence, see Fig. 3.4b.

As the transitions from –0.60% to –1.32% and back result from field changes of only 51 kV/cm (compared with 123 kV/cm when starting from zero), the heating effect associated with those transitions are only 17% of those involving the 0 to –0.60% levels (see blue squares), while leading to the same NDE magnitude. For these curve segments, 'heating' is practically negligible and the uncorrected data (diamonds) display transitions that are gradual in time. Also, the rise and decay curves associated with the –0.60% and –1.32% levels in Fig. 3.4b are more symmetric that those between the levels 0 and –0.60%. The solid and dashed lines in Fig. 3.4b demonstrate that all these features are captured by $\Delta_E S \propto P^2$ feature in eq. (3.12), again using the linear response $g(\tau_D)$ but with time constants that exceed the low field limit values by a factor of 1.7, identically for all six curves.

The original time-resolved entropy effect measurement (circles in Fig. 3.3[12] prior to accounting for the 'heating' effects) for glycerol suggested that the NDE disappears abruptly when the high dc bias field is removed. Such an abrupt return to the linear response behavior would be compatible with the scenario sketched in Fig. 3.1a, where the $P(E)$ curve near zero field never changes. By contrast, after unveiling the true gradual nature of the transition of the entropy effect with time (diamonds in Fig. 3.3 and Fig. 3.4, after accounting for the 'heating' effects) clearly invalidates Fig. 3.1a for the present NDE. Instead, it has to be assumed that the high field modifies the $P(E)$ curve also at $E \approx 0$, as implied in Fig. 3.1b. In other words, the main effect of the high dc field at the fundamental frequency of the small ac-field is to modify the (linear) susceptibility $\chi$ in eq. (3.1). Since $\chi$ is altered as a result of shifting time constants via configurational entropy, the time scale involved in this process is the equivalent of a structural recovery

time ($\tau_{rec}$).[44] It should be noted that the considerable polarization not only reduces entropy but in parallel will also lead to dielectric

### 3.4.2 Monohydroxy Alcohols

Glass-forming monohydroxy alcohols provide excellent testing grounds for linking the observed magnitudes and times scales of the NDE's to the anisotropy of polar order. Unlike more typical liquids such as glycerol, these alcohols display a considerable discrepancy between the time scales of the prominent (Debye type) dielectric retardation process and of mechanical and enthalpy relaxations.[30,37] The cases of 2E1H and 2E1B have particularly strong spectral separations of dielectric (D) and structural ($\alpha$) relaxation times, with $\tau_D/\tau_\alpha$ as high as 2000.[37,45] It should be noted that the alcohols used in this study and near their $T_g$ have high Kirkwood correlation factors, $g_K$, indicative of chain-like configurations dominating the hydrogen bonded structures.[46] Therefore, we do not expect a field induced ring-to-chain conversion and the concomitant increase in $\Delta\varepsilon$ for the present alcohols, a feature had been observed for 5-methyl-3-heptanol (5M3H).[6,47]

On the basis of the spectra of the relative change in dielectric loss in Fig. 3.5, we convince ourselves that the steady state NDE is mainly the result of modifying the time constant ($\tau_D$) associated with the Debye peak, consistent with the sigmoidal curves, $(\varepsilon''_{hi} - \varepsilon''_{lo})/\varepsilon''_{lo}$, with a magnitude that is approximately linear in $E_B^2$. The notion that only $\tau_D$ depends on field

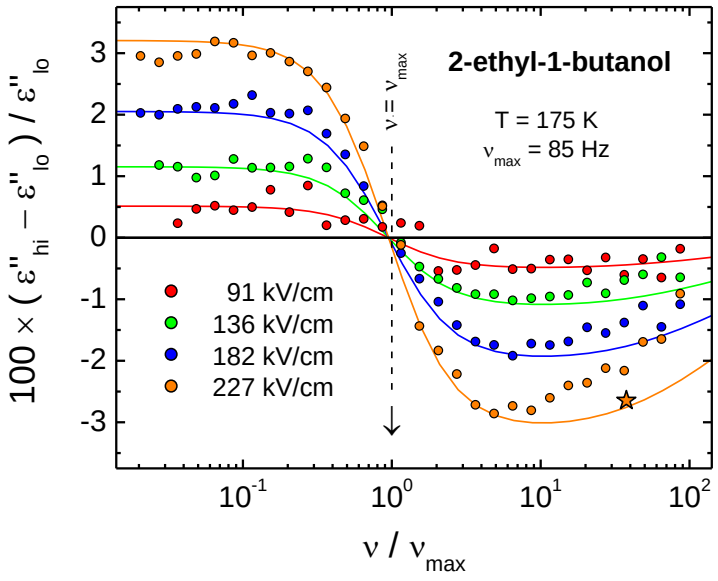


FIG. 3.5. Near steady state values of the field induced relative changes of the dielectric loss component, $(\varepsilon''_{hi} - \varepsilon''_{lo})/\varepsilon''_{lo}$, for 2-ethyl-1-butanol versus reduced frequency, $\nu/\nu_{max}$. The subscripts 'hi' and 'lo' refer to the high bias electric fields of $E_B$ as listed in the legend and $E_B = 0$, respectively. Experimental results (symbols) are for different fields, but for a common temperature $T = 175$ K. The lines are based on an HN fit to the low field data for $\varepsilon''_{lo}$, and the same HN curve but with $\tau_{HN}$ increased for the $\varepsilon''_{hi}$ case, e.g., by 3.2% at $E_B$ = 227 kV/cm. The star represents the steady state plateau of the time resolved result of Fig. 7, scaled by the field squared to $E_B = 227$ kV/cm.

in a quadratic manner is tested quantitatively by fitting the low field loss profile, $\varepsilon''_{lo}$, by the sum of a Debye and a HN type peak, using the imaginary component of

$$\varepsilon^*(\omega) = \varepsilon_\infty + \frac{\Delta\varepsilon_D}{1 + i\omega\tau_D} + \frac{\Delta\varepsilon_\alpha}{\left[1 + (i\omega\tau_\alpha)^\alpha\right]^\gamma} \quad . \tag{3.15}$$

Then, $(\varepsilon''_{hi} - \varepsilon''_{lo})/\varepsilon''_{lo}$ is determined with $\varepsilon''_{hi}$ calculated via eq. (3.15) with $\ln\tau_D$ increased with $E_B^2$, while all other parameters remain field invariant. The lines in Fig. 3.5 are obtained in this manner and demonstrate that the effect of field on permittivity is captured entirely by its impact on $\tau_D$, and that the modifications scale with $E_B^2$. The predicted

reduction of the effect towards high frequencies is due to the presence of the small α-peak with $\tau_\alpha << \tau_D$. For frequencies exceeding $10\,\nu_{max}$, the data show less NDE than predicted by the lines, most likely because steady state conditions have not been reached within the present experimental time window at the higher frequencies. This notion is supported by the star (at $\nu \approx 40\,\nu_{max}$) which represents the true steady state level for $E_B$ = 227 kV/cm derived from a time resolved measurement (see below).

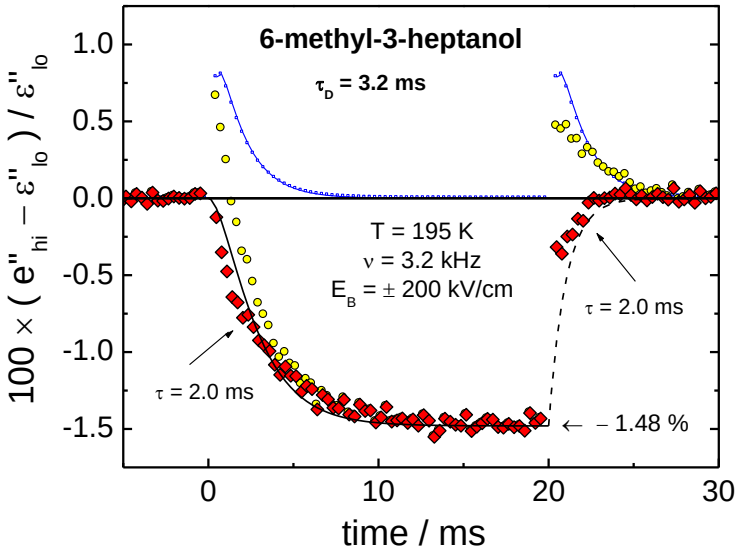


FIG. 3.6. Field induced relative change of the 'dielectric loss' component, $e''(t)$, probed at $\nu$ = 3.2 kHz for 6-methyl-3-heptanol at a temperature of $T$ = 195 K. The bias field $E_B$ is applied in the time range $0 \le t \le 20$ ms. Circles (yellow) represent the results from the average of the two signals with $E_B$ = +200 kV/cm and $E_B$ = –200 kV/cm, where the direct response to the bias step is cancelled. The diamonds (red) represent the experimental data after subtracting the heating effect shown as squares (blue). The solid and dashed curves are respective fits to the rise and decay of the NDE with the common parameters indicated.

An example of a time-resolved measurement is provided for 6M3H in Fig. 3.6, where the 'as observed' data for the relative change of the $e''$ (circles) display much more

pronounced 'heating' spikes towards positive values than in the case of glycerol in Fig. 3.3. Determining the 'heating' effect correction for monohydroxy alcohols is complicated by the problem that the heat capacity step, $\Delta C_{cfg}$, observed by calorimetric techniques is associated with the structural ($\alpha$) relaxation, not with the Debye process that occurs on a very different time scale.[32,38] Consequently, the value of $\Delta C_{cfg}$ in eq.(3.9) is treated as adjustable parameter. By requiring that the corrected curves (diamonds) extrapolate reasonably well to the level prior to changing the bias, the fit values of $\Delta C_{cfg}$ are determined within margins of around ± 20%. In agreement with previous high ac field measurements on monohydroxy alcohols[33] we find that using $\tau_T = \tau_D$ fails to generate smooth time dependences for the corrected curves (diamonds), while $\tau_T = \tau_\alpha$ yields the results shown in Fig. 3.6 and Fig. 3.7. This assumption that enthalpy relaxation times ($\tau_T$) match those of the structural relaxation process ($\tau_\alpha$) instead of the prominent dielectric peak ($\tau_D$) has been verified experimentally for 2E1H.[48]

The data treatment outlined above for 6M3H has been repeated for the other alcohols, 2E1B and 2E1H, and the results are compiled in Fig. 3.7. The adjusted $\Delta C_{cfg}$ values that yield the curves in Fig. 3.7 are significantly below the true calorimetric heat capacity steps, a consequence of the large $\tau_D/\tau_T$ ratios which imply that energy is absorbed from the field at a low rate ($1/\tau_D$) compared with that ($1/\tau_T$) at which heat is surrendered to the phonon bath. The values for $\Delta C_{cfg}$ in eq. (3.9) are smaller than the actual heat capacity step by factors of 19 for 6M3H, 830 for 2E1H, and 1300 for 2E1B. These values appear to correlate with the corresponding $\tau_D/\tau_\alpha$ ratios: 38 for 6M3H, 790 for 2E1H, and 2000

for 2E1B, suggesting that the spectral separation is a significant factor in determining the effective values for $\Delta C_{cfg}$ in eq. (9) for monohydroxy alcohols.

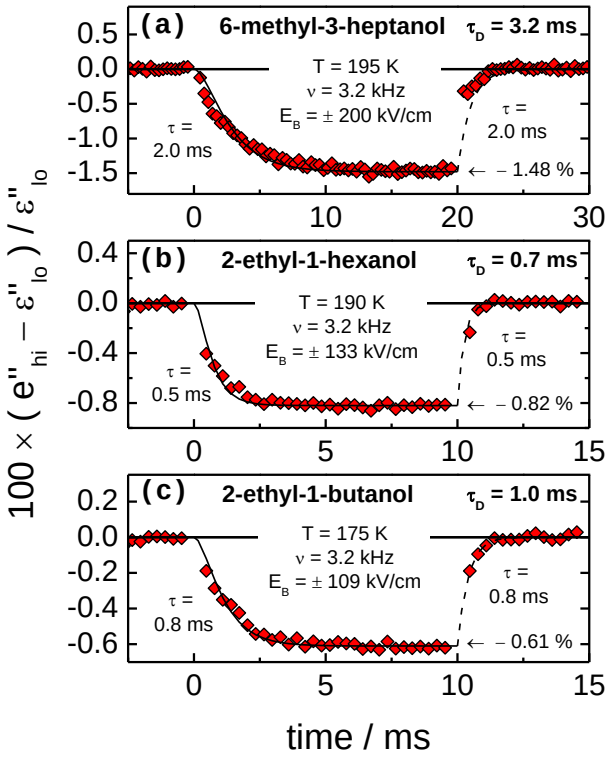


FIG. 3.7. Field induced relative change of the 'dielectric loss' component, $e''(t)$, for three different monohydroxy alcohols at the respective temperatures indicated. The bias field $E_B$ is applied in the time range $0 \le t \le 20$ ms (a) or $0 \le t \le 10$ ms (b,c). In each case, the $e''(t)$ data are probed at $\nu = 3.2$ kHz. The diamonds (red) represent the experimental data using the fields $\pm E_B$ as listed, after subtracting the heating effect. The solid and dashed curves are respective fits to the rise and decay of the NDE with the common parameters indicated.

The time evolutions of the NDE's obtained after 'heating' correction for the three alcohols display rise/decay asymmetries similar to the case of glycerol. For all cases shown in Fig. 3.7, the rise of the NDE is systematically slower than the subsequent decay of the effect. Still, both time dependences are again captured by the squared polarization

curves, eq. (3.12b), with identical parameters for the rise and decay curve for each compound. However, the time constants used in eq. (3.12b) are on average 70% of $\tau_D$, i.e., somewhat faster than the dielectric Debye time constant, see Fig. 3.7. Observing that the time scales associated with the rise and decay of this NDE are linked to those of the dielectric Debye process supports the connection to polar order, because processes governed by mechanical of enthalpy relaxation would be up to three decades faster.

The three measurements of Fig. 3.7 display high field steady state plateaus indicating field induced increases of the Debye times quantified by $\Delta_E \ln \tau_D$ = +1.48% for 6M3H, +0.82% for 2E1H, and +0.61% for 2E1B (since $d\ln\varepsilon''/d\ln\nu = -1$ at these frequencies). Based on the slopes $\partial\varepsilon_s/\partial T$ (–0.32 for 6M3H, –0.21 for 2E1H, and –0.27 for 2E1B) and the fields used, eq. (3.12b) leads to the following reductions of configurational entropies, $\Delta_E S_{cfg}$ in units of mJ $K^{-1}$ $mol^{-1}$: –90 for 6M3H, –26 for 2E1H, and –18 for 2E1B. Due to the lack of available parameters, an Adam-Gibbs type analysis analogous to that performed for glycerol is not possible. However, the activation parameters are similar for all three alcohols ($\partial \ln \tau/\partial T$ = –0.22 $K^{-1}$ for 6M3H, –0.26 $K^{-1}$ for 2E1H, and –0.24 $K^{-1}$ for 2E1B), and it may be expected that the magnitudes of the NDE in terms of $\Delta_E \ln \tau_D$ follow the order of the $\Delta_E S_{cfg}$. A scrutiny of the values listed above reveal that this expectation is justified.

### 3.4.3 Relation to the Electro Optical Kerr Effect

The electro-optical Kerr effect (EKE) describes the birefringence, $\Delta n$, induced by a static electric field by virtue of the anisotropy created in the case of dipolar liquids. The

effect is quadratic in the electric field, $\Delta n = B\lambda E^2$, where $B$ is the Kerr constant, $\lambda$ the optical wavelength, and $E$ the electric field.[49] Numerous time-resolved experiments have characterized the rise and decay behavior of the birefringence for viscous liquids, including glycerol,[48] 2-ethyl-1-hexanol (2E1H),[50] and 6-methyl-3-heptanol (6M3H).[5] Due to the fact that birefringence and the present NDE are both signatures of field induced anisotropy, the two experiments are very similar, but with the EKE typically measured at much smaller fields compared with the NDE of this work.

A survey of studies that compare dielectric retardation ($\tau_D$) with EKE rise ($\tau_{rise}$) and decay ($\tau_{decay}$) times reveals that $\tau_{rise}$ is usually larger than $\tau_{decay}$, and that the EKE time constants are near the dielectric times $\tau_D$, with a matching temperature dependence.[48,49,50,52,53] For the case of glycerol, linear fits to $\Delta n(t)$ resulted in $\tau_{rise} \approx 1.5\,\tau_{decay}$ and $\tau_D \approx 0.5\,\tau_{decay}$,[48] while the same analysis applied to the data (diamonds) in Fig. 3.3 would give $\tau_{rise} \approx 2\ \tau_{decay}$ and $\tau_D \approx 0.7\,\tau_{decay}$.

A complication in the Kerr effect analysis is that both first ($P_1 \propto \cos\theta$) and second ($P_2 \propto \cos^2\theta - 1/3$) order Legendre polynomials of the reorientational degrees of freedom are relevant.[54] Also, permanent and induced dipole moments will contribute differently to $\Delta n(t)$. To our knowledge, no attempt has been made to explain the asymmetry of experimental EKE rise and decay transients in terms of the quadratic field dependence as implied in eq.(3.12b). It would be interesting to explore to what extent the quadratic field dependence is capable of rationalizing this difference in rise and decay time constants observed in EKE measurements. Another consequence of $\Delta n \propto E^2$ and thus $\Delta n \propto P^2$ is

that EKE rise and decay time constants should not be expected to match linear response dielectric retardation times, contrary to previous assumptions.[49]

### 3.5 Summary and Conclusions

Time-resolved non-linear dielectric effects (NDE's) have been measured for various glass-forming polar liquids near their glass transition temperatures: glycerol and three monohydroxy alcohols. The dominant effects originating from dc bias electric fields in the 90 to 230 kV/cm range are due to changes of the dielectric retardation time constants rather than amplitudes. These field induced changes are monitored by evaluating the dielectric 'loss' versus time, $e''(t)$, with a resolution of one period of the small signal test frequency. The impact of the polarization responses to the large field steps that occurs when switching the bias field on and off is eliminated by averaging over two measurement, one with positive and one with negative bias of identical amplitudes. Transient effects analogous to local heating are observed subsequent to applying and removing the dc field. The resulting temporary reductions of time constants are corrected for, unveiling the time dependent effect of polarization anisotropy in the non-linear regime, observed as increases in the retardation time constants.

Apart from the 'heating' transients, the application of the bias field leads to a gradual increase of the dielectric time constants (slower dynamics, higher $T_g$). This rise of the NDE with time is seen to be slower than the subsequent decay that occurs when the field is removed again, analogous to what had been observed repeatedly for the rise/decay behavior of the electro-optical Kerr effect in similar systems. Since the magnitude of this NDE is quadratic in field, its time dependence should follow that of the polarization

squared, i.e., $(1 - e^{-t/\tau})^2$ and $(e^{-t/\tau})^2$ for the rise and decay of a Debye mode, respectively. It is demonstrated that this quadratic field dependence explains these asymmetric rise/decay patterns. For glycerol, the observed steady state change of the structural relaxation time ($\Delta_E \ln \tau_\alpha$ = 2.7%) agrees well with the field induced reduction of configurational entropy and its impact on the dynamics via the Adam-Gibbs relation, which predicts $\Delta_E \ln \tau_\alpha$ = 2.8%. Similar effects are observed for the three monohydroxy alcohols, where the rise and decay of the NDE is linked to the time scale of the prominent Debye type dielectric process. This lends strong support to the notion that the NDE is associated with the rise and decay of polarization anisotropy, as shear mechanical and enthalpy relaxations in these alcohols occur on very different time scales.

Based on the evidence compiled in this work, we conclude that the reduction in configurational entropy is a dominant factor in the non-linear dielectric behavior of polar liquids subject to high dc fields. Both the time dependence and the steady state level of the NDE can be rationalized on the basis of the change in entropy. The gradual decay of the NDE after removing the bias field is observed via a low field sinusoidal excitation, which implies that the modifications are described by a field and time dependence of the (linear) 'susceptibility', $\chi(E,t)$, rather than requiring higher order terms such as $\chi^{(3)}$, see Fig. 13..

We note that this entropy effect is likely at the origin of low frequency features that have been detected in non-linear dielectric measurements using high amplitude ac fields (without bias). The effect shows as an increase of the loss at frequencies below that of the dielectric loss peak and is bound to disappear near and above the loss peak frequency.

Indication of such features can be found for 2E1B,[33] for 5M3H,[6] and more clearly for plastic crystals.[55,56] Finally, it may be important to realize that an electric field may change entropy and thus relaxation time scales in much the same way as possible by small changes in temperature or pressure. However, a structural difference remains: in the presence of an electric field, a dipolar liquid becomes anisotropic, while changing entropy by temperature or hydrostatic pressure alone preserves the isotropic nature of the liquid.

### 3.6 References


1 R. Richert, Adv. Chem. Phys. **156**, 101 (2014).

2 J. Herweg, Z. Physik **3**, 36 (1920).

3 K. De Smet, L. Hellemans, J. F. Rouleau, R. Corteau, and T. K. Bose, Phys. Rev. E **57**, 1384 (1998).

4 D. V. Matyushov, J. Chem. Phys. **142**, 244502 (2015).

5 J. Małecki, J. Chem. Phys. **36**, 2144 (1962).

6 L. P. Singh and R. Richert, Phys. Rev. Lett. **109**, 167802 (2012).

7 B. Roling, J. Chem. Phys. **117**, 1320 (2002).

8 B. Roling, S. Murugavel, A. Heuer, L. Lühning, R. Friedrich, and S. Röthel, Phys. Chem. Chem. Phys. **10**, 4211 (2008).

9 J. Zioło and S. J. Rzoska, Phys. Rev. E **60**, 4983 (1999).

10 A. Drozd-Rzoska, S. J. Rzoska, J. Zioło, Phys. Rev. E **77**, 041501 (2008).

11 G. P. Johari, J. Chem. Phys. **138**, 154503 (2013).

12 S. Samanta and R. Richert, J. Chem. Phys. **142**, 044504 (2015).

13 J. K. Park, J. C. Ryu, W. K. Kim, and K. H. Kang, J. Phys. Chem. B **113**, 12271 (2009).

[14] V. Kaiser, S. T. Bramwell, P. C. W. Holdsworth, and R. Moessner, Nature Materials **12**, 1033 (2013).

[15] J. F. Scott, Annu. Rev. Mater. Res. **41**, 229 (2011).

[16] B. Schiener, R. Böhmer, A. Loidl, and R. V. Chamberlin, Science **274**, 752 (1996).

[17] T. Matsuo, H. Suga, and S. Seki, Bull. Chem. Soc. Jpn. **39**, 1827 (1966).

[18] A. Khalife, U. Pathak, and R. Richert, Eur. Phys. J. B **83**, 429 (2011).

[19] T. Bauer, P. Lunkenheimer, S. Kastner, and A. Loidl, Phys. Rev. Lett. **110**, 107603 (2013).

[20] W. Huang and R. Richert, J. Phys. Chem. B **112**, 9909 (2008).

[21] J.-P. Bouchaud and G. Biroli, Phys. Rev. B **72**, 064204 (2005).

[22] C. Crauste-Thibierge, C. Brun, F. Ladieu, D. L'Hôte, G. Biroli, and J.-P. Bouchaud, Phys. Rev. Lett. **104**, 165703 (2010).

[23] C. Brun, F. Ladieu, D. L'Hôte, M. Tarzia, G. Biroli, and J.-P. Bouchaud, Phys. Rev. B **84**, 104204 (2011).

[24] J. L. Déjardin. Y. P. Kalmykov, and P. M. Déjardin, Adv. Chem. Phys. **117**, 275 (2001).

[25] S. Havriliak and S. Negami, Polymer **8**, 161 (1967).

[26] H. Fröhlich, *Theory of Dielectrics* (Clarendon, Oxford, 1958).

[27] R. Richert, Thermochim. Acta **522**, 28 (2011).

[28] M. D. Ediger, Ann. Rev. Phys. Chem. **51**, 99 (2000).

[29] R. Richert, J. Phys.: Condens. Matter **14**, R703 (2002).

[30] R. Richert, Physica A **322**, 143 (2003).

[31] M. Goldstein, J. Chem. Phys. **123**, 244511 (2005).

[32] C. Hansen, F. Stickel, T. Berger, R. Richert, and E. W. Fischer, J. Chem. Phys. **107**, 1086 (1997).

[33] T. Blochowicz and E. A. Rössler, J. Chem. Phys. **122**, 224511 (2005).

[34] S. Weinstein and R. Richert, Phys. Rev. B **75**, 064302 (2007).

[35] W. Huang and R. Richert, J. Chem. Phys. **130**, 194509 (2009).

[36] G. Adam and J. H. Gibbs, J. Chem. Phys. **43**, 139 (1965).

[37] R. Richert and C. A. Angell, J. Chem. Phys. **108**, 9016 (1998).

[38] R. Böhmer, C. Gainaru, and R. Richert, Physics Reports **545**, 125 (2014).

[39] C. T. Moynihan and A. V. Lesikar, Ann. New York Acad. Sci. **371**, 151 (1981).

[40] D. L'Hôte, R. Tourbot, F. Ladieu, and P. Gadige, Phys. Rev. B **90**, 104202 (2014).

[41] L.-M. Wang and R. Richert, Phys. Rev. Lett. **99**, 185701 (2007).

[42] R. Kohlrausch, Pogg. Ann. Phys. **91**, 179 (1854).

[43] G. Williams and D. C. Watts, Trans. Faraday Soc. **66**, 80 (1970).

[44] I. M. Hodge, J. Non-Cryst. Solids **169**, 211 (1994).

[45] L.-M. Wang and R. Richert, J. Chem. Phys. **121**, 11170 (2004).

[46] C. J. F. Böttcher, *Theory of Electric Polarization, Vol 1* (Elsevier, Amsterdam, 1973).

[47] L. P. Singh, C. Alba-Simionesco, and R. Richert, J. Chem. Phys. **139**, 144503 (2013).

[48] H. Huth, L.-M. Wang, C. Schick, and R. Richert, J. Chem. Phys. **126**, 104503 (2007).

[49] M. S. Beevers, D. A. Elliott, and G. Williams, J. Chem. Soc. Faraday Trans. 2 **76**, 112 (1980).

[50] R. Coelho and D. Khac Manh, C. R. Acad. Sc. Paris - Serie C **264**, 641 (1967).

[51] J. Crossley and G. Williams, J. Chem. Soc. Faraday Trans. 2 **73**, 1906 (1977).

[52] M. S. Beevers, J. Crossley, D. C. Garrington, and G. Williams, Faraday Symp. Chem. Soc. **11**, 38 (1977).

[53] J. Crossley and G. Williams, J. Chem. Soc. Faraday Trans. 2 **73**, 1651 (1977).

[54] V. Rosato and G. Williams, J. Chem. Soc. Faraday Trans. 2 **77**, 1767 (1981).

[55] M. Michl, Th. Bauer, P. Lunkenheimer, and A. Loidl, Phys. Rev. Lett. **114**, 067601 (2015).

[56] B. Riechers, K. Samwer, R. Richert, J. Chem. Phys. **142**, 154504 (2015).

# CHAPTER 4

# FIELD INDUCED CHANGES IN THE RING/CHAIN EQUILIBRIUM OF HYDROGEN BONDED STRUCTURES: 5-METHYL-3-HEPTANOL

In this chapter, we look deeper into what governs the nonlinear effects of monohydroxy alcohols, by looking at a material that has a supramolecular structure of near unity between rings and chains. In the previous section, the materials studied had high Kirkwood correlation factors (> 1).The high $g_k$ values indicate there would be no measurable chemical effect. In this chapter the material studied has a $g_k$ of approximately 1, which allows us to measure the ring to chain conversion timescale as well as see a chemical effect in the measurements.

## 4.1 Introduction

Hydrogen bonds play a significant role regarding the properties of liquids such as water, alcohols, and amides. The dielectric properties of these materials have been studied extensively with the goal of understanding the role of the hydrogen bonds regarding the structure and dynamics in these liquids.[1] Many monohydroxy alcohols,[2,3] various amides,[4,5,6] and possibly water,[7,8] belong to a class of liquids for which the prominent dielectric relaxation process does not reflect the typical signatures of structural relaxation, such as the heat capacity step,[9,10,11] shear mechanical relaxation,[12,13] or density-density correlation functions.[14] Another common feature of these liquids is the Debye type nature of its prominent dielectric loss peak, which is retained even at the glass-transition for those cases where crystallization can be avoided.[1] It is generally accepted that hydrogen bonding is at the origin of these particular properties of this class

of liquids. In many cases, e.g., 1-propanol, chain structures connected by hydrogen bonding develop, especially at lower temperatures.[15]

The preferred supramolecular structures that develop through hydrogen bonding will depend on the structure of the compound involved. Steric hindrance can lead to a higher population of ring-like structures or inhibit intermolecular hydrogen bonding altogether.[16,17] In this respect, a series of isomeric octyl alcohols has received considerable attention. A number of these isomers has been studied by Dannhauser,[18] revealing that the position of a methyl group can modify the Kirkwood-Fröhlich correlation factor $g_K$ to a large extent. This factor gauges the strength of the effective dipole moment relative to the molecular dipole,[19]

$$g_K = \frac{\mu_{eff}^2}{\mu^2} = 1 + z\langle \cos\theta \rangle \ , \qquad (4.1)$$

which results from orientational correlation of dipole moments. Here, $z$ is the average number of neighbors and $\langle \cos\theta \rangle$ is the averaged cosine of the angle between the dipoles. The more parallel dipole alignment of chain structures leads to an enhancement of $\mu_{eff}/\mu$ and $g_K$ with a concomitant increase of the dielectric constant, $\varepsilon_s$. By contrast, ring-like dipole structures involve anti-parallel alignment that leads to $g_K$ values below unity. The case of $g_K \approx 1$ could indicate either uncorrelated dipoles or the coexistence of chains ($g_K > 1$) and rings ($g_K < 1$).[15]

Among the isomeric octyl alcohol series, 5-methyl-3-heptanol (5M3H) is particularly interesting because its net $g_K$ value changes from above to below unity across a relatively small temperature window.[18] The dielectric loss spectra and the temperature

variation of $g_K$ in this range of interest are shown in Fig. 4.1. This behavior suggests that ring and chain like structures have similar free energies in 5M3H around $T$ = 200 K and that the equilibrium constant for the ring and chain population is not far from unity.[20] Because chain structures are much more dipolar than rings, it is expected that this equilibrium may be influenced by an external electric field, which was the basis for recent high ac field dielectric studies of 5M3H and related liquids.[20,21] The conclusion from those experiments was that the electric field does enhance the relaxation amplitudes via an increase of $g_K$, but the effect fades at higher frequencies because the ring/chain conversion requires a time scale that is near that of the Debye process. Accordingly, the relaxation amplitudes return to the low field values for frequencies above those of the Debye peak loss maximum.

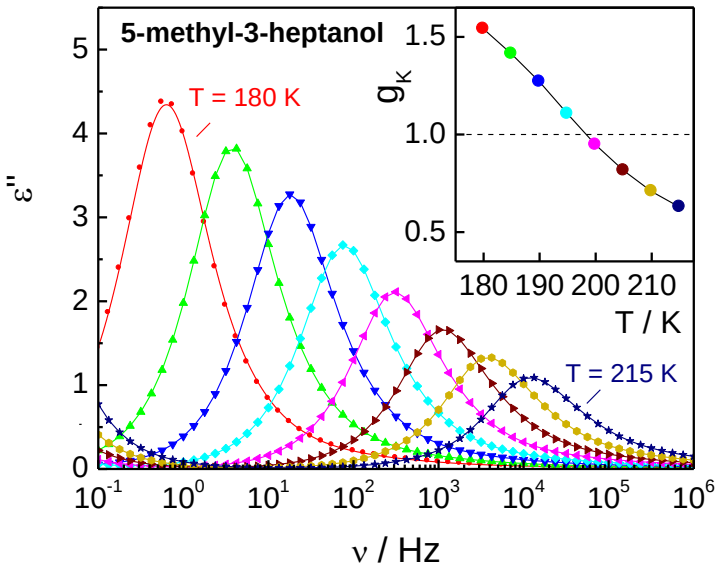


FIG. 4.1. Low field dielectric loss spectra of 5-methyl-3-heptanol for temperatures from 180 K to 210 K in steps of 5 K. The inset shows the Kirkwood correlation factor, $g_K$, of 5M3H for the same temperature range. Data taken from ref. 20 and 21.

The present study revisits 5M3H in terms of a time resolved dielectric study in which the ring/chain equilibrium is altered through high dc-bias (opposed to ac) electric fields. In the steady state case and for a field of $E_B$ = 171 kV cm$^{-1}$, we observe a relative change of the relaxation amplitude of $\Delta_E \ln \varepsilon_D$ = +11.0% and a relative change of the time constant of $\Delta_E \ln \tau_D$ = +12.6% concerning the Debye process. These two quantities are not only similar in their steady state magnitude, but also follow the same time dependence that closely matches the Debye time constant, $\tau_D$. The result is a cancellation effect that renders the high frequency permittivity practically field invariant. The observations suggest that a field induced ring-to-chain conversion not only increases the net Kirkwood correlation factor $g_K$ and thus $\Delta\varepsilon$, but also slows down the dynamics associated with the Debye process. This correlation explains a change in the spectral separation between Debye time and the primary structural relaxation whenever $g_K$ changes, i.e., usually as a function of temperature.

**4.2 Experiments**

The compound 5-methyl-3-heptanol (5M3H, purity unspecified) was purchased from Sigma-Aldrich and is used as received. Low field impedance measurements were obtained using a Solartron SI-1260 gain/phase analyzer with a Mestec DM-1360 transimpedance amplifier. Low field measurements are used to verify sample properties and to obtain an accurate electrode spacing through the comparison of the relaxation amplitude ($\Delta\varepsilon$) to reference data. This is necessary because at electrode spacer

thicknesses of around 10 μm, deviations between actual and nominal distance are common.

The high field cell capacitor consists of two spring loaded polished stainless steel electrodes (17 mm and 20 mm), separated by a 13 μm thick Kapton ring that leaves an inner area of 14 mm diameter for the sample. For all measurements, the cell is mounted onto the cold stage of a closed cycle He-refrigerator cryostat Leybold RDK 6-320 with Coolpak-6200 compressor. A Lakeshore Model 340 temperature controller stabilizes the temperature within several mK. High bias field experiments aimed at steady state results are performed using a Solartron 1260 gain/phase analyzer, with the voltage amplified by a Trek PZD-350 amplifier. The voltage at the sample is measured at the 'V1' input of the SI-1260 using the voltage monitor output of the Trek PZD-350 amplifier. The current is recorded as the voltage drop across an *RC* network shunt, the impedance of which is designed to increase from 250 Ω at $10^4$ Hz to 300 kΩ at 1 Hz in order to counteract the reduced current levels at low frequencies. The shunt output is ac-coupled ($RC$ = 0.12 s) to a buffer amplifier that protects the system from sample failure. The output of that buffer is analyzed via the 'V2' input of the SI-1260. For each frequency, the system is programmed to perform 15 measurements with the bias field $E_B$ on, followed by 15 measurements with no bias, where each measurement integrates the signal for the greater of 1 s or 18 periods. This protocol is meant to capture steady state impedance values at the high field, while avoiding excessive exposure to high fields and providing ample recovery time between high field measurements. Due to the lack of time resolution in this acquisition mode, the results could deviate from true steady state values.

Time resolved measurements are performed as described in detail earlier.[22] A Stanford Research Systems DS-345 programmable wave form generator supplies the voltage waveform, which is amplified by a factor of 100 using a Trek PZD-350 high voltage amplifier. The programmed sinusoidal waveforms, $V(t) = V_B + V_0\sin(\omega t)$, consist of an integer number of periods, where the bias voltage $V_B$ is applied only for some of the periods. In this case, $V_B/V_0$=4, so that the amplitude of the ac field component is practically in the regime of linear responses. The voltage and current ($R$ = 3 kΩ shunt) signals are recorded using a Nicolet Sigma 100 digitizing oscilloscope that averages over 5000 waveform repetitions. In order to eliminate the direct polarization response to applying or removing the bias field, all signal traces refer to an average of two measurements: one with positive bias voltage, and one with negative bias voltage of the same magnitude. These averaged voltage $V(t)$ and current $I(t)$ traces are subject to period-by-period Fourier analysis, yielding the amplitudes ($A$) and phases ($\varphi$) of the voltage ($A_V$, $\varphi_V$) and current ($A_I$, $\varphi_I$) for each period. The effect of the high bias field is quantified by the out-of-phase 'permittivity' evaluated for each measured period using

$$e'' = \left| \frac{A_I \cos(\varphi_I - \varphi_V)}{\omega A_V C_0} \right| , \qquad (4.2)$$

where $C_0$ is the geometric capacitance of the cell, nominally $C_0$ = 105 pF. The notation $e''$ is used instead of $\varepsilon''$ because this quantity changes with time in a non-equilibrium situation where permittivity $\varepsilon$ is not properly defined.

## 4.3 Results

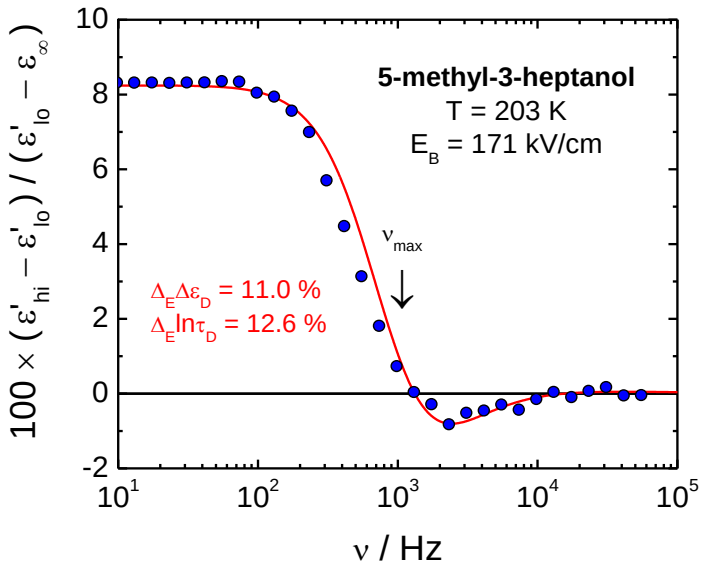


FIG. 4.2. Symbols represent the experimental field induced ($E_B$ = 171 kV cm$^{-1}$) steady state spectra of the relative change of the real part of permittivity, $(\varepsilon'_{hi} - \varepsilon'_{lo})/(\varepsilon'_{lo} - \varepsilon_\infty)$, for 5M3H at $T$ = 203 K. The value of $\varepsilon_\infty$ is subtracted from the $\varepsilon'$ data because it is considered field invariant. The line is calculated based on $\varepsilon'_{lo}$ determined from an HN fit to the low field data and with $\varepsilon'_{hi}$ given by the same fit but with the Debye amplitude and time constant modified according to $\Delta_E \ln \varepsilon_D$ = 11.0% and $\Delta_E \ln \tau_D$ = 12.6%, respectively. The arrow indicates the frequency position of the low field loss peak, $\nu_{max}$

The quasi steady state effects resulting from the high dc bias field of $E_B$ = 171 kV cm$^{-1}$ are presented graphically as the relative difference of the high and low field spectra of permittivity in Fig. 4.2 and Fig. 4.3. The storage component of the permittivity in Fig. 4.2 is represented as $(\varepsilon'_{hi} - \varepsilon'_{lo})/(\varepsilon'_{lo} - \varepsilon_\infty)$, where the infinite frequency dielectric constant, $\varepsilon_\infty$, is subtracted because electronic polarizability is considered field invariant. The main feature of Fig. 4.2 is the 8% increase of the quantity $(\varepsilon' - \varepsilon_\infty)$, which fades towards higher frequencies, similar to previous observations.[20,21] The dielectric loss counterpart is shown as $(\varepsilon''_{hi} - \varepsilon''_{lo})/\varepsilon''_{lo}$ in Fig. 4.3. These changes in $\varepsilon''$ are more

pronounced, but also approach practically zero for frequencies that exceed $10\times\nu_{max}$, where $\nu_{max}$ is the low field loss peak position (indicated by arrows in both figures).

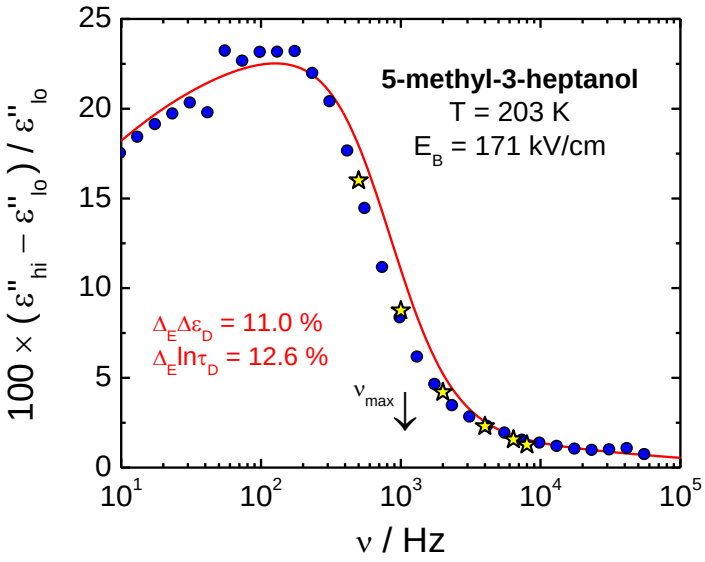


FIG. 4.3. Symbols represent the experimental field induced ($E_B$ = 171 kV cm$^{-1}$) steady state spectra of the relative change of the dielectric loss, $(\varepsilon''_{hi} - \varepsilon''_{lo})/\varepsilon''_{lo}$, for 5M3H at $T$ = 203 K. The line is calculated based on $\varepsilon''_{lo}$ determined from an HN fit to the low field data and with $\varepsilon''_{hi}$ given by the same fit but with the Debye amplitude and time constant modified according to $\Delta_E\ln\varepsilon_D$ = 11.0% and $\Delta_E\ln\tau_D$ = 12.6%, respectively. The arrow indicates the frequency position of the low field loss peak, $\nu_{max}$. Stars show the steady state plateau values from the time resolved experiments.

A time resolved measurement of $(\varepsilon''_{hi} - \varepsilon''_{lo})/\varepsilon''_{lo}$ at the frequency $\nu$ = 1.0 kHz is provided in Fig. 4.4. This measurement frequency is selected to closely match that of the loss peak, i.e., $\nu_{max}$ = 1075 Hz at this temperature of $T$ = 203 K. In this case, a steady state plateau value of 8.75% is reached after few ms. In this time resolved technique the temporal resolution is limited to one period, equivalent to 1 ms in the case of Fig. 4.4. Expectedly, the plateau level of 8.75% is consistent with the change seen in Fig. 4.2 at $\nu$ = 1.0 kHz Similar measurements performed at higher frequencies with $\nu > \nu_{max}$ are compiled in Fig.

4.5. The resulting steady state values for $\nu$ = 4.0, 6.4, and 8.0 kHz indicate field induced increases in $\varepsilon''$ of 2.30%, 1.56%, and 1.27%, respectively. All plateau values observed by time resolved experiments are included as stars in the spectrum of Fig. 4.3, with the agreement confirming the steady state nature of the spectrum.

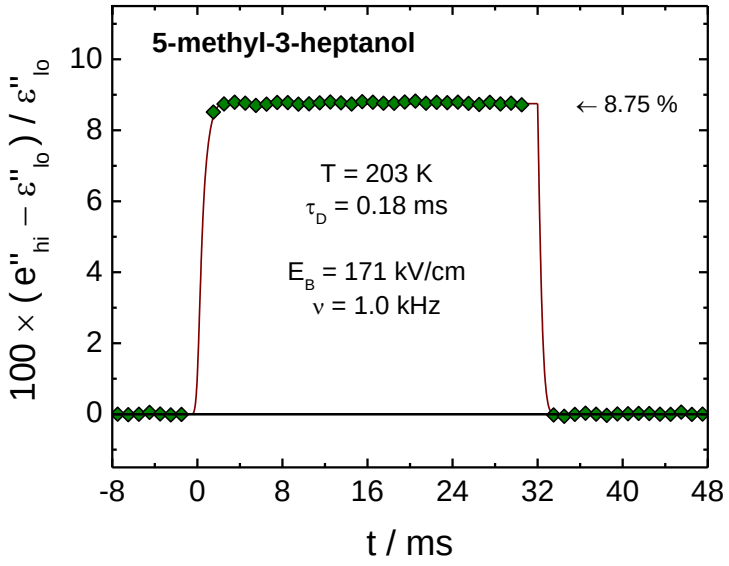


FIG. 4.4 Symbols represent the experimental field induced ($E_B$ = 171 kV cm$^{-1}$) relative change of the dielectric 'loss', ($e''_{hi} - \varepsilon''_{lo}$)/$\varepsilon''_{lo}$, versus time for 5M3H at $T$ = 203 K for a frequency $\nu$ = 1 kHz ($\approx \nu_{max}$). The line is calculated based on a squared exponential time dependence, $A\times[1 - \exp(-t/\tau)]^2$ and $A\times[\exp(-t/\tau)]^2$ with $A$ = 8.75% and $\tau$ = 0.24 ms.

The quadratic field dependence of the steady state effect has been verified by determining $\Delta_E \ln \tau_D$ at different fields. The results are $\Delta_E \ln \tau_D$ = 2.8% at $E_B$ = 82 kV cm$^{-1}$ and $\Delta_E \ln \tau_D$ = 12.6% at $E_B$ = 171 kV cm$^{-1}$. From these values, a power law relation with power lg(12.6/2.8)/lg(171/82) = 2.04 is found, consistent with the expected quadratic field dependence. We also note that qualitatively analogous results were found for

mixtures of 5M3H or 4-methyl-3-heptanol with 1-propanol, where the propanol content was around 5 to 10% by weight.

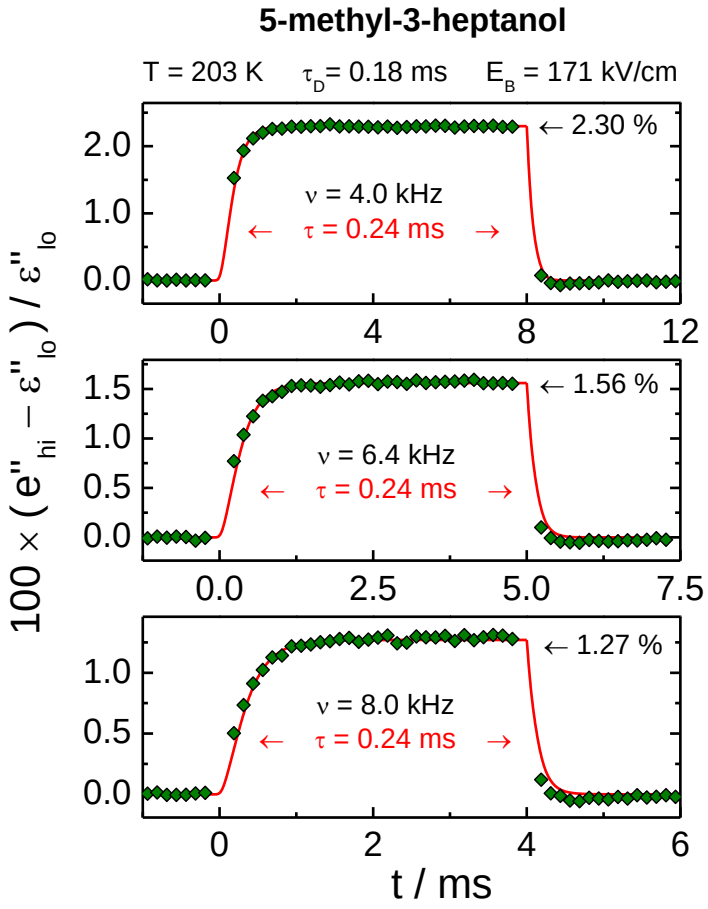


FIG. 4.5. Symbols represent the experimental field induced ($E_B$ = 171 kV cm$^{-1}$) relative change of the dielectric 'loss', $(e''_{hi} - \varepsilon''_{lo})/\varepsilon''_{lo}$, versus time for 5M3H at $T$ = 203 K for the frequencies $\nu$ = 4.0, 6.4, and 8.0 kHz (> $\nu_{max}$). The lines are calculated based on a squared exponential time dependence, $A\times[1 - \exp(-t/\tau)]^2$ and $A\times[\exp(-t/\tau)]^2$ with $A$ equal to the respective plateau value (as indicated) and with a common value of $\tau$ = 0.24 ms..

### 4.4 Discussion

The dc field induced changes of the quantity $(\varepsilon' - \varepsilon_\infty)$ observed in Fig. 4.2 are highly reminiscent of what had been seen earlier for 5M3H using high amplitude (bias free) ac

fields.[20,21] As in the previous studies, this field driven increase of $\Delta\varepsilon$ is understood as the result of the high field shifting the ring/chain equilibrium constant, $K_{r/c}$, towards the more polar species, i.e., favoring the chains and thus increasing the net $g_K$. In the present case, however, the disappearance of the amplitude enhancement for $\nu > \nu_{max}$ cannot be attributed to the frequency exceeding the rate at which $\varepsilon'(\omega)$ can change via $g_K$. The reason for this notion is that the alternating field component, $E_0$, is within the regime of linear response (applied electric field is $E(t) = E_B + E_0\sin(\omega t)$ with $E_B/E_0 = 4$) and thus has practically no impact on the ring/chain equilibrium, which now is only a matter of the static high field $E_B$. As a result, a different explanation for the frequency dependence of the non-linear effects must be found.

In order to rationalize the steady state results of Fig. 4.2 and Fig. 4.3, a quantitative analysis of these spectra is required. To this end, the low field loss spectra (see Fig. 4.1) are fit with the sum of a Debye type and a Havriliak-Negami (HN) type dielectric process.[23] These fits employ the permittivity function

$$\varepsilon^*(\omega) = \varepsilon_\infty + \frac{\Delta\varepsilon_D}{1+i\omega\tau_D} + \frac{\Delta\varepsilon_\alpha}{\left[1+(i\omega\tau_\alpha)^\alpha\right]^\gamma} \quad . \tag{4.3}$$

where $\varepsilon_\infty$ is the dielectric constant in the high frequency limit, and $\Delta\varepsilon_D$ and $\tau_D$ are the amplitude and time constant associated with the Debye process. The additional small signature of the primary ($\alpha$) relaxation mode is characterized by its amplitude $\Delta\varepsilon_\alpha$, its time constant $\tau_\alpha$, and the exponents $\alpha$ and $\gamma$ that define the symmetric and asymmetric broadening of the loss peak, respectively. Fits to the low field permittivity curves define $\varepsilon_\infty$, $\varepsilon'_{lo}$, and $\varepsilon''_{lo}$. Results for $\varepsilon'_{hi}$ and $\varepsilon''_{hi}$ are obtained by allowing $\Delta\varepsilon_D$ and $\tau_D$ to be

modified by the high field, whereas all parameters associated with the α-process are considered field invariant. The two field dependent quantities, $\Delta\varepsilon_D$ and $\tau_D$, are adjusted for a best fit to the experimental data for $(\varepsilon'_{hi} - \varepsilon'_{lo})/(\varepsilon'_{lo} - \varepsilon_\infty)$ in Fig. 4.2, and $(\varepsilon''_{hi} - \varepsilon''_{lo})/\varepsilon''_{lo}$ in Fig. 4.3. It turns out that the field effect on both the storage and the loss component can be described by the same parameters, with the field induced changes being quantified by $\Delta_E \ln\Delta\varepsilon_D$ = +11.0% and $\Delta_E \ln \tau_D$ = +12.6%. This 11% increase of $\Delta\varepsilon_D$ amounts to an 8.2% change of the total $\Delta\varepsilon = \Delta\varepsilon_D + \Delta\varepsilon_\alpha$, which appears as low frequency plateau level in Fig. 4.2. The curves calculated on the basis of the $\Delta_E \ln\Delta\varepsilon_D$ and $\Delta_E \ln \tau_D$ values are included as solid lines in both, Fig. 4.2 and Fig. 4.3. The coincidence of these fits with the experimental data validates that the field dependence of $\Delta\varepsilon_D$ and $\tau_D$ is sufficient to describe how the permittivity is modified by a static field of high amplitude.

In the previous studies of 5M3H based upon high amplitude ac fields,[20,21] the parameter $\Delta\varepsilon_D$ was the only variable considered to be sensitive to the high field. Presently, we find not only that both Debye peak parameters, $\Delta\varepsilon_D$ and $\tau_D$, change with $E_B$, but also that their relative changes are similar in magnitude. As a result, the field driven increase in peak amplitude and shift of the peak position to lower frequencies lead to a near perfect cancellation of the two effects, so that the high frequency regime of the permittivity appears field invariant. This cancellation feature does not seem to be accidental in the case of 5M3H, as the same behavior can be observed for mixtures of 5M3H or 4M3H with 1-propanol. Therefore, the basis for deriving a time scale for the ring-to-chain conversion from the frequency dependence of the earlier[20,21] high ac field experiments is no longer justified.

In order to assess the time scale of the ring/chain population to reach equilibrium after a change in the dc field, we turn to the time resolved experiments at selected frequencies shown in Fig. 44 and Fig. 4.5. The case of $\nu$ = 1.0 kHz in Fig. 4.4 picks up the time dependence of the amplitude change, $\Delta_E \ln \Delta\varepsilon_D$, selectively, because a lateral shift along the frequency axis remains undetected at the peak frequency $\nu_{max}$, where $\partial \ln\varepsilon / \partial \ln \nu = 0$. On the other hand, the limited time resolution of 1 ms is insufficient for resolving the dynamics. At the higher frequencies of Fig. 4.5, the changes are resolved across several periods in time, but these curves involve both $\Delta_E \ln \Delta\varepsilon_D$ and $\Delta_E \ln \tau_D$. In Fig. 4.5 it is particularly the $\nu$ = 8 kHz case that reveals the asymmetric response to applying and removing the field, where the fall time appears to be much shorter than the rise behavior.

In analogy to an earlier analysis of time-resolved non-linear effects,[24,25] we recognize that the steady state levels of $\Delta_E \ln \Delta\varepsilon_D$ and $\Delta_E \ln \tau_D$ depend quadratically on the field $E_B$. Because the deviations from the $P(E_B)$ linearity are still quite small, a reasonable approximation to the time dependence of the nonlinear effect is the proportionality to the squared time dependent polarization, $P$, where $P(t)$ is an exponential. Therefore, the curves in Fig. 4.5 are assumed to follow $\phi(t) \times [\varepsilon''_{hi}(t \to \infty) - \varepsilon''_{lo}]/\varepsilon''_{lo}$, with

$$\phi(t) = \begin{cases} \left(1 - e^{-(t-t_{on})/\tau}\right)^2 & , \quad t_{on} \le t \le t_{off} \\ \left(e^{-(t-t_{off})/\tau}\right)^2 & , \quad t \ge t_{off} \end{cases} , \tag{4.4}$$

where $t_{on}$ and $t_{off}$ are the times at which the field $E_B$ is applied and removed, respectively. For the four frequencies of Fig.4. 4 and Fig. 4.5, the solid lines demonstrate that eq. (4.4) with a common time constant of $\tau$ = 0.24 ms reproduces all observed rise and decay data

for these frequencies. We note that the birefringence $\Delta n$ stemming from the electro-optical Kerr effect is also quadratic in the electric field, $\Delta n \propto E^2$,[26] and a very similar rise/decay asymmetry is observed in $\Delta n(t)$ curves.[27,28,29,30] Given that the quantity $\tau$ = 0.24 ms associated with all fits is only 30% larger than the low field Debye time of $\tau_D$ = 0.18 ms, we conclude as before that it is the Debye time scale that governs this structural recovery process,[20,21] not the faster α-relaxation time. With this coincidence of the ring/chain conversion time $\tau$ with the Debye time $\tau_D$ of 5M3H, the present results are again supportive of the picture in which the fluctuation of the Kirkwood correlation factor $g_K$ is at the origin of the Debye process of monohydroxy alcohols and related liquids.[1,20,21,31] This is equivalent to fluctuations in the end-to-end distance of the chain or in the ring/chain type structural motif.

Based on the time dependence of the $(\varepsilon''_{hi} - \varepsilon''_{lo})/\varepsilon''_{lo}$ curves in Fig. 4.4 and Fig. 4.5, we observe that this quantity approaches its steady state level in a monotonic fashion and that this level, $[\varepsilon''_{hi}(t \rightarrow \infty) - \varepsilon''_{lo}]/\varepsilon''_{lo}$, is much smaller than $\Delta_E \ln \Delta\varepsilon_D$ or $\Delta_E \ln \tau_D$. This implies that for $\nu \geq \nu_{max}$ the cancellation of $\Delta_E \ln \Delta\varepsilon_D$ and $\Delta_E \ln \tau_D$ is effective for all times, not only in the steady state case. This suggests that both amplitude ($\Delta\varepsilon_D$) and time constant ($\tau_D$) vary concertedly with time, and furthermore that the Debye time scale changes with the ring/chain composition. In support of this notion and according to the results of Singh *et al.*,[21] the spectral separation of $\tau_D$ and $\tau_\alpha$ ($d\ln(\tau_D/\tau_\alpha)/dT = -0.029$ K$^{-1}$) and the relaxation amplitude ($d\ln(\Delta\varepsilon)/dT = -0.046$ K$^{-1}$) are similar regarding their sensitivity to temperature. When a high dc field is applied, these two quantities also change by similar relative amounts, i.e., $d\ln(\tau_D/\tau_\alpha)/dE \approx d\ln(\Delta\varepsilon)/dE$, see Fig.4. 2 and Fig.

4.3. As a result, when $g_K$ changes with temperature as a consequence of an altered ring/chain equilibrium, not only will the amplitude $\Delta\varepsilon_D$ change, but also the spectral separation of time constants, $\log(\tau_D/\tau_\alpha)$. We hypothesize that this feature is at the origin of the distinct temperature dependences of $\tau_D(T)$ and $\tau_\alpha(T)$ that seems more pronounced when $g_K$ varies considerably with $T$.

Finally, we assess the extent to which other known sources of non-linear dielectric behavior contribute to the present findings. Heating related effects can lead to considerable non-linearities in the case of ac fields,[32,33] but are suppressed in the present experiments on the basis of the static nature of the high electric field. A recently recognized source of a field induced change in relaxation time is due to the change in entropy that occurs at high fields, $\Delta_E S = \frac{1}{2}\varepsilon_0 \upsilon(\partial\varepsilon_s/\partial T)\times E_B^2$, where $\upsilon$ is the molar volume.[22,24,25,34] A study of various monohydroxy alcohols has shown that $\Delta_E \ln\tau_D$ is approximately proportional to $\Delta_E S$. For 6M3H the results were $\Delta_E \ln\tau_D$ = 1.48% and $\Delta_E S$ = –90 mJ $K^{-1}$ $mol^{-1}$ at $T$ = 195 K and $E_B$ = 200 kV $cm^{-1}$. For 5M3H at $T$ = 203 K and $E_B$ = 171 kV $cm^{-1}$, $\Delta_E S$ = –35 mJ $K^{-1}$ $mol^{-1}$ is obtained based on $\partial\varepsilon_s/\partial T$ = – 0.17 $K^{-1}$ and assuming equal molar volumes, $\upsilon_{5M3H} = \upsilon_{6M3H}$. Therefore, an entropy effect of $\Delta_E \ln\tau_D$ = 0.57% is estimated for 5M3H, less than 5% of the observed chemical effect. Similarly, dielectric saturation could counteract the present 'chemical' effect observed as positive $\Delta_E \ln\Delta\varepsilon_D$, but saturation at these fields tends to remain a $\Delta\varepsilon$ reduction of not more than 0.5%. In conclusion, we are confident that the large field effect of this study are dominated by the field driven ring/chain conversion.

## 4.5 Summary and Conclusion

The monohydroxy alcohol 5-methyl-3-heptanol near $T$ = 200 K is selected for a high dc bias field dielectric study because its Kirkwood correlation factor ($g_K \approx 1$) indicates the coexistence of ring- and chain-like structures with similar free energies. As realized earlier,[20] this situation gives rise to a strong sensitivity of structure and dynamics to an electric field, since rings and chains differ considerably in their net dipole moments. In contrast to the earlier approach to 5M3H based upon high ac fields,[21] employing steps in a dc bias field of sufficient magnitude allows us to directly observe the time dependence of the field induced changes in structure and dynamics.

Steady state spectra of the quantities that gauge the relative changes in permittivity, $(\varepsilon'_{hi} - \varepsilon'_{lo})/(\varepsilon'_{lo} - \varepsilon_\infty)$ and $(\varepsilon''_{hi} - \varepsilon''_{lo})/\varepsilon''_{lo}$, are analyzed and the observations are consistent with changes in both the amplitude ($\Delta_E \ln \Delta\varepsilon_D$ = +11.0%) and time constant ($\Delta_E \ln \tau_D$ = +12.6%) of the Debye process. The similarity of the two percentage change values leads to a cancellation effect at frequencies $\nu > \nu_{max}$, such that the high frequency sides of the dielectric spectra appear field invariant. The evolutions of these field induces changes are observed as a function of time after applying and after removing the high dc bias field. The resulting rise and decay curves are asymmetric, with the rise always appearing slower than the decay counterpart, analogous to observations for other non-linear dielectric effects[24,25] and for electro-optical Kerr effect curves.[27,28] The quadratic field dependence of the steady state effects, $\Delta_E \ln \Delta\varepsilon_D \propto E_B^2$ and $\Delta_E \ln \tau_D \propto E_B^2$, implies that squared exponential approaches, $[1 - \exp(-t/\tau)]^2$ and $[\exp(-t/\tau)]^2$, should represent the rise and decay behavior. We find that this quadratic approach captures the observed

rise/decay asymmetries, and that all transitions are associated with the same time constant of $\tau$ = 0.24 ms, only 30% higher than the Debye time constant, $\tau_D$ = 0.18 ms. We conclude that it is the fluctuation of the end-to-end vector of the hydrogen-bonded structures that gives rise to the Debye process, more akin to a fluctuation of the magnitude of a dipole moment (of $g_K$) rather than the reorientation of a permanent dipole.

The observation that the Debye time scale $\tau_D$ is also a matter of the ring/chain equilibrium constant can help to understand the common feature that the Debye process fails to track the temperature dependence of the α-process of monohydroxy alcohols. In other words, the spectral separation of the Debye- and α-peaks, $\log(\tau_D/\tau_\alpha)$, depends on temperature in these liquids. The present study suggests that $\log(\tau_D/\tau_\alpha)$ will change whenever $g_K$ displays a considerable sensitivity to temperature, which is a common feature of monohydroxy alcohols in their viscous regime.[15]

### 4.6 References


1 R. Böhmer, C. Gainaru, and R. Richert, Physics Reports **545**, 125 (2014).

2 S. S. N. Murthy, J. Phys. Chem. **100**, 8508 (1996).

3 L.-M. Wang and R. Richert, J. Phys. Chem. B **109**, 11091 (2005).

4 L.-M. Wang and R. Richert, J. Chem. Phys. **123**, 054516 (2005).

5 C. Gainaru, T. Hecksher, N. B. Olsen, R. Böhmer, and J. C. Dyre, J. Chem. Phys. **137**, 064508 (2012).

6 C. Gainaru, S. Bauer, E. Vynokur, H. Wittkamp, W. Hiller, R. Richert, and R. Böhmer, J. Phys. Chem. B **119**, 15769 (2015).

7 W. Huang and R. Richert, J. Phys. Chem. B **112**, 9909 (2008).

8 J. S. Hansen, A. Kisliuk, A. P. Sokolov, and C. Gainaru, Phys. Rev. Lett. **116**, 237601 (2016).

[9] H. Huth, L.-M. Wang, C. Schick, and R. Richert, J. Chem. Phys. **126**, 104503 (2007).

[10] S. S. N. Murthy and M. Tyagi, J. Chem. Phys. **117**, 3837 (2002).

[11] L.-M. Wang, Y. Tian, R. Liu, and R. Richert, J. Chem. Phys. **128**, 084503 (2008).

[12] T. A. Litovitz and G. E. McDuffie, J. Chem. Phys. **39**, 729 (1963).

[13] B. Jakobsen, C. Maggi, T. Christensen, and J. C. Dyre, J. Chem. Phys. **129**, 184502 (2008).

[14] C. Hansen, F. Stickel, T. Berger, R. Richert, and E. W. Fischer, J. Chem. Phys. **107**, 1086 (1997).

[15] C. J. F. Böttcher, *Theory of Electric Polarization, Vol 1* (Elsevier, Amsterdam, 1973).

[16] P. Bordewijk, F. Gransch, and C. J. F. Böttcher, J. Phys. Chem. **73**, 3255 (1969).

[17] G. P. Johari, O. E. Kalinovskaya, and J. K. Vij, J. Chem. Phys. **114**, 4634 (2001).

[18] W. Dannhauser, J. Chem. Phys. **48**, 1911 (1968).

[19] H. Fröhlich, *Theory of Dielectrics* (Clarendon, Oxford, 1958).

[20] L. P. Singh and R. Richert, Phys. Rev. Lett. **109**, 167802 (2012).

[21] L. P. Singh, C. Alba-Simionesco, and R. Richert, J. Chem. Phys. **139**, 144503 (2013).

[22] S. Samanta and R. Richert, J. Chem. Phys. **142**, 044504 (2015).

[23] S. Havriliak and S. Negami, Polymer **8**, 161 (1967).

[24] A. R. Young-Gonzales, S. Samanta, and R. Richert, J. Chem. Phys. **143**, 104504 (2015).

[25] S. Samanta, O. Yamamuro, and R. Richert, Thermochim. Acta **636**, 57 (2016).

[26] M. S. Beevers, D. A. Elliott, and G. Williams, J. Chem. Soc. Faraday Trans. 2 **76**, 112 (1980).

[27] R. Coelho and D. Khac Manh, C. R. Acad. Sc. Paris - Serie C **264**, 641 (1967).

[28] J. Crossley and G. Williams, J. Chem. Soc. Faraday Trans. 2 **73**, 1906 (1977).

[29] M. S. Beevers, J. Crossley, D. C. Garrington, and G. Williams, Faraday Symp. Chem. Soc. **11**, 38 (1977).

[30] J. Crossley and G. Williams, J. Chem. Soc. Faraday Trans. 2 **73**, 1651 (1977).

[31] C. Gainaru, R. Meier, S. Schildmann, C. Lederle, W. Hiller, E. A. Rössler, and R. Böhmer, Phys. Rev. Lett. **105**, 258303 (2010).

[32] W. Huang and R. Richert, J. Chem. Phys. **130**, 194509 (2009).

[33] R. Richert, Adv. Chem. Phys. **156**, 101 (2014).

[34] G. P. Johari, J. Chem. Phys. **138**, 154503 (2013).

# CHAPTER 5

# MODIFING HYDROGEN-BONDED STRUCTURES BY PHYSICAL VAPOR DEPOSITION:4-METHYL-3-HEPTANOL

In the previous section, it was shown that supramolecular structures could be modified with the application of a high field, and the changes occurred on the Debye timescale. In this chapter, physical vapor deposited films of 4-methyl-3-heptanol measured and analyzed to test the connectivity between the absence of polarity and hydrogen bonded rings in conditions that are meant to suppress the formation of supramolecular structures.

## 5.1 Introduction

In liquids such as water, alcohols, amides, and some other cases, hydrogen bonding can have a significant impact on the structure and dynamics.[1] In particular, glass forming monohydric alcohols have been studied extensively in recent years in order to gain a deeper insight into the role of hydrogen bonding in such systems.[2] Due to the considerable molecular dipole moment arising mainly from the hydroxyl group, alcohols can have a high dipole density.[1] Moreover, hydrogen bonding induces a preferred parallel alignment within clusters of dipoles in many of these alcohols, leading to an effective dipole moment, $\mu_{\text{eff}}$, that is larger than $\mu$ itself.[1] Such alcohols, in contrast to simple liquids, display a Debye type loss peak as the most prominent dielectric polarization feature that is associated with end-to-end vector fluctuations of hydrogen-bonded supramolecular structures. Therefore, this mode does not correspond to the structural relaxation process identified by mechanical or calorimetric experiments.[3,4,5,6,7,8,9] This

enhancement of $\mu_{eff}$ by orientational correlations is captured by the Kirkwood correlation factor, $g_K = 1 + z\langle\cos\theta\rangle$, where $z$ is the number of neighbor dipoles and $\langle\cos\theta\rangle$ gauges their average orientation.[10] The impact of $g_K$ on the dielectric constant, $\varepsilon_s$, can be quantified by the Kirkwood-Fröhlich equation.[10] Hydrogen bonded dipole chains are found in many *n*-alcohols and lead to positive values for $\langle\cos\theta\rangle$ and thus $g_K$ values reaching levels near 4, thereby enhancing the dielectric constant over the reference liquid with uncorrelated dipole orientation ($g_K = 1$).[1]

In contrast, other monohydric alcohols have been found to have much *lower* dielectric constants than what is expected for a simple liquid on the basis of the dipole density, i.e., when $g_K$ is set to unity. A well-known case is the series of octanol isomers studied by Dannhauser,[11] where the methyl group position alone is observed to change the Kirkwood correlation factor from 0.1 to 4.2, while the dipole density remains unchanged. In such alcohols, values of $g_K$ below unity are believed to be due to the hydrogen bond induced formation of ring-like structures,[1] in which anti-parallel orientations give rise to an effective cancellation of dipole moments. Within this series of octanol isomers with virtually constant dipole density, the dielectric relaxation amplitude, $\Delta\varepsilon = \varepsilon_s - \varepsilon_\infty$, changes from 0.5 to 27, indicating a substantial change in the structure of hydrogen-bonded clusters.[12] Consequently, the dielectric properties of these liquids are sensitive indicators of any changes in their supramolecular structures.

The above notions regarding alcohols all refer to the bulk equilibrium liquid state, with values of $g_K$ that are far from unity being observed mostly in liquids supercooled from above the melting temperature to near $T_g$.[1,13] Liquids can also be prepared by

warming a glass created by physical vapor deposition (PVD), a technique that has been recognized to create glasses of exceptional qualities.[14] Molecular glasses fabricated by PVD often display higher density, lower enthalpy, and higher kinetic stability relative to the standard glasses prepared by cooling the liquid to below $T_g$. These results are expected when surface mobility is high enough to allow substantial equilibration during deposition even below $T_g$. However, glasses of monohydric alcohols and other hydrogen bonding liquids prepared by PVD can show little to no enhancement of the kinetic stability,[15,16] and direct measurements indicate that hydrogen-bonding impedes surface mobility.[17,18] Thus it is possible that vapor deposition of hydrogen-bonded systems, particularly at low temperatures, will yield glasses with structures that are trapped exceptionally far from equilibrium. Recent work by Wübbenhorst and coworkers on glycerol and other polyols can be interpreted in this manner.[19,20] They found that vapor-deposited glycerol, when heated above $T_g$, formed an unusual liquid in which the Kirkwood factor $g_K$ was substantially higher than in the ordinary supercooled liquid.

PVD fabrication is explored for its capability to change the hydrogen-bonded structures and thus the Kirkwood factor, $g_K$, of monohydric alcohols relative to the ordinary supercooled liquid. Focus is given to 4-methyl-3-heptanol (4M3H), an alcohol that has a Kirkwood correlation factor of $g_K = 0.11$ in the bulk near its glass transition ($T_g$ = 162 K), indicative of predominantly ring-like structures. Glasses of 4M3H were prepared by vapor-deposition onto substrates held between 0.6 $T_g$ and $T_g$. When glasses prepared at the lower substrate temperatures are heated, they displayed dielectric losses ($\varepsilon''$ between 200 Hz and 20 kHz) that were at least an order of magnitude higher than

those of the ordinary supercooled liquid, indicating that $g_K \geq 1$ for the as-deposited glass. Near $T$ = 162 K, these as-deposited films convert to a state with significantly lowered $g_K$ and/or increased $\tau_D$ by annealing on a time scale of about 2000 s, which is near the Debye relaxation time of the ordinary liquid. Surprisingly, even at temperatures as high as $T_g$ + 40 K, the PVD film of 4M3H does not convert back to the state of the ordinary liquid that is obtained by supercooling. Instead, it enters a state with orientational mobility of the dipoles, but with a dielectric loss that remains considerably higher and with dynamics that are frustrated relative to the standard supercooled state. Vapor deposited structures therefore retain memory of the deposition history even well above $T_g$.

**5.2 Experiments**

The material 4-methyl-3-heptanol (4M3H, ≥ 99%) was purchased from Sigma-Aldrich and was used as received. About 1 mL of the liquid was held in a glass reservoir which can be evacuated. This reservoir was connected via a pressure regulator, a shutoff valve, a regulating needle valve and another shutoff valve to an opening in the vacuum enclosure of a closed-cycle helium cryostat (Leybold RDK 10-320) in order to facilitate vapor deposition onto a cold substrate. The cryostat was evacuated to a pressure lower than $10^{-3}$ Pa using a turbo pump supported by the cryo-pump action of the cold-finger within the vacuum system. The substrate holder temperature can be adjusted between 30 and 300 K by a Lakeshore Mod. 340 temperature controller equipped with DT-470 diode sensors. The substrate holder was surrounded by a radiation shield held near 100 K with an aperture that is aligned with the molecular beam.

The surface onto which the vapor was deposited was a microlithographically fabricated interdigitated electrode (IDE) cell, IME 1050.5-FD-Au from ABTECH Scientific, based upon a borosilicate substrate.[21,22] The comb electrode capacitor has been determined to have a geometric capacitance of $C_{geo}$ = 1.14 pF and the effective height of the electric field is estimated to be $d$ = 7 μm ($d \approx \lambda/3$, where $\lambda$ = 20 μm is the spatial periodicity).[23] A 4M3H glass has a dielectric constant of $\varepsilon_\infty$ = 2.4 ($\chi_\infty = \varepsilon_\infty - 1$ = 1.4), so that during deposition an incremental capacitance of $C_{geo}\chi_\infty h/d$ = 0.16 pF per $h$ = 1 μm film thickness, where $h$ is the thickness of the dielectric sample. Capacitance values were recorded with an Andeen-Hagerling ultra precision bridge (AH-2700A) at frequencies in the range $\nu$ = 100 Hz to 20 kHz. All dielectric loss values are corrected for the fraction of sample volume to capacitor geometry volume, $\approx h/d$.

During the physical vapor deposition process, capacitance and substrate temperature are recorded as a function of time with the initial rate and total capacitance change being evaluated to yield the deposition rate $v_{dep}$ and film thickness $h$, respectively. After the deposition process is completed, samples are cooled to a set-point temperature of about 30 K and subject to three subsequent temperature scans during which temperature and permittivity ($\varepsilon'$ and $\varepsilon''$) are recorded: initial scan (run 1) of the as deposited film from 30 to 162 K, isothermal recording of permittivity at 162 K for 5 hours, a scan (run 2) of the partially annealed sample from 30 to 190 K, and a final scan (run 3) from again 30 K to 220 K. All scan rates are 0.5 K/min, and near the end of 'run 3' the permittivity is observed to drop abruptly due to sample evaporation.

The permittivity data obtained from the IDE cell contains contributions from the borosilicate glass substrate. In order to subtract this substrate signal, the permittivity of the empty cell was measured after the complete evaporation of each sample. These baselines were recorded using the same temperature scan employed for the sample measurements: 30 K to 220 K at a rate of 0.5 K/min. The logarithmic $\varepsilon''(T)$ values obtained in this manner are subject to fifth order polynomial fits to facilitate interpolation to the actual temperatures recorded for run 1, 2 and 3 for that particular sample. Approximate baseline values are $\varepsilon''$ = 0.010, 0.013, 0.030, and 0.090 at the respective temperatures $T$ = 50, 100, 150, and 200 K.

**5.3 Results**

A typical set of dielectric loss results for vapor deposited 4M3H is depicted in Fig. 5.1, where the following deposition condition were used: substrate temperature $T_{dep}$ = 130 K (= 0.80$T_g$), deposition rate $\nu_{dep}$ = 3.6 nm/s, and a final film thickness of $h$ = 5.6 μm. The graph shows the fixed frequency scan of $\varepsilon''(\nu$ = 1 kHz) from 30 K to 162 K for the as-deposited sample as 'run 1'. At the end of this first scan, the sample is held at the final temperature of that scan, $T$ = 162 K, for 5 hours in order to allow it to equilibrate. The following scan labeled 'run 2' starts also at 30 K but extends to a higher temperature of $T$ = 190 K, and at the end of this scan the temperature is dropped to 30 K again. The last scan, 'run 3', represents the annealed state and reaches temperatures of $T$ = 220 K. For temperatures in excess of about 205 K, the signal drops rapidly as a result of sample evaporation (open symbols in Fig. 5.1). The main feature of this result is the significantly

increased dielectric loss of the as-deposited sample over the annealed case, amounting to a factor of $\varepsilon''_{dep}/\varepsilon''_{ann} = 11$ at $T = 162$ K.

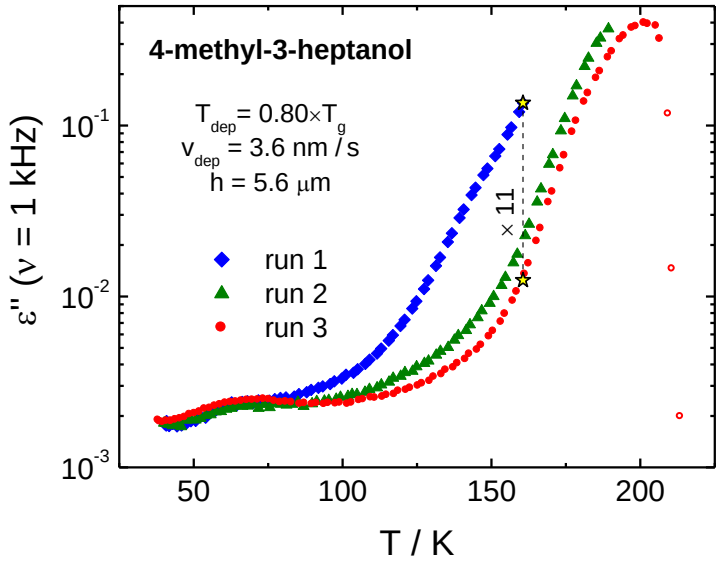


FIG. 5.1. Dielectric loss of 4-methyl-3-heptanol at a fixed frequency $\nu = 1$ kHz for a sample deposited at a rate of $v_{dep} = 3.6$ nm/s onto a substrate temperature $T_{dep} = 130$ K (= $0.80T_g$) with a film thickness of $h = 5.6$ μm. Curves represent three subsequent temperature up-scans at a rate of 0.5 K/ min, each starting at $T = 30$ K: blue diamonds are for the as-deposited sample (run 1, 30 - 162 K), green triangles are for the partially annealed sample (run 2, 30 - 190 K), red circles are for the completely annealed sample (run 3, 30 - 220 K. The two stars connected by the dashed line indicate the loss ratio between the as-deposited and fully-annealed sample, $\varepsilon''_{dep}/\varepsilon''_{ann} = 11$ in this case.

For the initial and final temperature scan of the same sample for which the $\nu = 1$ kHz results are shown in Fig. 5.1, the frequency dependence for each temperature is outlined in Fig. 5.2, showing 'run 1' and 'run 3' curves for three different frequencies each: $\nu = 200$ Hz, 2 kHz, and 20 kHz. Values that rise above the near constant loss level of around $3\times10^{-3}$ are indicative of slopes $\partial\lg\varepsilon''/\partial\lg\nu \approx -0.5$ for both the as-deposited and the annealed sample.

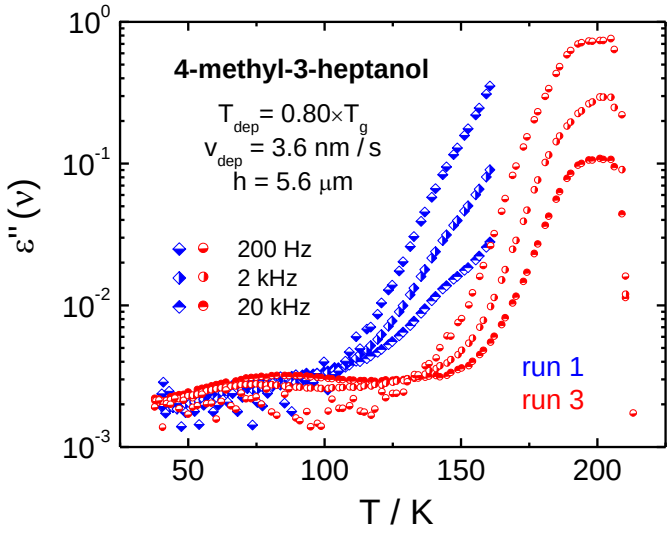


FIG.5.2. Dielectric loss of 4-methyl-3-heptanol for 'run 1' and 'run 3' of the same sample that led to the data in Fig. 5.1, but for three different frequencies each run as indicated: $\nu$ = 20 kHz, 2 kHz, and 200Hz.

Deposition of 4M3H at virtually the same conditions as above (deposition rate $v_{dep}$ = 3.2 nm/s, final film thickness $h$ = 5.6 μm) but onto a substrate temperature of $T_{dep}$ = 160 K (= 0.99$T_g$) yields a sample whose dielectric behavior is practically identical to that of the bulk liquid. This is shown in Fig. 5.3, which compares both the as-deposited (run 1) and annealed (run 3) PVD film with the bulk liquid measured at constant temperatures in the range 120 to 211 K.

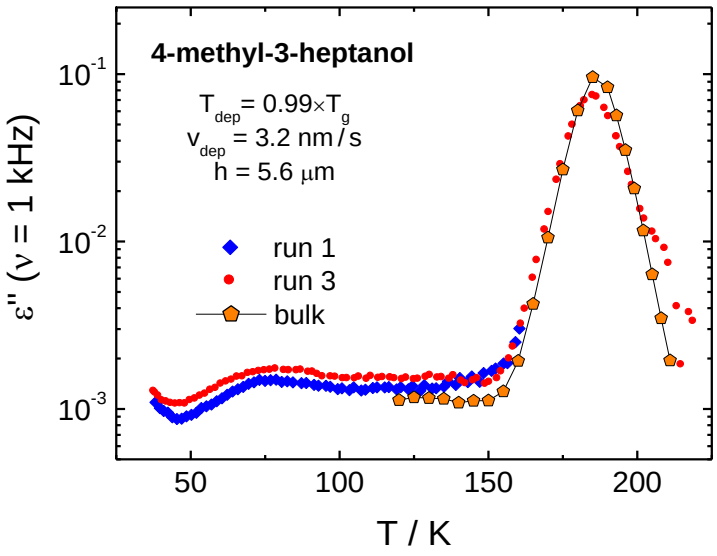


FIG. 5.3. Dielectric loss of 4-methyl-3-heptanol at a fixed frequency $\nu$ = 1 kHz for a sample deposited at a rate of $v_{dep}$ = 3.2 nm/s onto a substrate temperature $T_{dep}$ = 160 K (= 0.99 $T_g$) with a film thickness of $h$ = 5.6 μm. Curves represent two temperature up-scans at a rate of 0.5 K/ min, each starting at $T$ = 30 K: blue diamonds are for the as-deposited sample (run 1, 30 - 162 K), red circles are for the completely annealed sample (run 3, 30 - 220 K. The orange pentagons represent the loss of the ordinary bulk liquid in equilibrium. Minor differences between the curves are expected, because the films are measured during a $T$-scan and the bulk liquid data is recorded at constant temperatures.

The effect of deposition temperature far below $T_g$ is addressed in Fig. 5.4, which depicts the first and third scans of two samples, one with $T_{dep}$ = 130 K (= 0.80$T_g$) and one with $T_{dep}$ = 100 K (= 0.62$T_g$). Both samples are deposited at a rate of $v_{dep}$ = 6.0 nm/s until a final film thickness of $h$ = 5.5 μm is achieved. The ratios of the loss values of the as-deposited and annealed film, $\varepsilon''_{dep}/\varepsilon''_{ann}$, taken at $T$ = 162 K are very similar for the two different deposition substrate temperatures: $\varepsilon''_{dep}/\varepsilon''_{ann}$ = 10 for $T_{dep}$ = 0.62$T_g$ and 13 for $T_{dep}$ = 0.80$T_g$. The deposition conditions ($T_{dep}$, $v_{dep}$, $h$) for all samples of this study are compiled in Table 5.1, along with the values for $\varepsilon''_{dep}/\varepsilon''_{ann}$, which gauge the enhancement

of the dielectric loss at $T$ = 162 K of the as-deposited film over the annealed counterpart (which is not yet the standard supercooled liquid).

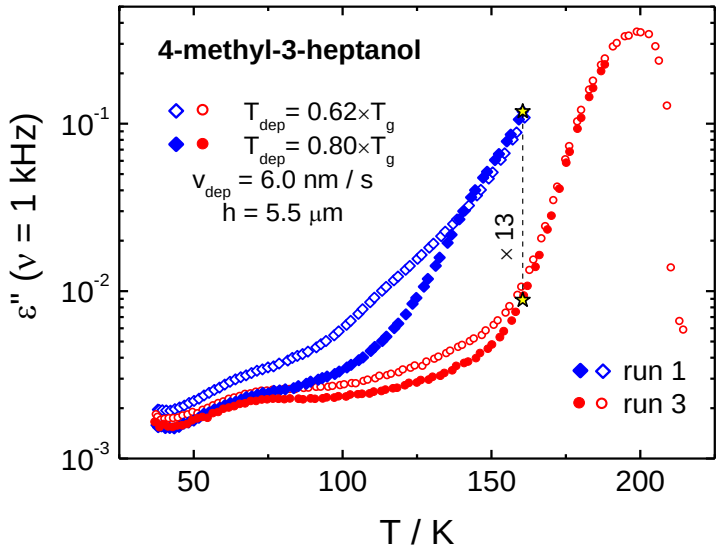


FIG. 5.4. Dielectric loss of 4-methyl-3-heptanol at a fixed frequency $\nu$ = 1 kHz for a sample deposited at a rate of $v_{dep}$ = 6.0 nm/s onto a substrate temperature $T_{dep}$ = 130 K (= 0.80$T_g$, solid symbols) and $T_{dep}$ = 100 K (= 0.62$T_g$, solid symbols), both with a film thickness of $h$ = 5.5 μm. Curves represent two temperature up-scans at a rate of 0.5 K/ min, each starting at $T$ = 30 K: blue diamonds are for the as-deposited sample (run 1, 30 - 162 K), red circles are for the completely annealed sample (run 3, 30 - 220 K. The two stars connected by the dashed line indicate the loss ratio between the as-deposited and fully-annealed sample for the $T_{dep}$ = 0.8 $T_g$ case, $\varepsilon''_{dep}/\varepsilon''_{ann}$ = 13 in this case.

For each PVD sample mentioned above, the sample is held at $T$ = 162 K for 5 hours directly after 'run 1' is completed and prior to cooling it down to near 30 K and beginning 'run 2'. During this annealing time, the dielectric loss is recorded every 3 minutes in order to monitor the effect of annealing on $\varepsilon''$ at a frequency of $\nu$ = 1 kHz. A typical curve for such a measurement is depicted in Fig. 5.5, revealing a monotonic reduction of the loss towards the lower values observed in the subsequent 'run 2' scan (see Fig. 5.1, which

refers to the same sample as Fig. 5.5). The initial rise of $\varepsilon''$ that occurs during the first ≈ 6 minutes is due to the actual sample temperature still adjusting to the $T$ = 162 K set-point immediately after the 0.5 K/min scan.

| $T_{dep}$ / $T_g$ | $v_{dep}$ / (nm $s^{-1}$) | $h$ / μm | $\varepsilon''_{dep}/\varepsilon''_{ann}$ | Figure |
|---|---|---|---|---|
| 0.80 | 3.6 | 5.6 | 11 | 5.1, 5.2, 5.5 |
| 0.99 | 3.2 | 5.6 | 1 | 5.3 |
| 0.62 | 6.0 | 5.5 | 10 | 5.4 |
| 0.80 | 6.0 | 5.5 | 13 | 5.4 |
| 0.80 | 0.94 | 5.5 | 14 | - |
| 0.80 | 5.9 | 5.6 | 12 | - |

TABLE 5.1. Preparation conditions for different samples in terms of the ratio of deposition temperature to glass transition temperature ($T_{dep}/T_g$), deposition rate ($v_{dep}$), and film thickness ($h$). The quantity $\varepsilon''_{dep}/\varepsilon''_{ann}$ designates the ratio of the dielectric loss values $\varepsilon''$(ν = 1 kHz) at $T$ = 162 K for the as-deposited (dep) and annealed (ann) sample. The last column identifies the figure number in which data for that sample are shown.

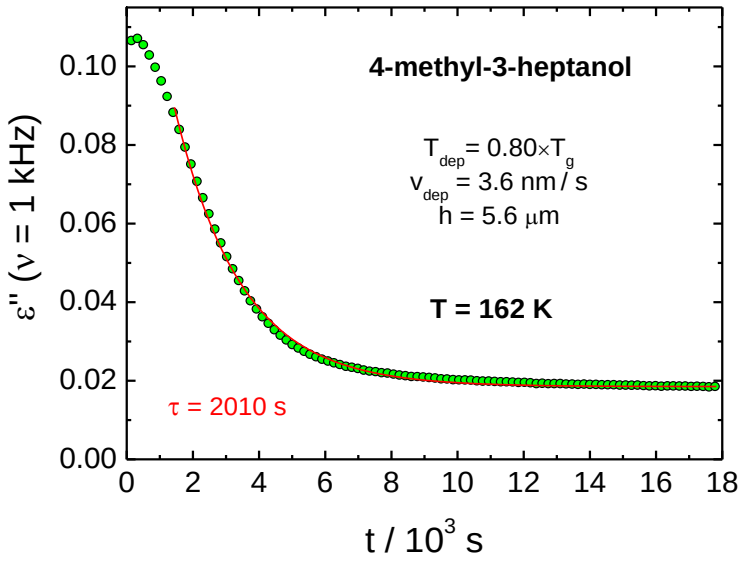


FIG. 5.5. Dielectric loss of 4-methyl-3-heptanol at a fixed frequency $\nu$ = 1 kHz for a sample deposited at a rate of $v_{dep}$ = 3.6 nm/s onto a substrate temperature $T_{dep}$ = 130 K (= 0.80$T_g$) with a film thickness of $h$ = 5.6 μm. The symbols represent the time dependence of the loss at a constant temperature ($T$ = 162 K), measured immediately after the completion of 'run 1' and prior to 'run 2' and 'run 3' (along the dashed vertical line of Fig. 1). The initial rise is due to temperature equilibration from $T$ = 160.5 to 162 K. The red line shows an exponential fit to the final decay behavior with time constant $\tau$ = 2010 s.

**5.5 Discussion**

The dielectric properties of the monohydric alcohol 4-methyl-3-heptanol has been studied extensively.[11,12,13,24,25,26,27,28] A survey of the results reveals that some disagreement regarding the relaxation amplitude ($\Delta\varepsilon = \varepsilon_s - \varepsilon_\infty$) exists, partly due to the four distinct diastereoisomers of 4M3H, as discussed by Bauer *et al.* in a recent report.[22] Many monohydric alcohols, such as ethanol or 1-propanol, are highly polar as a result of hydrogen-bonded chain-like structures in which the neighboring dipoles prefer a more parallel alignment, thereby enhancing the Kirkwood correlation factor $g_K$ and the

dielectric constant $\varepsilon_s$, with these two quantities being connected via the Kirkwood-Fröhlich equation,[10]

$$\frac{(\varepsilon_s - \varepsilon_\infty)(2\varepsilon_s + \varepsilon_\infty)}{\varepsilon_s(\varepsilon_\infty + 2)^2} = \frac{\rho N_A \mu^2}{9 k_B T \varepsilon_0 M} \times g_K \ , \qquad (5.1)$$

where $\varepsilon_s$ and $\varepsilon_\infty$ are the dielectric constants in the limits of low and high frequency, respectively. In eq. (5.1), $N_A$ is Avogadro's constant, $\rho$ is the density, $M$ is the molar mass, $k_B$ is Boltzmann's constant, and $\varepsilon_0$ represents the permittivity of vacuum.

4M3H is an unusual alcohol in the sense that $\Delta\varepsilon \approx 0.5$ is very small for the dipole density of an octanol, and accordingly $g_K$ is around 0.1 near the glass transition at $T_g$ = 162 K. The rationale for such a low value of $g_K$ is based on the anti-parallel orientation of dipoles that stems from the formation of hydrogen-bonded ring-like structures.[11] Because dipole cancellation in this liquid suppresses the dielectric relaxation amplitude, $\Delta\varepsilon$, by about a factor of ten, small deviations from the mostly anti-parallel dipole orientation (either by subtle structural changes or by contamination) can have a large impact on $\Delta\varepsilon$. This sensitivity may be a further factor contributing to the different findings regarding $\Delta\varepsilon$ of 4M3H, consistent with the variations in $\Delta\varepsilon$ originating from the Debye peak amplitude.[22]

The above explanation for the small dielectric constant of 4M3H implies that the supramolecular structure of the liquid is a critical factor in defining its dielectric properties. Upon cooling the bulk liquid towards the glass transition at a typical cooling rate, say up to 20 K/min, the structure has no trouble equilibrating to the preferred hydrogen-bonded clusters, i.e., ring-like structures near $T_g$. For the supercooled liquid

state, it has been observed that this equilibration of the hydrogen-bonded structures (and thus $g_K$) occurs on the time scale ($\tau_D$) of the Debye process, i.e., somewhat slower than structural relaxation ($\tau_\alpha$).[29] If the liquid is not given sufficient time for the supramolecular structure to emerge, one should expect very different dielectric properties. This could be accomplished by a very fast quench of the liquid from above the melting temperature, $T > T_m$, to $T < T_g$, or, alternatively, by physical vapor deposition (PVD). In any case, if the ring-like supramolecular structures were absent, one would expect a lack of the dipole cancellation effect, thus $g_K \approx 1$ (or higher if chains are formed) instead of 0.1, and accordingly a much higher level of $\varepsilon_s$.

The values for $\varepsilon''_{dep}/\varepsilon''_{ann}$ in Table 5.1 demonstrate that in most cases the as-deposited film has a dielectric loss that is higher than that of the annealed liquid by about an order of magnitude. However, one case can be found in which this factor is in fact unity: the case of a deposition at $T_{dep} = 0.99T_g$ ($v_{dep} = 3.2$ nm/s) where the as deposited films displays bulk liquid behavior (see Fig. 5.3). For this situation, we assume that the system is given sufficient time to approach the equilibrium supramolecular structure that leads to the low loss configuration. Samples, including alcohols, deposited by PVD at $T_{dep} \approx T_g$ are known to have practically the same properties as the ordinary liquid counterparts.[9,16]

For the remaining cases in Table 5.1 for which the loss ratio of the as-deposited over the annealed film is much larger than unity, the values of $\varepsilon''_{dep}/\varepsilon''_{ann}$ are characterized by an average of 12 with standard deviation 1.6. The relatively small fluctuation of these numbers with deposition condition implies that $\varepsilon''_{dep}/\varepsilon''_{ann} \approx 12$ is a robust result that is not very sensitive to deposition temperature in the range from $0.62T_g$ to $0.80T_g$ and to

deposition rate in the range 0.94 to 6.0 nm/s. In order to explain the observation of $\varepsilon''_{dep} \approx 12\varepsilon''_{ann}$, different scenarios can be envisioned: annealing reduces the relaxation amplitude, annealing increases the dielectric relaxation time scale $\tau_D$, or a combination of these two effects. A very plausible explanation for an annealing induced drop in $\varepsilon''$ at a virtually constant dipole density and temperature is a considerable increase in the fraction of ring-like configurations and the concomitant reduction of the Kirkwood correlation factor $g_K$. An increase of $\tau_D$ could emerge from the annealing induced development of hydrogen-bonding. Either scenario points towards a structural change away from uncorrelated molecules closer to the hydrogen-bonded structures that are characteristic of the ordinary liquid.

To scrutinize the notion of an amplitude reduction quantitatively, we determine what a factor of 12 regarding $\Delta\varepsilon$ means in terms of a change of $g_K$. For the purpose of calculating the Kirkwood correlation factor, the ordinary equilibrium liquid can be characterized by $\varepsilon_\infty$ = 2.2 and $\varepsilon_s$ = 2.7[22] i.e., $\Delta\varepsilon$ =0.5, as well as $M$ = 130.23 g/mol, $\rho$ = 0.93 g/cm$^3$, and $\mu$ = 1.68 D. Inserting these values into eq. (5.1) yields a correlation factor $g_K$ = 0.11 for the ordinary liquid, consistent with literature values.[12,19,20,21,22] The minimum value of $g_K$ for the average as-deposited situation is then estimated by replacing $\Delta\varepsilon$ =0.5 by 12×$\Delta\varepsilon$, with all other parameters unchanged, assuming that $g_K$ = 0.11 is the lowest value that 4M3H can assume. For this situation eq. (5.1) yields $g_K \geq 1.1$, consistent with practically uncorrelated dipole orientations and possibly some chain formation in the as-deposited films. Therefore, such a higher dielectric relaxation

amplitude is expected when the deposition conditions do not give the molecules sufficient time to rearrange into ring-like configurations.

That this estimate yields only a lower bound for $g_K$ is a consequence of the dielectric data not providing $\Delta\varepsilon$ directly. Instead, it is observed in Fig. 5.2 that the present frequency range captures the high frequency wing of the loss profile, with slopes $\partial\lg\varepsilon''/\partial\lg\nu \approx -0.5$ for both the as-deposited and the annealed sample (see Fig. 5.2, where at a given $T$ the curves reveal reductions in $\varepsilon''$ by about a factor of 10 for an increase in frequency by two decades). This slope is near the value of –0.4 found for the ordinary supercooled liquid.[12,22] For the as-deposited sample, the loss at the lowest frequency, $\nu$ = 200 Hz, is $\varepsilon''$ = 0.35. The minimum value for $\Delta\varepsilon$ can be estimated from a Cole-Davidson type dielectric profile,

$$\hat{\varepsilon}(\omega) = \varepsilon'(\omega) - i\varepsilon''(\omega) = \varepsilon_\infty + \frac{\Delta\varepsilon}{(1+i\omega\tau)^\gamma} \ , \qquad (5.2)$$

with $\Delta\varepsilon$ set to unity and $\gamma$ = 0.5, which defines the slope, $\partial\lg\varepsilon''/\partial\lg\nu$, at high frequencies. Numerically, such a loss profile reaches $\varepsilon''_{max}$ = 0.35 (at $\nu = \nu_{max}$) and the highest loss value followed by a slope $\partial\lg\varepsilon''/\partial\lg\nu \approx -0.5$ is about 0.3 (at $\nu \approx 2\nu_{max}$) . Therefore, observing $\varepsilon''$ = 0.35 at the low frequency end of a loss segment with the logarithmic slope of –0.5 implies a $\Delta\varepsilon$ = 0.35/0.3 = 1.2 for the as-deposited film if $\nu_{max} \approx$ 100 Hz, and higher for the more likely case that $\nu_{max} <<$ 100 Hz. The smallest possible $\Delta\varepsilon$ of the annealed film should be that of the ordinary liquid, $\Delta\varepsilon$ = 0.5, so that the as-deposited film should display a $\Delta\varepsilon$ = 12×0.5 = 6 or higher, consistent with the lower bound of 1.2. A

liquid with the same dipole density but strongly favoring chain formation is the isomer 6-methyl-3-heptanol, with $\Delta\varepsilon = 27$ and $g_K = 4.2$ near its $T_g$, values that may serve as upper bounds for 4M3H. Even if the as-deposited film had this maximal value $\Delta\varepsilon = 27$, a reduction by a factor of 12 would bring the correlation factor down to $g_K \approx 0.4$, implying anti-correlated dipoles and ring-like configurations in the films annealed at $T = 162$ K.

Annealing of the vapor deposited films is accompanied by a significant reduction in the level of the dielectric loss in the 200 Hz to 20 kHz range, as evident from Fig. 5.1, Fig. 5.2, Fig. 5.4, Fig. 5.5, and Table 5.1. Based on the estimate of the $g_K$ change associated with annealing, waiting at $T = 162$ K ($= T_g$) or scanning towards temperatures in excess of $T_g$ can be understood as facilitating ring formation and the concomitant dipole cancellation that leads to the small dielectric constant in the annealed film, but contributions from changes in the relaxation times cannot be excluded. A trace of isothermal annealing at $T = 162$ K is shown in Fig. 5.5, and the longer time approach towards equilibrium is approximated by an exponential decay regarding $\varepsilon''(\nu = 1$ kHz) with time constant $\tau_{ann} = 2\times10^3$ s, somewhat larger than the dielectric Debye time of $\tau_D = 3\times10^2$ s at $T = 162$ K. Recall that equilibration of the supramolecular structures and $g_K$ was found to occur on the time scale of $\tau_D$ in supercooled alcohols.[12,28] It can also be observed in Fig. 5.5 that the initial ($t < 1500$ s) decay rate is slower than the long time limit. Both features, the large value of $\tau_{ann}$ relative to $\tau_D$ and the time evolution of $\tau_{ann}$, could indicate a slightly enhanced kinetic stability over the ordinary glass or liquid.

By the time a sample has completed 'run 2', the system appears to be near its steady state condition because the changes at $T_g$ towards the end of the time scale in Fig. 5.5

become minute, and a subsequent excursion to 190 K induces only minor additional reductions in $\varepsilon''$, as the curve for 'run 2' is much closer to that of 'run 3' relative to that of 'run 1' in all cases, see Fig. 5.1. Still, the final 'run 3' traces, i.e., $\varepsilon''(\nu = 1\ \text{kHz})$ versus $T$, for all PVD samples with $\varepsilon''_{\text{dep}} >> \varepsilon''_{\text{ann}}$ fail to match the bulk curve of Fig. 5.3, which is characterized by a loss peak at $T = 185$ K where $\varepsilon''(\nu = 1\ \text{kHz})$ reaches a level of 0.1. The dielectric loss values are relatively high and frequency dependent in these films, see Fig. 5.2, which excludes crystallization as an explanation for the unusual dielectric behavior. In fact, the PVD samples display no loss peak (for $\nu > 100$ Hz) below the temperature at which the sample evaporates, around $T = 205$ K. This suggests that the PVD film of 4M3H in this metastable state is subject to frustrated dynamics and altered supramolecular structures relative to the ordinary liquid, even after annealing above $T_g$. Applying the arguments following eq. (5.2) to the data at $T_g + 40$ K would place the loss peak frequency in the range from $\nu_{\text{max}} = 1$ Hz to 100 Hz, i.e., much below the $\nu_{\text{max}} \approx 3$ kHz of the ordinary liquid.

Above the $T_g$ of the ordinary liquid, the loss amplitude of the annealed film in the situation of 'run 3' is higher than that of the regular equilibrium liquid. This can be derived from the observation that the curves labeled 'run 3' in Fig. 5.1 and Fig. 5.4 reach values around $\varepsilon''_{\text{max}} = 0.4$, implying that the PVD films near 200 K have higher loss amplitudes than the regular liquid, $\varepsilon''_{\text{max}} = 0.1$, see Fig. 5.3. An estimate based on the data of Fig. 5.2, $\varepsilon''(\nu = 200\ \text{Hz}) = 0.7$, and the approach outlined using eq. (5.2) with $\partial \lg \varepsilon'' / \partial \lg \nu \approx -0.5$ yields $\Delta\varepsilon \geq 2.3$, whereas the ordinary liquid shows $\Delta\varepsilon = 0.4$ at 200 K. Therefore, even 40 K above the $T_g$ of the ordinary liquid, these liquids prepared by PVD

appear to possess at least 6 times the dielectric relaxation amplitude of the ordinary liquid at the same temperature. It should be kept in mind that the small dielectric constant of the regular supercooled liquid in the range $T = T_g$ to 200 K is a matter of cancellation of large dipoles, and that $g_K$ can change considerably with temperature. In fact, the ordinary liquid displays a rapid rise of $\varepsilon''_{max}$ upon heating above 240 K as a results of a diminished preference for ring-like structures,[21] but even at 300 K the level of $\varepsilon''_{max}$ does not exceed 0.2. Similarly, it is possible that the ring-like structures in the annealed films are not as robust as those in the ordinary supercooled state, leading to their disintegration that sets in already at a temperature below 240 K and thus giving rise to an increase in $\Delta\varepsilon$. Regardless of how the high dielectric relaxation amplitudes of the PVD films are explained, it remains that physical vapor deposition leads to considerably different dielectric properties and thus structures relative to the ordinary liquid, and that these differences persist well above $T_g$. As a point of reference, the Debye time of supercooled 4M3H at $T = T_g + 40$ K is $\tau_D \approx 50$ μs,[12] implying that the supramolecular structure would have equilibrated practically instantaneously (relative to the scan rate of 0.5 K/min) if the film was similar to the ordinary liquid in this regard. Unfortunately, the evaporation of the sample within the vacuum cryostat limits the temperature range of this study, so that dielectric relaxation time constants or the temperature at which the sample would revert to true equilibrium cannot be determined.

In the liquid state, different supramolecular structures related to hydrogen bonding motifs are associated with different densities[23] and dielectric relaxation times.[28] For instance, under isochronal conditions, a pressure of about 800 MPa leads to an increase of

the loss peak value, $\varepsilon''_{max}$, by a factor of ten,[23] indicating that ring structures demand a relatively high amount of volume. As this is factor is near the enhancement value of the loss observed for the as-deposited glass, it may be inferred that these films have an initial density that is considerably higher that of the glass obtained by ordinary cooling techniques. Therefore, the annealing induced formation of the ring-like structures that characterize the ordinary liquid may require an expansion of the film, while being molecularly tethered via hydrogen-bonding to the substrate surface. This could be a further factor in preventing the recovery of the equilibrium state just above $T_g$.

Observing a significantly altered dielectric behavior of a hydrogen bonding liquid that is induced by vapor deposition onto $T_{dep} < T_g$ and that persists well above $T_g$ is not a new feature. As reported by Wübbenhorst and collaborators,[17,18] various vapor deposited polyols have shown increased dielectric relaxation amplitudes in the liquid state by factors of up to 4.5. As an example, a 126 nm film of glycerol was observed to have a $\Delta\varepsilon$ that is 3.7 times that of the ordinary supercooled liquid as well as time constants that were larger by a factor of 4.5, and this state persisted at temperatures of $T_g$ + 50 K. Kasina *et al.* have proposed a picture of rotational diffusion of 'rigid polar clusters' with sizes of order 4-5 nm to explain the high kinetic stability, the specific calorimetric signatures, the enhanced strength, and the longer time scale associated with the dielectric α-relaxation. Glycerol differs from the 4M3H situation in that its Kirkwood correlation factor is well above unity near $T_g$, not well below unity as is the case for 4M3H.

Because the dipole density of 4M3H is virtually independent of sample preparation (vapor deposition versus cooling the liquid at moderate rates), changes in the dielectric

relaxation amplitude, $\Delta\varepsilon$, imply changes in the Kirkwood correlation factor, $g_K$, and thus in supramolecular structure. As a result, the present findings clearly demonstrate that PVD is capable of modifying the supramolecular arrangement of 4M3H considerably, and that this modification can persist at temperatures well beyond the ordinary glass transition of that alcohol. Qualitatively, such deposition induced modifications of supramolecular structures are analogous to previous effects reported for glycerol and other polyols,[23] and they may explain that vapor deposited amorphous solid water (ASW) does not display the dielectric amplitude expected on the basis of bulk water.[30]

**5.6 Summary and Conclusion**

The liquid 4-methyl-3-heptanol is a monohydric alcohol that readily forms a glass upon cooling. Near its glass transition at $T_g$ = 162 K, the supercooled 4M3H displays a very low dielectric constant ($\Delta\varepsilon \approx 0.5$) relative to its dipole density, indicative of hydrogen-bonded ring-like supramolecular structures that lead to dipole moment cancellation and a small Kirkwood correlation factor of $g_K \approx 0.1$. As a result, the dielectric relaxation behavior of 4M3H is very sensitive to changes in the supramolecular structure. Vapor deposition of 4M3H onto a substrate held at a temperature of $0.99T_g$ generates a film that has virtually the same dielectric behavior (and thus the same structure) as the samples prepared by supercooling the melt.

We have vapor deposited films of 4M3H onto interdigitated electrode cells held at temperatures well below the $T_g$ of the ordinary liquid. In the glassy state of these films, we observe dielectric loss levels that are higher than those of the supercooled liquid, and annealing at $T_g$ = 162 K leads to a reduction of $\varepsilon''(\nu = 10$ kHz) by a factor of around 10.

A very plausible explanation for these features is that vapor deposition did not give the molecules sufficient time to arrange in the ring-like structures that are required for the slower dynamics and the low loss levels of the ordinary liquid. Subsequent annealing at $T_g$ then facilitates a structural change that is consistent with effective dipole cancellation and the concomitant reduction in dielectric amplitudes and $g_K$. Surprisingly, further heating the film up to temperatures of $T_g$ + 40 K fails to restore the structure and dynamics of the ordinary liquid, even though supercooled 4M3H would structurally relax within about 50 μs at $T_g$ + 40 K. Instead, the dielectric loss data suggests that these vapor deposited films have a higher dielectric relaxation amplitude and longer relaxation times than the same material prepared by cooling the melt. In conclusion, the vapor deposited films appear to have supramolecular structures that differ considerably from those of the ordinary liquid, and this feature persists when heating the film to $T_g$ + 40 K at the slow rate of 0.5 K/min.

**5.7 References**


1 C. J. F. Böttcher, *Theory of Electric Polarization, Vol 1* (Elsevier, Amsterdam, 1973).

2 R. Böhmer, C. Gainaru, and R. Richert, Physics Reports **545**, 125 (2014).

3 C. Hansen, F. Stickel, T. Berger, R. Richert, and E. W. Fischer, J. Chem. Phys. **107**, 1086 (1997).

4 T. A. Litovitz and G. E. McDuffie, J. Chem. Phys. **39**, 729 (1963).

5 L.-M. Wang and R. Richert, J. Chem. Phys. **123**, 054516 (2005).

6 L.-M. Wang, Y. Tian, R. Liu, and R. Richert, J. Chem. Phys. **128**, 084503 (2008).

7 B. Jakobsen, C. Maggi, T. Christensen, and J. C. Dyre, J. Chem. Phys. **129**, 184502 (2008).

[8] H. Huth, L.-M. Wang, C. Schick, and R. Richert, J. Chem. Phys. **126**, 104503 (2007).

[9] Y. Z. Chua, A. R. Young-Gonzales, R. Richert, M. D. Ediger, and C. Schick, J. Chem. Phys. **147**, 014502 (2017).

[10] H. Fröhlich, *Theory of Dielectrics* (Clarendon, Oxford, 1958).

[11] W. Dannhauser, J. Chem. Phys. **48**, 1911 (1968).

[12] L. P. Singh, C. Alba-Simionesco, and R. Richert, J. Chem. Phys. **139**, 144503 (2013).

[13] S. S. N. Murthy, J. Phys. Chem. **100**, 8508 (1996).

[14] S. F. Swallen, K. L. Kearns, M. K. Mapes, Y. S. Kim, R. J. McMahon, M. D. Ediger, T. Wu, L. Yu, and S. Satija, Science **315**, 353 (2007).

[15] M. Tylinski, M. S. Beasley, Y. Z. Chua, C. Schick, and M. D. Ediger, J. Chem. Phys. **146**, 203317 (2017).

[16] M. Tylinski, Y. Z. Chua, M. S. Beasley, C. Schick, and M. D. Ediger, J. Chem. Phys. **145**, 174506 (2016).

[17] Y. Chen, W. Zhang, and L. Yu, J. Phys. Chem. B **120**, 8007 (2016).

[18] Y. Chen, M. Zhu, A. Laventure, O. Lebel, M. D. Ediger, and L. Yu, J. Phys. Chem. B **121**, 7221 (2017).

[19] S. Capponi, S. Napolitano, and M. Wübbenhorst, Nat. Commun. **3**, 1233 (2012).

[20] A. Kasina, T. Putzeys, and M. Wübbenhorst, J. Chem. Phys. **143**, 244504 (2015).

[21] L. Yang, A. Guiseppi-Wilson, and A. Guiseppi-Elie, Biomed. Microdevices **13**, 279 (2011).

[22] H.-B. Yu, M. Tylinski, A. Guiseppi-Elie, M. D. Ediger, and R. Richert, Phys. Rev. Lett. **115**, 185501 (2015).

[23] M. C. Zaretsky, L. Mouyad, and J. R. Melcher, IEEE Trans. Electr. Insul. **23**, 897 (1988).

[24] W. Dannhauser, J. Chem. Phys. **48**, 1918 (1968).

[25] S. S. N. Murthy and M. Tyagi, J. Chem. Phys. **117**, 3837 (2002).

[26] S. Bauer, K. Burlafinger, C. Gainaru, P. Lunkenheimer, W. Hiller, A. Loidl, and R. Böhmer, J. Chem. Phys. **138**, 094505 (2013).

[27] S. Bauer, H. Wittkamp, S. Schildmann, M. Frey, W. Hiller, T. Hecksher, N. B. Olsen, C. Gainaru, and R. Böhmer, J. Chem. Phys. **139**, 134503 (2013).

[28] S. Pawlus, M. Wikarek, C. Gainaru, M. Paluch, and R. Böhmer, J. Chem. Phys. **139**, 064501 (2013).

[29] A. R. Young-Gonzales and R. Richert, J. Chem. Phys. **145**, 074503 (2016).

[30] A. L. Agapov, A. I. Kolesnikov, V. N. Novikov, R. Richert, and A. P. Sokolov, Phys. Rev. E **91**, 022312 (2015).

# CHAPTER 6

# FURTHER INVESTIGATION INTO ELECTRORHEOLOGICAL EFFECTS

This chapter will look further into the "entropy" effect discussed in chapter 3. Here we measure the third harmonic of glycerol and model the contributions from the different nonlinear effects (saturation, 'chemical' effect, frustrated dynamics, and accelerated dynamics) contribute to the overall "hump" feature of the third harmonic signature. In the second part of this chapter we look at the nonlinear effects at the fundamental frequency and the third harmonic of highly polar propylene carbonate derivatives. These highly polar materials display a narrow relaxation peak, similar to the Debye type peaks seen in monohydroxyl alcohols. The work I contributed to this chapter is the third harmonic measurements of glycerol, and the measurement and analysis of the propylene carbonate derivatives containing a hydroxyl or methoxy group.

## 6.1 Third Harmonic Experiments of Non-linear Dielectric Effect vs. a Phenomenological Model

Relaxation experiments performed in the non-linear regime are being recognized for their potential to advance our understanding of liquid dynamics and the glass transition phenomenology. In the case of dielectric relaxation,[1,2] the high electric fields employed to drive the system beyond the linear response regime can modify the permittivity at constant temperature in various ways: 1) an increase of the relaxation amplitude ($\Delta\varepsilon$) by an enhancement of the net dipole moment termed 'chemical' effect;[3,4] 2) a reduction of $\Delta\varepsilon$ by means of dielectric saturation;[5,6,7] 3) accelerated dynamics originating from the sample absorbing energy from a time dependent field;[8,9,10,11] and 4)

frustrated dynamics due to the field induced entropy reduction.[12,13,14] While the chemical effects occur only in particular materials, the three other non-linear dielectric effects will inevitably occur in all polar liquids.

In the situation of harmonic excitation with a sinusoidal field, $E(t) = E_0\sin(\omega t)$, the signatures of non-linearity are seen as changes in the permittivity, $\hat{\varepsilon}(\omega)=\varepsilon'(\omega)-i\varepsilon''(\omega)$, at the fundamental frequency $\omega$. An alternative approach is to detect the third harmonic response, i.e., amplitude and phase of the polarization at the frequency $3\omega$, quantified by the susceptibility $\chi_3(\omega)$ or by $\chi_3(\omega)E_0^2$. Literature results for such $\chi_3(\omega)$ spectra document two main features: a plateau at low frequencies and a peak in $|\chi_3|(\omega)$ with a maximum that is positioned on the frequency axis below the peak frequency, $\nu_{max}$, of the low field dielectric loss, $\varepsilon''(\omega)$.[15] Additionally, the amplitude of this $|\chi_3|$ 'hump' is found to increase with decreasing temperature, an observation that has been used to conclude on a growing number of dynamically correlated molecules, $N_{corr}$, as a supercooled liquid approaches the glass transition via cooling.[16,17] This temperature trend of $N_{corr}$ has been linked to the temperature dependence of the apparent activation energy associated with the primary structural relaxation dynamics.[18,19,20]

The aim of the present study is to employ known properties of three non-linear dielectric effects in order to calculate the changes in the permittivities $\varepsilon'(\omega)$ and $\varepsilon''(\omega)$, the third harmonic susceptibility $\chi_3(\omega)$ and its temperature dependence, as well as the Fourier component of polarization at $5\omega$, quantified by $\chi_5(\omega)$. The sources of non-linearity accounted for in the present model are dielectric saturation, field induced entropy reduction, and energy absorption from a time dependent field. Experimentally,

these three effects can be quantified separately because energy absorption remains absent for a static field, which then reveals the saturation and entropy effect as respective changes of the dielectric relaxation amplitude and relaxation time scale.[14] The consequences of energy absorption can be isolated via a high amplitude ac field experiment, because they dominate on the high frequency side of the loss peak, where the other two effects are negligible. While the individual effects have been characterized, mainly in terms of their impact on the susceptibility at the fundamental frequency ($\chi_1$), their combined higher harmonic responses to large ac fields have not been studied to date. We find that the model captures the low frequency plateau and the 'hump' features in $|\chi_3|$ and $|\chi_5|$, including the increasing amplitude of the $|\chi_3|$ maximum as the temperature is lowered. For the case of glycerol, semi-quantitative agreement with experimental data is achieved. The individual contributions of the three sources of non-linear effects to the $|\chi_3|(\omega)$ spectra are identified.

### 6.1.1 Experiments

The materials employed for this study are glycerol (99.5+%, spectrophotometric grade), *N*-methyl-ε-caprolactam (99%), and 2-methyltetrahydrofuran (99+%, anhydrous), all of which are used as received from Sigma-Aldrich. According to a previous characterization,[21] this glycerol sample has 710 ppm water content and no signatures of conductivity are seen for at least two decades below the loss peak frequency. The sample capacitor cell is made of two spring-loaded polished stainless steel disks (16 and 20 mm ∅), which are separated by a Teflon ring of $d$ = 10 μm thickness with an inner area of 14 mm diameter for the sample. The resulting nominal geometric capacitance is $C_0$ = 136

pF. This cell is loaded with the sample material and then mounted onto the cold stage of a closed-cycle He-refrigerator cryostat Leybold RDK 6-320 with Leybold Coolpak-6200 compressor. Temperature stability within several mK is achieved using a Lakeshore Model 340 temperature controller equipped with DT-470-CU sensor diodes.

Permittivity experiments are performed for frequencies $\nu = \omega/2\pi$ ranging from 1 Hz to 100 kHz using a Stanford Research Systems SRS-830 lock-in amplifier. High voltages are achieved by boosting the sine wave output of the SRS-830 with a Trek PZD-350 amplifier, set to multiply by a factor of 100. The current is measured as voltage drop across a shunt whose impedance is designed to vary from $|Z| = 6$ kΩ at $\nu = 1$ Hz to $|Z| = 8$ Ω at $\nu = 100$ kHz by virtue of a seven component *RC* network. This shunt voltage is routed to the lock-in amplifier input via a linear voltage follower that sustains 500 V at the input, which protects the system against damages from sample failures. The system has been calibrated at every test frequency (1 Hz $\leq \nu \leq$ 10 kHz, step $\Delta \log \nu = 0.125$) with known low loss ($\tan\delta < 10^{-4}$) capacitances.

Lower field permittivity values ($\varepsilon'$, $\varepsilon''$) are recorded using a voltage of 50 $V_{rms}$ applied to the sample, while the lock-in amplifier is set to detect amplitude and phase of the current signal at the fundamental frequency. While non-linear effects are detectable in glycerol at this field, deviations from the low field limits remain below 0.5 %,[22] and are thus negligible for the purpose of determining loss peak positions. The relaxation amplitude $\Delta\varepsilon$ derived from these loss spectra are used to determine the actual sample thickness, which turned out to be $d = 10.5$ μm. As a result, the field corresponding to the 50 $V_{rms}$ voltage has a peak value of $E_0 = 68$ kV cm$^{-1}$.

In order to measure the third harmonic susceptibility, $\chi_3(\omega)$, a voltage of 100 $V_{rms}$ is applied to the sample, leading to a peak field of $E_0$ = 135 kV $cm^{-1}$, and the lock-in unit is set to analyze at the third harmonic frequency. These measurements are conducted for frequencies $\nu/3$, where $\nu$ are the frequencies (1 Hz ≤ $\nu$ ≤ 10 kHz) at which the system had been calibrated. In this manner, calibration data is valid at the third harmonic, i.e., at $3\times(\nu/3) = \nu$. The signal-to-noise ratio is improved by performing a sequence of 50 measurements at the field $E_0$ = 135 kV $cm^{-1}$ at each frequency, followed by 50 measurements at a lower field of $E_0$ = 27 kV $cm^{-1}$ to allow for sample recovery. For an individual measurement, the voltage is applied for the greater of 27 periods or 1.1 second, with the initial 9 periods or 0.1 second used for equilibration and the subsequent 18 periods or 1 second used for data acquisition. The final result is calculated from the average of 50 such measurements. Third harmonic results are reported in terms of the frequency dependent quantity

$$\left|\chi^3\right|E_0^2 = \frac{\left|I_{3\omega}\right|/\left|V\right|}{3\omega C_0} = \frac{\left|P_{3\omega}\right|}{\varepsilon_0 E_0}\ , \tag{6.1}$$

where $V$ is the applied voltage, and $I_{3\omega}$ and $P_{3\omega}$ denote the $3\omega$ Fourier components of current and polarization, respectively.

### 6.1.2 Model Considerations

In order to model non-linear dielectric effects, the sample is considered a dielectric at constant temperature between electrodes with uniform separation $d$, so that an applied voltage $V(t)$ leads to a uniform electric field $E(t) = V(t)/d$. For the present study, only harmonic fields characterized by a peak amplitude $E_0$ and frequency $\omega = 2\pi\nu$ are

considered, $E(t) = E_0\sin(\omega t)$, with zero bias (dc) field. The dielectric is characterized by its permittivity, $\hat{\varepsilon}(\omega) = \varepsilon'(\omega) - i\varepsilon''(\omega)$, and expressed as superposition of Debye type contributions subject to the probability density $g(\tau)$ regarding the time constants, $\tau$,

$$\hat{\varepsilon}(\omega) = \varepsilon_\infty + \int_0^\infty \frac{\Delta\varepsilon}{1+i\omega\tau} g(\tau) d\tau \approx \varepsilon_\infty + \sum_{i=1}^{N} \frac{\Delta\varepsilon_i^0}{1+i\omega\tau_i} \quad . \tag{6.2}$$

The relaxation amplitude is defined as $\Delta\varepsilon = \sum_i \Delta\varepsilon_i^0 = \varepsilon_s - \varepsilon_\infty$, with $\varepsilon_s$ and $\varepsilon_\infty$ being the low and high frequency limits of the permittivity, respectively. The superscript '0' indicates values associated with the low field limit. The function $g(\tau)$ can be determined from a Havriliak-Negami (HN) fit to the permittivity data.[23] In order to match the case of glycerol, the HN parameters are set to $\alpha_{HN} = 0.94$, $\gamma_{HN} = 0.64$, with $\tau_{HN}$ following a Vogel-Fulcher-Tammann (VFT) relation according to $\log_{10}(\tau_{HN}/\text{s}) = A + B/(T - T_0)$, with $A = -15.25$, $B = 1065$ K, and $T_0 = 126$ K. The temperature dependence of $\varepsilon_s$ is approximated by the empirical relation $\varepsilon_s = -24.08 + 19456\text{ K} / T$,[24] while a value of 3 is used for $\varepsilon_\infty$.

The initial condition of the model system is defined by the absence of an electric field, $E(t < 0) = 0$, and the depolarized state of the dielectric, i.e., with polarization $P(t < 0) = 0$. For times $t \geq 0$, the applied field is given by $E(t) = E_0\sin(\omega t)$. For the numerical calculation, the spectrum of retardation times, $g(\tau)$, is approximated by a discrete sum of ($N = 170$) modes indexed by '$i$' with time constants $\tau_i$, see Eq. (6.2). For each mode the polarization $P_i(t)$ changes in time according to the differential equation

$$\frac{dP_i(t)}{dt} = \frac{\varepsilon_0 \Delta\varepsilon_i(t) E(t)}{\tau_i(t)} - \frac{P_i(t)}{\tau_i(t)}\,, \tag{6.3}$$

with $\varepsilon_0$ = 8.854×10$^{-12}$ AsV$^{-1}$m$^{-1}$. From the individual $P_i(t)$'s, the total polarization is obtained via

$$P(t) = (\varepsilon_\infty - 1)\varepsilon_0 E(t) + \sum_i P_i(t) = P_\infty + \Delta P(t)\,. \tag{6.4}$$

In the linear response case, i.e., when $P \propto E$, the values of $\tau_i$ and $\Delta\varepsilon_i$ in Eq. (6.3) would be time invariant and the resulting $P(t)$ would recover the original HN permittivity. In the present approach, the small deviations from linear response are introduced by the high electric fields modifying the time constant $\tau_i$ and the relaxation amplitude $\Delta\varepsilon_i$ of each dielectric mode, thereby leading to time dependent parameters, $\tau_i(t)$ and $\Delta\varepsilon_i(t)$. The fact that these deviations from linearity remain below the 1% level justifies using these terms within linear response relations as good approximations. This is analogous to the time-honored models of physical aging, where the non-linear effect of a temperature change is accounted for by a temperature $T$ and structure (fictive temperature, $T_{fic}$) dependent relaxation time.[25,26] In the present context, field $E$ and polarization $P$ take the roles of $T$ and $T_{fic}$, respectively. The fictive temperature of a non-equilibrium system is the temperature at which the equilibrium counterpart would show the same property under consideration, e.g., the same relaxation time.

In general, four distinct non-linear dielectric effects have been established to occur in simple liquids: reduction of the relaxation amplitude $\Delta\varepsilon$ by dielectric saturation,[5,6,7] enhancement of $\Delta\varepsilon$ by chemical effects (increase of net dipole moments),[3,4] reduction of

time constants $\tau$ by energy absorption,[8,9,10,11] and an increase of $\tau$ values through a field induced lowering of the thermodynamic entropy.[12,13,14] Since glycerol displays no known chemical effect, only the three other sources of non-linear behavior will be considered in what follows.

A material will absorb energy from a time dependent field whenever the loss $\varepsilon''$ at the relevant frequency is not negligible.[1] In the present case of low frequencies (relative to vibrational modes), the effect amounts to an increase of the mode specific fictive temperatures, $T_i$, whose magnitude is a matter of the balance between a Joule 'heating' term and thermal relaxation of $T_i$ towards the bath temperature $T$.[8,21,27,28] As has been discussed and experimentally verified extensively in the literature,[29,30,31,32,33] the time dependence of $T_i$ follows the relation

$$\frac{dT_i(t)}{dt} = \left(\frac{\partial P_i(t)}{\partial t}\right)^2 \frac{\tau_i(t)}{\varepsilon_0 \Delta\varepsilon_i(t) \times \rho\Delta C_i f_C} - \frac{T_i(t) - T}{\tau_i(t)} \quad , \tag{6.5}$$

where $\rho\Delta C_i = \rho\Delta C(\Delta\varepsilon_i^0/\Delta\varepsilon)$ quantifies the heat capacity contribution of mode '$i$', with the total glass-to-liquid heat capacity step of glycerol being $\rho\Delta C$ = 1.2 J K$^{-1}$ cm$^{-3}$. Because only the configurational fraction of the experimentally determined excess heat capacity step should be relevant in Eq. (6.5), the factor $f_C = C_{cfg}/C_{exc}$ is included, which has been found to be $f_C$ = 0.8 for glycerol.[14,34] The impact of ($T_i - T$) on the time constants $\tau_i$ is via the overall activation parameter, $\partial \ln \tau_\alpha / \partial T$ (see below), whereas the relaxation amplitude $\Delta\varepsilon_i$ is considered independent of $T_i$.

When a static electric field $E_0$ polarizes a dielectric at constant temperature, the thermodynamic entropy $S$ is modified relative to its zero field value according to[35]

$$\Delta_E S = \frac{\varepsilon_0 M}{2\rho}\frac{\partial \varepsilon_s}{\partial T}\times E_0^2 \ , \tag{6.6}$$

where $M$ = 92.09 g mol$^{-1}$ is the molar mass and $\rho$ the density, which for glycerol is $\rho(T)$ = $\rho_0$ (1−$\alpha T$) with $\rho_0$ = 1.521 g cm$^{-3}$ and $\alpha$ = 6.01×10$^{-4}$ K$^{-1}$.[36] The sign of $\Delta_E S$ is usually negative, because $\partial\varepsilon_s/\partial T$ < 0 is observed for most liquids. [12] A possible connection between configurational entropy and relaxation time is given by the Adam-Gibbs (AG) model of super-Arrhenius type dynamics in glass forming liquids,[37] which is often expressed in terms of the more easily accessible excess entropy,

$$\log(\tau/s) = A_{AG} + \frac{C_{AG}}{TS_{exc}(T)} \ . \tag{6.7}$$

Here, the excess entropy, $S_{exc}(T)$, is the difference between the liquid and the crystal entropies and, within the AG model of Eq. (6.7), its magnitude determines how the apparent activation energy changes with temperature. The case of glycerol can be approximated by the parameters $C_{AG}$ = 67.4 kJ mol$^{-1}$ and $S_{exc}(T) = S_\infty(1 - T_K/T)$ with $S_\infty$ = 105 J K$^{-1}$ mol$^{-1}$ and $T_K$ = 140 K. Assuming that the AG relation applies also to field induced entropy changes,[12] the steady state effect of a static high field of magnitude $E_0$ on dielectric retardation times can be written as

$$\Delta_E \ln\tau = -\frac{\ln(10) C_{AG}}{T\times S_{exc}^2(T)}\frac{f_{S,E}}{f_{S,T}}\frac{\varepsilon_0 M}{2\rho}\frac{\partial\varepsilon_s}{\partial T}\times E_0^2 \ , \tag{6.8}$$

where $f_S = S_{cfg}/S_{exc}$ denotes the configurational fraction of the excess entropy,[38] with $f_{S,E}$ and $f_{S,T}$ denoting this fraction for field and temperature induced entropy changes,

respectively. Experimentally, a value of $f_{S,E}/f_{S,T}$ = 0.64 has been found to quantify this static field effect for glycerol.[39]

The magnitude of the dielectric saturation effect is determined experimentally for glycerol using a static field of $E_0$ = 225 kV cm$^{-1}$, where a reduction of –0.45% in $\Delta\varepsilon$ is observed. Assuming a quadratic dependence on the static electric field $E_0$, saturation in glycerol can by quantified by

$$\Delta_E \ln \Delta\varepsilon = -8.9\times10^{-11}\ \mathrm{V}^{-1}\ \mathrm{m}\times E_0^2\ , \tag{6.9}$$

which represents the relative change in $\Delta\varepsilon$ induced by a static field $E_0$.

Both factors introduced above, $\Delta_E \ln\tau$ and $\Delta_E \ln\Delta\varepsilon$, are steady state quantities that vary quadratically with field $E_0$. Following a field step, it has been observed that the field induced changes in relaxation time and amplitude approach their steady state values by tracking the time dependence of $\Delta P^2(t)$, i.e., the square of the relaxing polarization contribution.[38,40,41] Therefore, the time dependence of the entropy effect, Eq. (6.8), and of dielectric saturation, Eq. (6.9), can be accounted for by a common term $[\Delta P(t)/(\varepsilon_0\Delta\varepsilon E_0)]^2$, which represents the square of the time dependent polarization, $\Delta P(t)$, divided by its steady state value, $\Delta P(t\rightarrow\infty)$.

With the parameters given above, each individual component of the present model (energy absorption, entropy reduction, and saturation) has been found to describe the respective separate non-linear dielectric effect for glycerol as gauged by the changes in the permittivity, i.e., at the fundamental frequency.[14,21,28,33,38,39] Based on the above relations, we are now in the position to formulate how the time dependent parameters $\tau_i(t)$

and $\Delta\varepsilon_i(t)$ can be determined from their respective low field values, $\tau_i^0$ and $\Delta\varepsilon_i^0$. Two distinct scenarios can be envisioned for these structural recovery functions: the 'multiple fictive temperature' case where $\tau_i(t)$ and $\Delta\varepsilon_i(t)$ are governed by polarization state ($P_i$) and fictive temperature ($T_i$) of only the particular mode '*i*' in question, and the 'single fictive temperature' case where $\tau_i(t)$ and $\Delta\varepsilon_i(t)$ are governed by the average polarization state ($\Delta P$) and average fictive temperature ($T_{fic}$) of the entire sample.

The relations for the situation in which modes are mutually independent regarding structural recovery (multi-$T_f$) read

$$\tau_i(t) = \tau_i^0 \times \left(1 + \left(\frac{P_i(t)}{\varepsilon_0 \Delta\varepsilon_i^0 E_0}\right)^2 \times \Delta_E \ln\tau_i + \left(T_i(t) - T\right)\frac{\partial \ln\tau_\alpha}{\partial T}\right), \tag{6.10a}$$

$$\Delta\varepsilon_i(t) = \Delta\varepsilon_i^0 \times \left(1 + \left(\frac{P_i(t)}{\varepsilon_0 \Delta\varepsilon_i^0 E_0}\right)^2 \times \Delta_E \ln\Delta\varepsilon_i\right). \tag{6.10b}$$

For the case of a single fictive temperature, the mode specific quantities $P_i(t)$ and $T_i(t)$ in Eq. (6.10a) and $P_i(t)$ in Eq. (6.10b) have to be replaced by their respective averages, $T_{fic} = \langle T_i \rangle$ and $\Delta P = \langle P_i \rangle$. In Eq. (6.10a) the activation quantity $\partial \ln\tau_\alpha/\partial T$ would be obtained from the VFT parameters via $-B\ln(10)/(T-T_0)^2$.

The next step is to calculate the total non-linear polarization and its Fourier components, with all three sources of non-linear behavior accounted for. To this end, the differential equations, Eq. (6.3) and Eq. (6.5), are solved for all modes '*i*' of the sum of Eq. (6.2) with $\tau_i(t)$ and $\Delta\varepsilon_i(t)$ given by either version of Eq. (6.10). Each period of the resulting polarization, $P(t)$, is subject to Fourier analysis according to

$$P'_n(\omega)=\frac{\omega}{\pi}\int_{t}^{t+2\pi/\omega}\sin(n\omega t')P(t')dt' \quad , \quad P''_n(\omega)=\frac{\omega}{\pi}\int_{t}^{t+2\pi/\omega}\cos(n\omega t')P(t')dt' \quad , \tag{6.11}$$

where $t$ progresses in increments of $2\pi/\omega$. Here, $P'_n$ and $P''_n$ denote the in-phase and out-of-phase amplitudes for the first ($n$ = 1), third ($n$ = 3), or fifth ($n$ = 5) Fourier component of the polarization, $\hat{P}_n(\omega)$, respectively. For each frequency $\omega$, quasi steady state results are achieved by continuing the calculation in time for at least $3\tau_\alpha$, and then until the value of $|\chi_3|$ or $|\chi_5|$ determined for the current period differs less than 0.5% from the value obtained for the previous period. Based on this procedure, steady state values for $\varepsilon'_{lo}$, $\varepsilon''_{lo}$, $(\varepsilon''_{hi}-\varepsilon''_{lo})/\varepsilon''_{lo}$, are determined using

$$\varepsilon'(\omega)=1+\frac{\sqrt{P_1'^2+P_1''^2}}{\varepsilon_0 E_0}\times\cos\arctan(P_1''/P_1'), \tag{6.12a}$$

$$\varepsilon''(\omega)=-\frac{\sqrt{P_1'^2+P_1''^2}}{\varepsilon_0 E_0}\times\sin\arctan(P_1''/P_1'), \tag{6.12b}$$

where the indices 'lo' and 'hi' refer to the zero field limit and the $E_0$ = 135 kV cm$^{-1}$ case, respectively. The low field limit results are obtained by forcing $\tau_i(t) \equiv \tau_i^0$ and $\Delta\varepsilon_i(t) \equiv \Delta\varepsilon_i^0$. The relation employed for determining the third ($n$ = 3) and fifth ($n$ = 5) harmonic result is

$$|\chi_n(\omega)|E_0^{n-1}=\frac{\sqrt{P_n'^2+P_n''^2}}{\varepsilon_0 E_0} \quad . \tag{6.13}$$

Note that this method of determining $\chi_3$ is lacking the factor of 4 used elsewhere.[17]

### 6.1.2 Results and Discussion

For the case of glycerol, the experimental dielectric loss spectra, $\varepsilon''(\omega)$, obtained at a relatively low field of $E_0$ = 68 kV cm$^{-1}$ are recorded for temperatures between 210 K and 219 K. For this field, the deviations from the low field limit are expected to remain below about 0.5%, implying that non-linearities are negligible for the purpose of verifying the dielectric behavior of this $d$ = 10.5 μm thin sample and for quantifying the loss peak frequencies, $\nu_{max}$. These results are compiled as solid symbols in Fig.6.1, which includes the values of $\nu_{max}(T)$ as arrows. For the three lower temperatures, $T$ = 210, 213, and 216 K, third harmonic susceptibility spectra have been obtained, which are shown in Fig. 6.2.

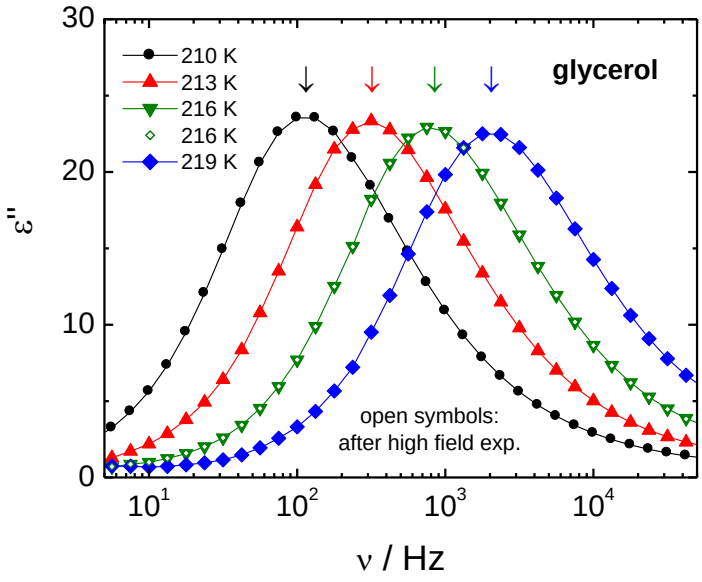


FIG. 6.1. Dielectric loss spectra, $\varepsilon''(\omega)$, for glycerol measured using a relatively low field ($E_0$ = 68 kV cm$^{-1}$) at the four temperatures indicated in the legend. Solid symbols are for the fresh sample, i.e., prior to the high field experiments. Open smaller symbols for $T$ = 216 K are obtained after all high field $\chi_3$ measurements have been completed and they coincide with the solid symbols for $T$ = 216 K. Arrows indicate the loss peak frequency positions, $\nu_{max}$. Lines serve as guides only.

The low field loss peak positions, $\nu_{max}$, are indicated by arrows in this figure. The inset of Fig. 6.2 demonstrates the very good agreement with literature results, after rescaling both curves to a common field of $E_0 \rightarrow 100$ kV cm$^{-1}$ and to the present definition of $\chi_3(\omega)$ in Eq. (6.13). The data for the glassy state at $T = 180$ K in Fig. 6.2 is meant to demonstrate that $|\chi_3|$ is practically zero when no relaxation is present in this frequency window. Repeating a low field measurement after the $\chi_3(\omega)$ data acquisition reveals that all field induced changes are entirely reversible, see open symbols for $T = 216$ K in Fig. 6.1, which coincide with the spectrum taken prior to the high field measurements.

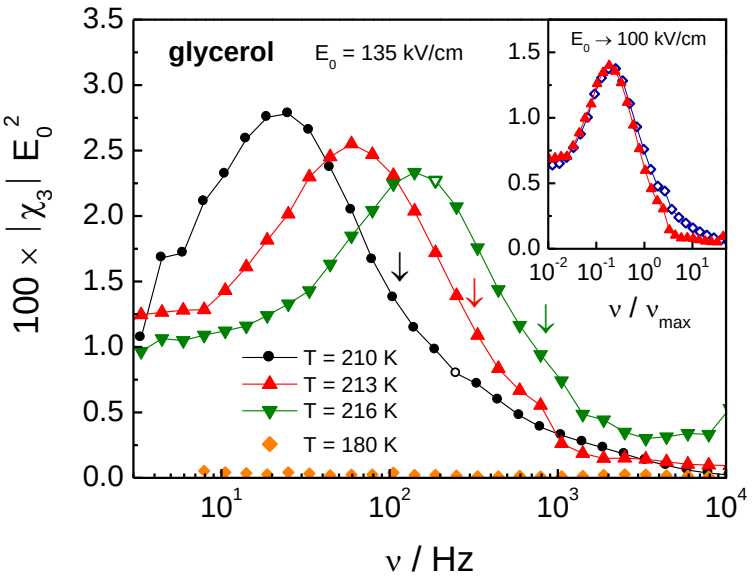


FIG. 6.2. Spectra of the third harmonic susceptibility for glycerol at the four temperatures indicated, reported in terms of the quantity $|\chi_3|E_0^2$. Note that the symbols near zero for $T = 180$ K are for the glassy state. These measurements are based on peak fields of $E_0 = 135$ kV cm$^{-1}$. The two open symbols reflect values determined by interpolation. Arrows indicate the low field loss peak frequency positions, $\nu_{max}$. The inset compares the present results for $T = 213$ K (solid symbols) with those reported by Bauer

*et al.* in ref. 18 (open symbols). Both data sets are field-squared rescaled to $E_0 \rightarrow 100$ kV cm$^{-1}$ and shown on a frequency scale reduced to the peak frequency $\nu_{max}$.

On comparing Fig. 6.2 with Fig. 6.1, it is obvious that the increase of the $|\chi_3|$ maximum heights observed for the lower temperatures greatly exceeds that of the $\varepsilon''$ amplitudes and thus of $\Delta\varepsilon$. The qualitative features seen for glycerol in Fig. 6.2 are observed also for *N*-methyl-ε-caprolactam and 2-methyltetrahydrofuran, but the results are not shown due inferior signal-to-noise levels for these samples. Together with reports of $|\chi_3|(\omega)$ spectra in the literature,[15,17,18,19] this suggests that the $|\chi_3|(\omega)$ results for glycerol are representative of the behavior of many polar glass-forming liquids.

Prior to comparing experiment and model, it should be pointed out that the values that define the magnitude of the saturation and entropy effect are determined from a high static field experiment, while their time dependence is derived from time resolved experiments following a field step.[14,39] The only adjustment that seemed necessary to achieve good agreement with the present $|\chi_3|$ findings was to reduce the saturation level by a factor of two, which then leads to matching the observed low frequency plateau level of $|\chi_3|E_0^2$. The reason for this is not clear, but the value of $\Delta_E \ln\Delta\varepsilon$ had been measured using a field of $E_0 = 225$ kV cm$^{-1}$, i.e., much higher than the present value of $E_0 = 135$ kV cm$^{-1}$. The parameters associated with energy absorption are taken from previous high ac field measurements at frequencies $\nu > \nu_{max}$, where energy absorption clearly dominates the nonlinear effects.[14,21,28,33] It is important to realize that by using ac and dc field protocols and by analyzing the amplitude and relaxation time changes separately, the impacts of the three sources of non-linear behavior can be gauged individually.

With all the required parameters obtained independently (except for the saturation level) and employed as outlined in Section 6.2.2, the model calculation for the three temperatures realized in the experiment gives rise to the curves shown in Fig. 6.3. A key result of this study is that these $|\chi_3|(\omega)$ model curves display all the characteristic features of the experimental results of Fig. 6.2. A more quantitative comparison reveals that the model curves are shifted 0.15 on the $\log_{10}(\nu)$ scale to the right and 5% higher in amplitude relative to the experimental values. We note that the same qualitative features of $|\chi_3|(\omega)$ spectra are obtained for the case of a Debye type response, i.e., repeating the calculation with HN exponents $\alpha_{HN} = \gamma_{HN} = 1$.

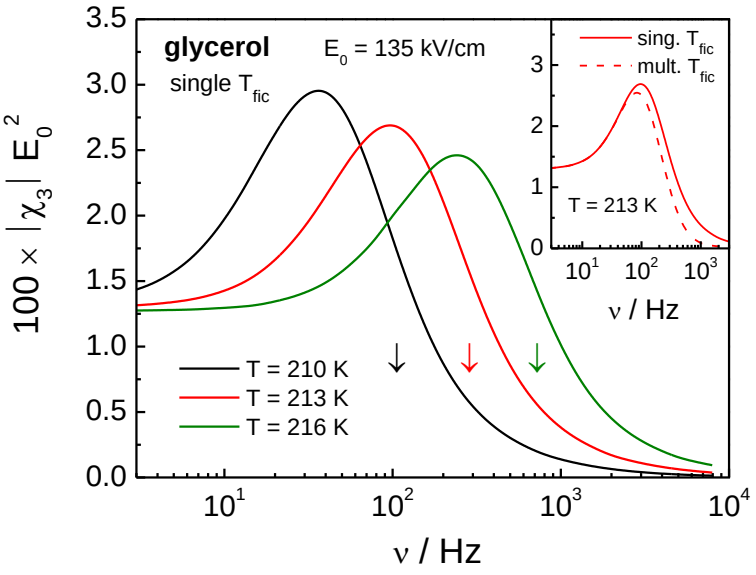


FIG. 6.3. Calculated steady state spectra of the third harmonic susceptibility in terms of $|\chi_3|E_0^2$ at $E_0$ = 135 kV cm$^{-1}$. Curves reflect the case of a single fictive temperature with the parameters selected to represent glycerol at the three temperatures indicated. Arrows indicate the low field loss peak frequency positions, $\nu_{max}$. The inset compares the single versus the multiple fictive temperature scenario for $T$ = 213 K, calculated for otherwise identical parameters.

The inset of Fig. 6.3 compares the single versus the multiple $T_f$ scenarios, i.e., global versus mode-specific structural recovery dynamics. While the difference between these two cases is not substantial, the single-$T_f$ calculation yields somewhat wider $|\chi_3|(\omega)$ spectra that match better the experimental observation. This preference for a single fictive temperature is equally observed in other measurements of structural recovery, namely physical aging and scanning calorimetry.[24,25,42,43]

Although not forced by parameter adjustment, the peak amplitudes, $|\chi_3|_{max}$, of the calculated $|\chi_3|(\omega)$ spectra of Fig. 6.3 agree favorably with the observed values. For instance, the calculated $|\chi_3|_{max}E_0^2$ value at $T$ = 213 K is 0.027, while the experimental counterpart is 0.026. The temperature dependence of the model $|\chi_3|_{max}$ values amounts to a 18.6 % change across the 6 K temperature range, again matching the 18.5% change observed in the experiment. This sensitivity of $|\chi_3|_{max}$ to temperature greatly exceeds that of $\Delta\varepsilon$, so it is of interest to identify the origin of this effect, particularly because this amplitude change is the key ingredient to deriving the number $N_{corr}$ of dynamically correlated particles in the framework of an approach to $\chi_3$ for systems close to a critical point.[16] In the present model, this temperature dependence stems predominantly from the temperature dependent apparent activation energy that is inherent in Eq. (6.10a) via $\Delta_E \ln\tau$ and $\partial \ln\tau_\alpha/\partial T$. A more detailed analysis reveals that the activation parameter $\partial \ln\tau_\alpha/\partial T$ increases by 14% and the relaxation amplitude $\Delta\varepsilon$ increases by 4% when the temperature is reduced from 216 to 210 K. Therefore, the temperature variation of both $\partial \ln\tau_\alpha/\partial T$ and $\Delta\varepsilon$ combined appear to be responsible for the ≈18% amplitude increase of $|\chi_3|_{max}$. The

question remains which of the non-linear effects dominates in creating this 'hump' feature in the $|\chi_3|(\omega)$ spectra.

With the aim of assessing the individual contributions of the three non-linear effects to the $|\chi_3|(\omega)$ spectra, the calculation for $T$ = 213 K has been repeated with only one of the effects activated at a time. Deactivating the effects of saturation, entropy reduction, and energy absorption can be accomplished by respectively setting $\Delta_E \ln \Delta\varepsilon \equiv 0$, $\Delta_E \ln \tau \equiv 0$, or $\partial \ln \tau_\alpha / \partial T \equiv 0$ in Eq. (6.10). The outcomes are shown in Fig. 6.4, which reiterates the total $|\chi_3|(\omega)$ curve as solid line, but includes the third harmonic results for the individual effects of saturation, entropy reduction, and energy absorption. Expectedly, saturation governs the low frequency plateau of $|\chi_3|$, and its impact fades towards higher frequencies. The individual effects of entropy reduction and energy absorption seen in Fig. 6.4 agree with previous assessments of these effects.[44,45]

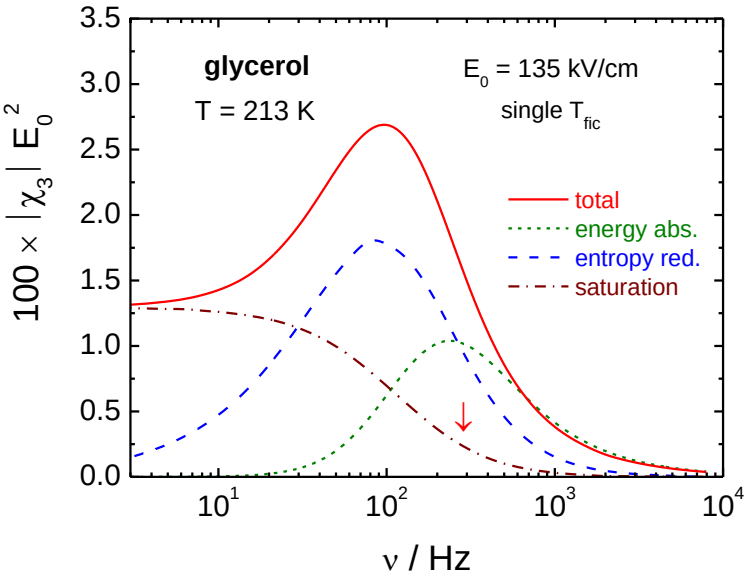


FIG. 6.4. Calculated steady state spectra of the third harmonic susceptibility in terms of $|\chi_3|E_0^2$ at $E_0$ = 135 kV cm$^{-1}$. Curves reflect the case of a single fictive temperature

with the parameters selected to represent glycerol at $T$ = 213 K. The solid line represents the total $\chi_3$ that includes all sources of non-linearity (as in Fig. 6.3), other curves are for the individual contributions from energy absorption, entropy reduction, and saturation (see legend). The arrow indicates the loss peak frequency position, $\nu_{max}$

The 'hump' amplitude appears to be governed by the entropy effect, implying that its temperature variation depends largely on the variation of $\Delta_E \ln \tau$, which in the present model is a matter of the apparent activation energy inherent in the Adam-Gibbs term, Eq. (6.8). The present particular choice of the Adam-Gibbs model for relating dynamics to entropy is computationally convenient, but not considered critical for reproducing this temperature dependence of $|\chi_3|_{max}$. Quite generally, a certain field induced entropy reduction, $\Delta_E S_{cfg}$, will have more impact at a lower temperature, were the configurational entropy of the material, $S_{cfg}(T)$, is decreased and the relative change, $\Delta_E S_{cfg}/S_{cfg}(T)$, is accordingly higher. When comparing the curves representing the three individual contributions in Fig. 6.4, it seems to require a field dependent relaxation time $\tau$ to generate a maximum in $|\chi_3|$. Consistent with calculations for non-interacting dipoles,[46,47,48] the present results for saturation itself (sometimes referred to as trivial effect) yields a monotonic dependence of $|\chi_3|$ on frequency.

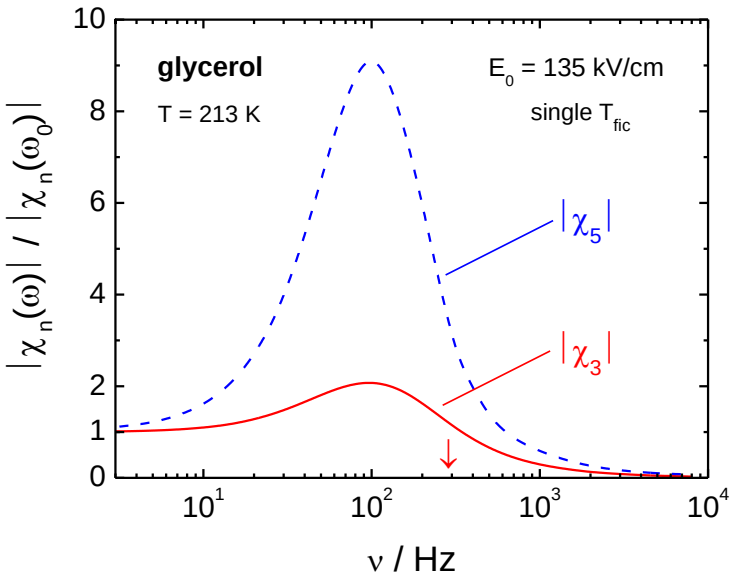


FIG. 6.5. Calculated steady state spectra of the third ($n$ = 3, solid line) and fifth ($n$ = 5, dashed line) harmonic susceptibility in terms of $|\chi_n| E_0^{n-1}$ at $E_0$ = 135 kV cm$^{-1}$. Curves reflect the case of a single fictive temperature with the parameters selected to represent glycerol at $T$ = 213 K. The curves are normalized to unity at a low frequency, $\omega_0 \approx 1$ Hz. The arrow indicates the loss peak frequency position, $\nu_{max}$.

It should be stressed that the present results do not exclude the existence of dynamical correlations as important features of the structure and dynamics of glass-forming materials. For instance, future studies might reveal that such correlations are necessary for rationalizing the field induced increase in viscosity that correlates with the reduction in thermodynamic entropy. What the present study does tell us is that glassy correlations may not be the only approach to understanding non-linear dielectric effects in supercooled liquids.

The fifth harmonic susceptibility of the model glycerol at $T$ = 213 K has also been evaluated, and the result is shown as $|\chi_5|$ in Fig. 6.5, which includes $|\chi_3|$ for

comparison. Both curves, $|\chi_3|(\omega)$ and $|\chi_5|(\omega)$, are normalized to their values at the low frequency end of the calculated spectra, i.e., near 1 Hz. The fifth harmonic susceptibility appears to display a maximum at practically the same frequency position as the $3\omega$ counterpart, but the $|\chi_5|$ peak rises higher than the $|\chi_3|$ curve for the present scaling. The relation of the two peaks is reminiscent of experimental results reported by Albert *et al.* for glycerol,[49] where $|\chi_5|$and $|\chi_3|$ are normalized to their respective low frequency plateau value. In the present model, the Taylor series expansion of $\Delta\varepsilon$ versus field is truncated at the $E_0^2$ term, see Eq. (6.9). For the static limit of the higher Fourier components, this implies a finite value for $|\chi_3|$, but $|\chi_5|$ will eventually approach zero in the $\omega \to 0$ limit. Adding the next non-zero term, $\propto E_0^4$, to the saturation component of the model would generate a low frequency plateau for $|\chi_5|(\omega)$, but its magnitude cannot be determined independently for a complex condensed dipole system such as glycerol. This limitation prohibits a quantitative test of the $|\chi_5| \approx |\chi_3|^2$ feature reported for the experiment of Albert and coworkers.[48] The normalization of $|\chi_n|(\omega)$ to $|\chi_n|(1\text{ Hz})$ in Fig. 6.5 generates overlap also on the high frequency side, similar to what is seen in the experimental curves.[48]

Finally, we show in Fig. 6.6 the non-linear dielectric effect of the present model if analyzed at the fundamental frequency, i.e., if gauged by the field indu6.ced relative change of the dielectric loss. In terms of $\varepsilon''(\omega)$, the strongest modification is observed at the frequencies that exceed the loss peak at $\nu_{max}$, with the position of $\nu_{max}$ indicated by the arrow. These large positive values of $(\varepsilon''_{hi} - \varepsilon''_{lo})/\varepsilon''_{lo}$ for $\nu > \nu_{max}$ as well as the

negative values just below $\nu_{max}$ originate from the energy absorbed from the field and the concomitant increases in the fictive temperature.[21,29,31]

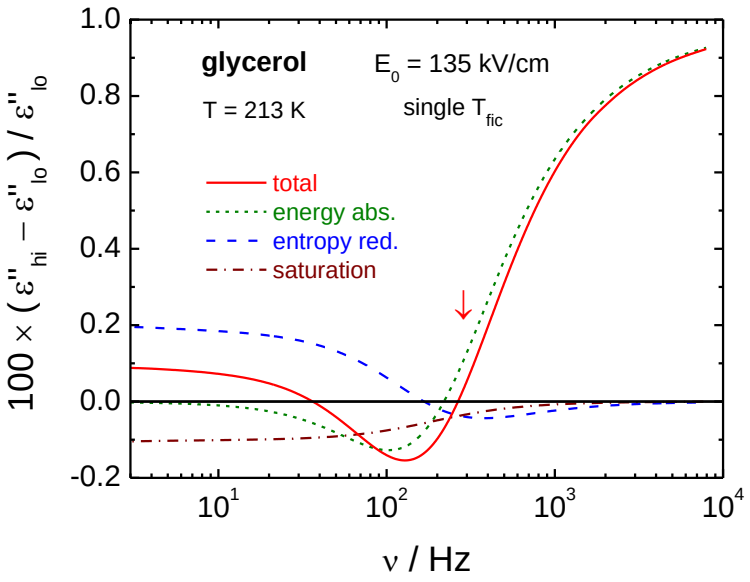


FIG. 6.6. Calculated steady state spectra of the relative change of the dielectric loss, $(\varepsilon''_{hi} - \varepsilon''_{lo})/\varepsilon''_{lo}$, for glycerol at $E_0$ = 135 kV cm$^{-1}$ and for $T$ = 213 K. The solid line represents the total field induced change of the loss that includes all sources of non-linearity, other curves are for the individual contributions from energy absorption, entropy reduction, and saturation (see legend). The arrow indicates the loss peak frequency position, $\nu_{max}$.

The positive effects that occur for frequencies $\nu < \nu_{max}$ are the consequence of the field induced entropy reduction and the resulting increase in the structural relaxation times. This enhancement, however, is damped to some extent via the saturation effect that reduces $\Delta\varepsilon$. In the case of plastic crystals, the entropy effect can be as pronounced as the energy absorption feature, and, as a result, the loss curves appear symmetrically widened at high ac fields relative to the low field limit.[19,20,50] Entropy reduction and saturation are both linked to the extent of polarization, and thus, within the present model, they display

the same time and frequency dependence. It may be more realistic to treat this as a single source of non-linear dielectric behavior which acts on both the dielectric amplitude and the relaxation time scale.

### 6.1.3 Summary

We have measured the third harmonic response of glycerol and two other glass-formers to a high amplitude ac electric field for temperatures for which the loss peak frequency, $\nu_{max}$, covers the range from about 100 to 1000 Hz. Together with literature reports, the present results confirm that the following three features of the $|\chi_3|(\omega)$ spectra are common to polar glass-forming liquids in their viscous state: a non-zero plateau level for sufficiently low frequencies, a maximum in $|\chi_3|$ positioned near $0.2\,\nu_{max}$ on the frequency scale, and a peak height, $|\chi_3|_{max}$, that increases with decreasing temperature. Moreover, $|\chi_3|_{max}(T)$ tracks the added temperature variations of the apparent activation energy, $\partial \ln \tau_\alpha / \partial(1/T)$, and of the relaxation amplitude, $\Delta\varepsilon(T)$.

With the aim of identifying the origins of non-linear effects and the extents to which they contribute to the higher harmonic responses, $\chi_3$ and $\chi_5$, we have devised a phenomenological model of non-linear dielectric responses that accounts for three distinct effects that occur at high fields relative to the low field limit: amplitude reductions via saturation, increased relaxation times due to field induced reductions of entropy, and accelerated dynamics due to enhanced fictive temperatures that occur when a dielectric absorbs energy from a time dependent field. Instead of approaching the problem on the basis of non-linear responses to higher orders of the field, we introduce the effect of high fields indirectly via field dependent relaxation amplitudes and time

constants. The fact that deviations from linearity remain below the 1% level justifies that linear response concepts remain good approximations. The approach is similar to many models of physical aging, where the non-linearity in temperature is indirectly accounted for by the fictive temperature concept.

Using parameters that are tailored to represent glycerol at the temperatures $T$ = 210, 213, and 216 K, the present model reproduces the observed $|\chi_3|(\omega)$ spectra in a semi-quantitative fashion. Specifically, good agreement between model and experiment is found for the absolute values and the temperature dependence of the third harmonic susceptibility maxima, $|\chi_3|_{max}(T)$, after adjusting only the parameter that controls the saturation level. Moreover, the maximum displayed by $|\chi_5|(\omega)$ matches the peak position of $|\chi_3|(\omega)$, but its peak height exceeds that of $|\chi_3|_{max}$ if normalized to the low frequency levels. This again is consistent with recent observations on glycerol.[48] Within the framework of this model, we can then discern the three distinct contributions to $|\chi_3|(\omega)$, which suggests that the entropy reduction effect dominates in defining the $|\chi_3|$ 'hump'. Although the box-model (which focuses solely on the effect of energy absorption) has been compared to third harmonic susceptibility spectra,[51] the present results show that the energy absorption effects alone will not provide a complete explanation of the $|\chi_3|$ peak.

At this stage, several models exist that deliver a rationale for non-monotonic $|\chi_3|(\omega)$ spectra that are reminiscent of the experimental findings. Among these, the present approach and a non-linear response theory for Markov processes[52] do not involve length scales of dynamical correlations explicitly, while another is associated with such glassy

correlations in terms of $N_{corr}(T)$.[16] Because we can explain higher harmonic susceptibilities without reference to glassy correlations, employing $|\chi_3|(\omega,T)$ results to conclude on an increasing $N_{corr}(T)$ when the temperature is lowered requires the demonstration that $N_{corr}(T)$ is the only valid explanation for the temperature dependence of $|\chi_3|_{max}$ or for the super-Arrhenius behavior of these liquids.

## 6.2 Nonlinear Dielectric Features of Highly Polar Derivatives of Propylene Carbonate

In the previous section, nonlinear effects in the third harmonic excitation are explicitly modeled and discussed. In this section, an overall study of nonlinear dielectric effect and nonlinear susceptibility studies for highly polar materials are studied. The work from the previous section is employed and expanded on in the understanding of the nonlinear effects at the fundamental frequency.

Nonlinear dielectric effects of considerable amplitude are expected for liquids with static dielectric constants, $\varepsilon_s$, that strongly exceed the high frequency permittivity, $\varepsilon_\infty$. Such materials will consist of molecules that possess large dipole moments, and the resulting coupling to external electric fields may give rise to pronounced nonlinear effects that are then accessible by experiment.

Studies of nonlinear dielectric effects have been reported for liquids that cover a wide range of polarities, with their dielectric constants ranging from about $\varepsilon_s \approx \varepsilon_\infty$ to levels reaching $\varepsilon_s = 100$. Dipole densities in glass forming liquids are rarely high enough to yield $\varepsilon_s$ values much higher than 100, except when hydrogen-bonding promotes high orientational correlations of dipoles, which increases the static dielectric constant.

Recently, dielectric properties of a series of propylene carbonate (PC) derivatives have been reported by Jedrzejowska, Ngai, and Paluch.[56] These compounds are simple glass-forming polar liquids with glass transition temperatures between $T_g$ = 170 K and 200 K, and dielectric constants in the viscous regime that are in the range of 70 < $\varepsilon_s$ < 250. In particular, hydrogen-bonding effects in these liquids are insufficient to lead to significant chemical effects, i.e., the field induced increase of $\varepsilon_s$ resulting from species with different dipole moments coexisting in thermodynamic equilibrium. Therefore, these liquids would appear to be ideal candidates for studying the generic nonlinear dielectric effects of saturation and electro-rheological behavior. Dielectric saturation amounts to a reduction in the relaxation amplitude, $\Delta\varepsilon = \varepsilon_s - \varepsilon_\infty$, while the electro-rheological response to a static electric field shifts the loss peak to lower frequencies, equivalent to increasing relaxation times and to a positive $T_g$ shift.

Nonlinear susceptibilities can be obtained either by a high dc bias field on top of a small amplitude oscillatory field, i.e., using $E(t) = E_B + E_0\sin(\omega t)$ with $E_0 < E_B$, or by a large ac field without bias, i.e., with $E_B = 0$. In the present context, the first ($n$ = 1) and third ($n$ = 3) order Fourier components of polarization, $\hat{P}_n(\omega)$, can be expressed by:

$$\frac{\hat{P}_1(\omega)}{\varepsilon_0 E_0} = \hat{\chi}_1^{(1)}(\omega) + \hat{\chi}_1^{(3,ac)}(\omega)E_0^2 + \hat{\chi}_1^{(3,dc)}(\omega)E_B^2 + \dots \,, \tag{6.14a}$$

$$\frac{\hat{P}_3(\omega)}{\varepsilon_0 E_0} = \hat{\chi}_3^{(3)}(\omega)E_0^2 + \dots \,, \tag{6.14b}$$

where the quantities $\chi_k^{(n)}$ represent contributions from the $n^{th}$ power of the field (ac or dc) in the $k^{th}$ Fourier component. Higher order terms such as $\chi_k^{(5)}$ may be required for very

high fields. As a result, nonlinear effects can be measured either in terms of deviations from the linear term, $\chi_1^{(1)}$, at the fundamental frequency, i.e., via $\chi_1^{(3,ac)}$ or $\chi_1^{(3,dc)}$, or by higher harmonics, e.g., $\chi_3^{(3)}$. In the following, the shorter notations $\chi \equiv \chi_1^{(1)}$ and $\chi_3 \equiv \chi_3^{(3)}$ will be used.

In this work, several PC derivatives have been studied in the highly supercooled regime regarding their nonlinear dielectric features: hydroxy-PC, vinyl-PC, R-methoxy-PC, S-methoxy-PC, and some mixtures thereof. All cases display significant dielectric saturation effects at levels that are expected on the basis of their dielectric constants. The electro-rheological effect of slowing down relaxation dynamics by a static electric field was observed for vinyl-PC, but, surprisingly, remained absent for the other pure liquids that are characterized by $\varepsilon_s > 130$. Also unexpected is the observation that the magnitude of this electro-rheological effect does not correlate with the field induced change in entropy, a correlation that has been suggested,[12] and supported by initial experimental studies.[14,40] In particular, for the most polar of these liquids, the methoxy-PC's, no signature of a field induced shift of the loss peak was found. It was also observed that the presence or absence of an electro-rheological effect correlates with the respective presence or absence of a pronounced maximum ('hump') in the cubic susceptibility, $\chi_3(\omega)$. Moreover, both the magnitudes of the electro-rheological effect and of the 'hump' in $|\chi_3(\omega)|$ vary linearly with the apparent activation energy when the temperature is altered. This supports the previous notion that this $\chi_3(\omega)$ hump is associated with the electro-rheological effect.[45,57] This particular nonlinear effect has been referred to as 'entropy effect', but because the present results question the role of entropy for the field

induced change in dynamics, the label 'electro-rheological effect' appears more appropriate. Note, however, that the dynamics are probed via dielectric relaxation times and not by rheological experiments.

### 6.2.1 Experiments

The compounds employed in this study were purchased from Sigma-Aldrich (S-A) and Tokyo Chemical Industries (TCI) and used as received: propylene carbonate (PC, S-A, 99.7 %, anhydrous, racemic mix of (*S*)-(–)-propylene carbonate and (*R*)-(+)-propylene carbonate), 4-vinyl-1,3-dioxolan-2-one (vinyl-PC, S-A, 99 %), (*S*)-(–)-4-methoxymethyl-1,3-dioxolan-2-one (S-MeO-PC, TCI, > 98 %), (*R*)-(+)-4-methoxymethyl-1,3-dioxolan-2-one (R-MeO-PC, TCI, > 98 %), 4-hydroxymethyl-1,3-dioxolan-2-one (hydroxy-PC, TCI, > 90 %). Two 50/50 volumetric mixtures have been prepared from the above compounds: a racemic mixture of S-MeO-PC and R-MeO-PC (S/R-mix-PC) and a mixture of R-MeO-PC and vinyl-PC (R/V-mix-PC). Linear response dielectric relaxation experiments were performed at peak fields not exceeding 200 V/cm using an Invar/sapphire cell described earlier,[58] which was held at the desired temperature with a Novocontrol Quatro ℓ-$N_2$ cryostat. Permittivity, $\hat{\varepsilon}(\omega)=\varepsilon'(\omega)-i\varepsilon''(\omega)$, was measured using a Solartron SI-1260 gain/phase analyzer equipped with a Mestec DM-1360 transimpedance amplifier and calibrated based on the empty capacitor cell ($C_{geo} = \pi\varepsilon_0 r^2/d$ = 28.2 pF, $r$ = 9 mm, $d$ = 80 μm).

High field experiments employed a cell in which two polished stainless steel or titanium electrodes (17 and 20 mm diameter) are held at a distance $d$ using a ring shaped spacer with 20 mm outer and 14 mm inner diameter that is subject to a constant stress

provided by a spring washer. The sheets used as spacer material were made of polytetrafluorethylene ($d$ = 10 μm) or polyimide ($d$ = 8 or 13 μm). The cell was temperature controlled via a closed cycle He-cryostat (Leybold RDK 6-320) and a heater control unit (Lakeshore Mod. 340). Spectra of nonlinear effects were measured with the SI-1260 analyzer, with the generator voltage amplified by a Trek PZD-350 voltage booster. The current detection is based on a passive shunt with frequency dependent impedance, a dc-blocking capacitor when dc fields are applied, and a buffer amplifier meant to protect the analyzer against sample failure.[45] This setup was used for both types of experiments, high ac fields with no bias and high dc-bias fields with a small ac field superposed.

A different technique is required to capture the nonlinear effects as a function of time after applying or removing the large dc-component of the field. To this end, an arbitrary waveform generator (Stanford Research Systems DS-345) was programmed to typically generate 16 periods of a sine-wave without dc bias, then 32 periods with a positive dc bias, and finally another 16 periods without bias. In each segment the field is given by $E(t) = E_B + E_0\sin(\omega t)$, with $E_0$ constant for all periods and either $E_B = 0$ or $E_B = 9\times E_0$ . This pattern was repeated 5000 times at low duty cycle to allow for signal averaging. In order to eliminate the polarization response to the field steps, the measurement was repeated with a negative bias field and the average of the two results was analyzed.[40] The voltage was enhanced by a Trek PZD-350 high voltage amplifier and the voltage across the sample and current running through an ohmic shunt ($R$ = 1 kΩ) were recorded with a Nicolet Sigma 100 digitizing oscilloscope. These signal traces, current $I(t)$ and voltage

$V(t)$, were subjected to a period-by-period Fourier analysis at the fundamental frequency $\omega$, yielding time dependent amplitudes $A$ and phases $\varphi$ for the current ($A^{(\mathrm{I})}$, $\varphi^{(\mathrm{I})}$) and for the voltage ($A^{(\mathrm{V})}$, $\varphi^{(\mathrm{V})}$) signals. Then, with $\Delta\varphi = |\varphi^{(\mathrm{I})} - \varphi^{(\mathrm{V})}|$,the time dependent equivalents of $\varepsilon'$ and $\varepsilon''$ are obtained via

$$\varepsilon' - i\varepsilon'' = \frac{A^{(I)}}{\omega A^{(V)} C_{geo}} \left(\sin\Delta\varphi - i\cos\Delta\varphi\right) , \tag{6.15}$$

where $C_{\mathrm{geo}} = \varepsilon_0 A/d$ is the geometric capacitance. Because these quantities are calculated for each period as if the system were in equilibrium, the notation $\varepsilon'$ and $\varepsilon''$ is used, even though permittivities are properly defined only for steady state conditions.

Cubic susceptibilities were measured using a Stanford Research Systems 830 lock-in amplifier, combined with a Trek PZD-350 high voltage amplifier. The setup differed only in the shunt used for current detection from the approach described previously. [45] In this work, a purely ohmic shunt ($R$ = 50 Ω) was used, and its voltage drop was fed through a low-pass filter (with cutoff frequency $f_{\mathrm{c}}$ = 3450 Hz) into the amplifier input to compensate for the near linear increase of the current with frequency. This detection circuit turned out intrinsically more linear than a shunt with frequency dependent impedance.

### 6.2.2 Results

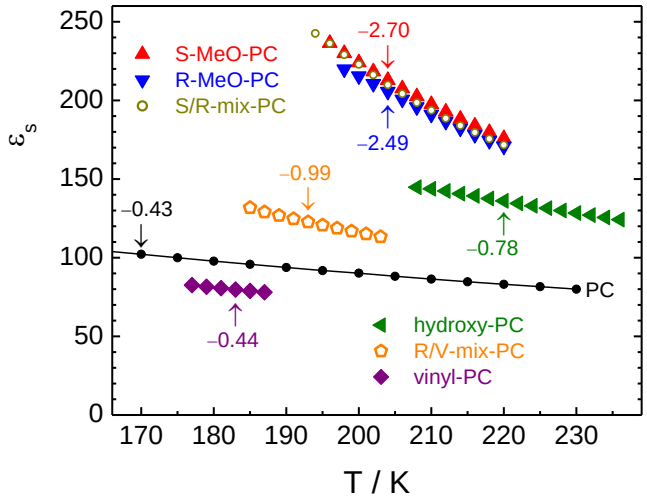


FIG. 6.7. Dielectric constant ($\varepsilon_s$) versus temperature ($T$) for propylene carbonate (dots and line) and all its derivatives (symbols) of the present study. The values for the slopes, $\partial\varepsilon_s/\partial T$, are given in units of $K^{-1}$ for the temperature to which the arrow points, where the loss peak position is $\nu_{max} \approx 300$ Hz (see Table 6.1).

The low field dielectric spectra derived from the Invar/sapphire cell were analyzed for the liquids under study with respect to the static dielectric constants, $\varepsilon_s$, in a range of temperatures above the glass transitions. The results for $\varepsilon_s(T)$ are compiled in Fig. 6.7, reiterating the impressive polarities of these PC derivatives. The current values for $\varepsilon_s$ are somewhat higher (≈ 15 %) than those of a previous report ($\Delta\varepsilon$ = 75 for PC, 185 for S-MeO-PC, 75 for vinyl-PC, and 114 for hydroxy-PC),[56] likely due to a deviation of the actual spacer thicknesses from the nominal values, which are used by Jedrzejowska *et al.* to determine $C_{geo}$. The reproducibility of the geometry of the present spacer free cell makes overestimating the true values almost impossible at this level of $\varepsilon_s$. The $\varepsilon_s(T)$ values for PC itself (racemic mix) are about 4.5 % lower than those reported by Simeral

and Amey,[59] but a straightforward comparison is not possible because the enantiomer composition for that sample is not provided. The remaining features such as loss peak position and spectral shape are in full agreement with the earlier dielectric spectra.[56] From these $\varepsilon_s(T)$ curves, the $\varepsilon_s$ levels and the slopes $\partial\varepsilon_s/\partial T$ have been determined for temperatures for which the peak loss frequency is at $\nu_{max} \approx 300$ Hz, which correspond to the temperatures near which the high field experiments were performed. The values are compiled in Table 6.1, along with the slopes $\partial \ln\Delta\varepsilon/\partial \ln T$ that gauge the sensitivity of $\Delta\varepsilon$ to changes in $T$ on relative scales.

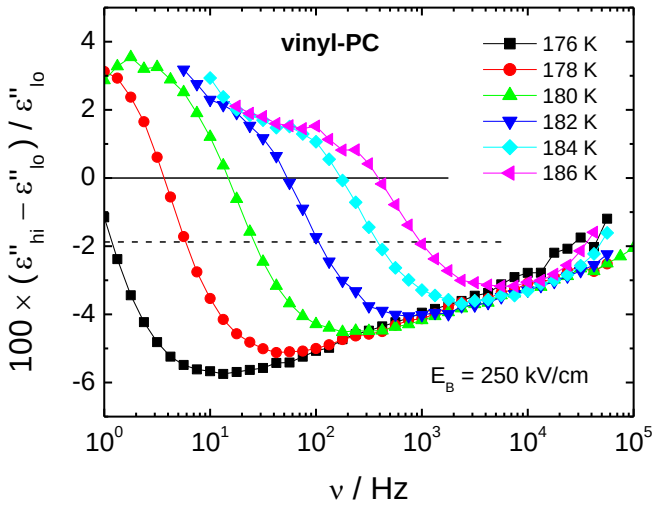


FIG. 6.8. Field induced relative change of the dielectric loss, $(\varepsilon''_{hi} - \varepsilon''_{lo})/\varepsilon''_{lo}$, versus frequency for vinyl-PC at the temperatures indicated, recorded for a common static field of $E_B = 250$ kV/cm. The dashed line at −1.88 % indicates the average level of dielectric saturation, and the curves cross this line at their respective loss peak frequency, $\nu_{max}$.

Spectra of steady state nonlinear effects due to high static fields are shown in terms of the relative change of the loss, $(\varepsilon''_{hi} - \varepsilon''_{lo})/\varepsilon''_{lo}$, versus frequency for vinyl-PC in Fig. 6.8 for a set of different temperatures. Qualitatively, the appearance of these curves is

analogous to what has been observed for numerous other viscous liquids:[55] a field induced reduction of the loss for the high frequency side, $\varepsilon''(\nu > \nu_{max})$, and enhancement of $\varepsilon''(\nu < \nu_{max})$ on the other side of $\nu_{max}$.

| sample | $T$ [K] | $\varepsilon_s$ | $\partial\varepsilon_s/\partial T$ [$K^{-1}$] | $\partial\ln\Delta\varepsilon/\partial\ln T$ | $100\times\Delta_E\ln\Delta\varepsilon$ | $100\times\Delta_E\ln\tau$ |
|---|---|---|---|---|---|---|
| S-MeO-PC | 204 | 213 | –2.70 | –2.64 | –5.0 | ≈ 0 |
| R-MeO-PC | 204 | 206 | –2.49 | –2.51 | -- | -- |
| hydroxy-PC | 220 | 136 | –0.78 | –1.30 | –0.55 | ≈ 0 |
| vinyl-PC | 183 | 79 | –0.44 | –1.06 | –0.28 | +0.63 |
| S/R-mix-PC | 204 | 210 | –3.01 | –2.98 | –4.6 | ≈ 0 |
| R/V-mix-PC | 193 | 123 | –0.99 | –1.59 | –1.25 | +0.21 |
| PC | 170 | 102 | –0.43 | –0.75 | –0.46 | +0.63 |

Table 6.1. Characteristic dielectric parameters for four PC derivatives, two of their mixtures, and PC itself. The values of $\varepsilon_s$, $\partial\varepsilon_s/\partial T$, and $\partial\ln\Delta\varepsilon/\partial\ln T$ are derived from low field experiments, with peak field $E_0$ < 200 V/cm and zero bias. High field results for $\Delta_E\ln\Delta\varepsilon$ and $\Delta_E\ln\tau$ are normalized for a common field of $E_B \rightarrow 100$ kV/cm those for PC are taken from ref. 15. All values are for the temperature indicated as $T$, at which the loss peak frequency is approximately $\nu_{max}$ = 300 Hz.

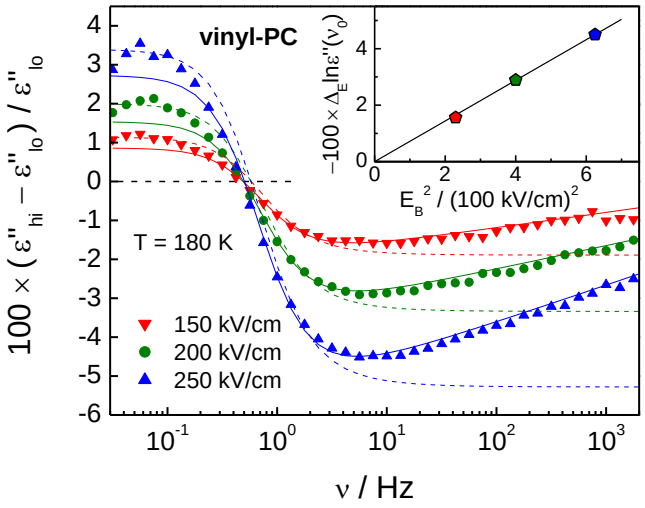


FIG. 6.9. Field induced relative change of the dielectric loss, $(\varepsilon''_{hi} - \varepsilon''_{lo})/\varepsilon''_{lo}$, versus frequency for vinyl-PC at a temperature of $T$ = 180 K, recorded for three different static fields of $E_B$ = 150, 200, and 250 kV/cm. The two sets of fit lines are explained in the text. The inset shows the amplitude of each curve at $\nu_0$ = 6 Hz versus $E_B^2$, demonstrating that these nonlinear effects scale with electric field squared.

This represents a clear indication of a shift of the loss peak to lower frequencies, equivalent to increased relaxation time constants and a positive $T_g$ shift. For the vinyl-PC case, it is demonstrated in Fig. 6.9 that the magnitudes of these nonlinear effects increase linearly with $E^2$, while the spectral shape remains unchanged. This quadratic field dependence has been observed for all nonlinear effects addressed in this study. The field induced peak shift of vinyl-PC is contrasted with the behavior of S-MeO-PC, S/R-mix-PC, and hydroxy-PC in Fig. 6.10, revealing that the methoxy and hydroxy derivatives of PC display no such field induced peak shift at a comparable dc bias field, but a very high level of dielectric saturation. The effect of a high field on the loss spectrum has also been recorded for the volumetric 50/50 mixture of R-MeO-PC and vinyl-PC, R/V-mix-PC, for a series of temperatures, with the results depicted in Fig. 6.11. Interestingly, the extent of

the field induced peak shift for the R/V-mix-PC changes from being as strong as for pure vinyl-PC to practically zero across this 10 K temperature range.

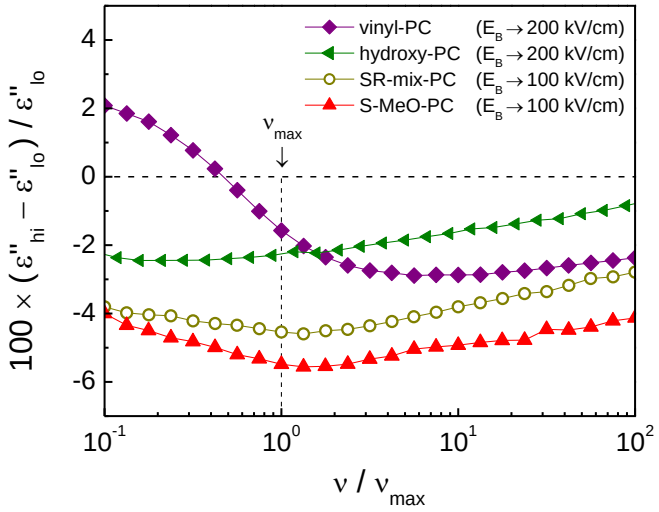


FIG. 6.10. Field induced relative change of the dielectric loss, $(\varepsilon''_{hi} - \varepsilon''_{lo})/\varepsilon''_{lo}$, versus normalized frequency, $\nu/\nu_{max}$, for four different samples: vinyl-PC ($T$ = 180 K, $\nu_{max}$ = 32 Hz), hydroxy-PC ($T$ = 219 K, $\nu_{max}$ = 200 Hz), S/R-mix-PC ($T$ = 202 K, $\nu_{max}$ = 240 Hz), and S-MeO-PC ($T$ = 201 K, $\nu_{max}$ = 75 Hz). Data for S/R-mix-PC and S-MeO-PC have been rescaled with $E_B^2$ to reflect the behavior at $E_B$ = 100 kV/cm. The curves for vinyl-PC and hydroxy-PC are scaled for $E_B$ = 200 kV/cm, i.e., expanded a factor of 4 relative to the other curves for clarity. The vertical line labeled $\nu_{max}$ marks the loss peak frequency position. Only the vinyl-PC curve indicates a field induced shift of the loss peak to lower frequencies in addition to saturation

Steady state spectra of nonlinear dielectric effects have also been recorded for high amplitude ac fields with no dc bias. As is typical for polar viscous liquids, these $(\varepsilon''_{hi} - \varepsilon''_{lo})/\varepsilon''_{lo}$ curves are practically zero for $\nu < \nu_{max}$, but rise to a positive plateau level for $\nu > \nu_{max}$. After normalizing the data to an ac electric field of $E_0 \rightarrow$ 100 kV/cm, the following plateau values for the increases of $\varepsilon''$ were found: +2.7 % for S-MeO-PC, +1.8 % for hydroxy-PC, +2.6 % for vinyl-PC, +2.8 % for S/R-mix/PC, and +2.5 % for R/V-mix-PC. These quantities are needed to eliminate the effects of transient energy

absorption when the field is switched on and off in the course of the time resolved experiments (see below).

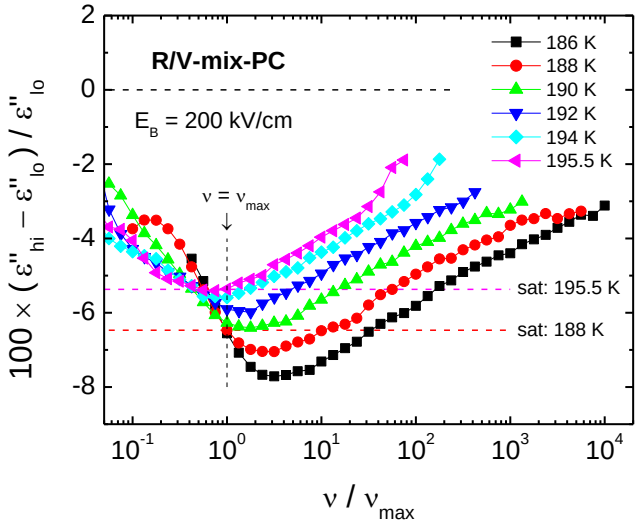


FIG. 6.11. Field induced relative change of the dielectric loss, $(\varepsilon''_{hi} - \varepsilon''_{lo})/\varepsilon''_{lo}$, versus normalized frequency for hydroxy-PC at the temperatures indicated, recorded for a common static field of $E_B$ = 200 kV/cm. The dashed lines at –5.4 % and –6.5 % indicate the saturation level at $T$ = 195.5 K and 188 K, respectively, and intersect the curves at their respective loss peak frequency, $\nu_{max}$.

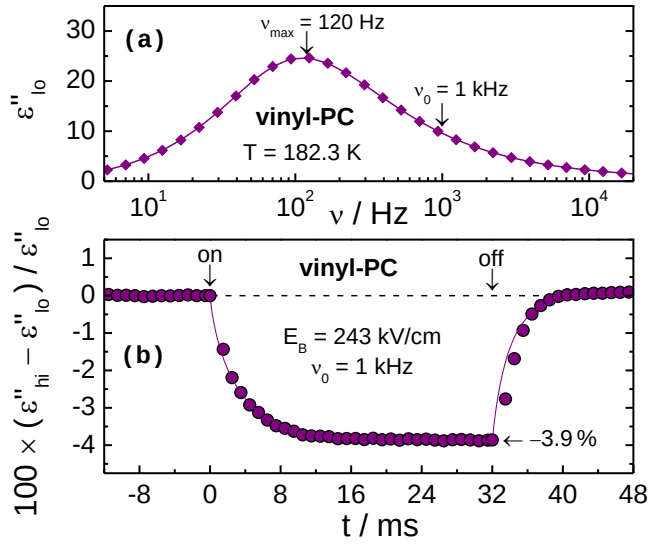


FIG. 6.12. (a) Low field loss profile of vinyl-PC at $T$ = 182.3 K, indicating the peak frequency $\nu_{max}$ = 120 Hz and the position of the fixed frequency $\nu_0$ = 1 kHz used to

obtain $\varepsilon''_{hi}(t)$. (b) Time-resolved field induced relative change of the dielectric loss, $(\varepsilon''_{hi} - \varepsilon''_{lo})/\varepsilon''_{lo}$, for vinyl-PC at a temperature of $T = 182.3$ K, recorded at a fixed frequency of $\nu_0 = 1$ kHz. The static field of $E_B = \pm 243$ kV/cm was turned on at $t = 0$ and turned off at $t = 32$ ms. Lines serve as guides only.

Time resolved data of nonlinear effects resulting from high dc bias fields have been recorded for numerous samples, temperatures and frequencies, partly to confirm that the spectra of $(\varepsilon''_{hi} - \varepsilon''_{lo})/\varepsilon''_{lo}$ are consistent with the long time plateau values of the time resolved traces. Using a method described in detail elsewhere and the above results from the nonlinear ac-field experiments, the time resolved curves are corrected for energy absorption that occurs during field on/off transitions.[40] Two representative examples are shown, one for vinyl-PC in Fig. 6.12 and one for S-MeO-PC in Fig. 6.13. Both cases are for a fixed frequency $\nu_0$ that is above the low field loss peak position $\nu_{max}$, as indicated in panel (a) of each figure. Also, both traces of the field induced relative change of $\varepsilon''$ display the rise/decay asymmetry observed for all structural recovery processes that depend quadratically on the field.[55,40]

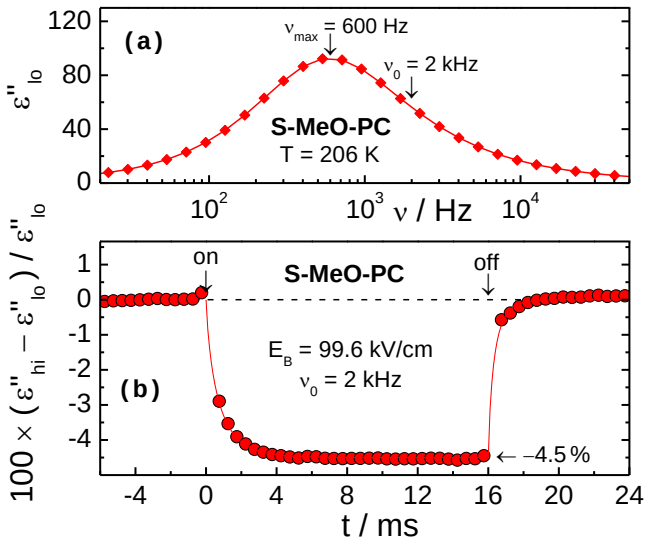


FIG. 6.13. (a) Low field loss profile of S-MeO-PC at $T$ = 206 K, indicating the peak frequency $\nu_{max}$ = 600 Hz and the position of the fixed frequency $\nu_0$ = 2 kHz used to obtain $\varepsilon''_{hi}(t)$. (b) Time-resolved field induced relative change of the dielectric loss, $(\varepsilon''_{hi} - \varepsilon''_{lo})/\varepsilon''_{lo}$, for S-MeO-PC at a temperature of $T$ = 206 K, recorded at a fixed frequency of $\nu_0$ = 2 kHz. The static field of $E_B$ = ±99.6 kV/cm was turned on at $t$ = 0 and turned off at $t$ = 16 ms. Lines serve as guides only.

Cubic susceptibilities in terms of $|\chi_3(\omega)|E_0^2$ are depicted in Fig. 6.14 for vinyl-PC at various temperatures. While the low-frequency plateau level changes only little with temperature, the peak amplitudes, $\chi_{3,max}$, of these curves decrease systematically with increasing temperature. The $|\chi_3(\omega)|$ behavior of the methoxy derivatives differs qualitatively from that of vinyl-PC. This is represented in Fig. 6.15 by the $|\chi_3(\omega)|$ curves obtained for the S/R-mix-PC case, which generated the best cubic susceptibility data due to its higher crystallization resistance compared with the pure enantiomers.

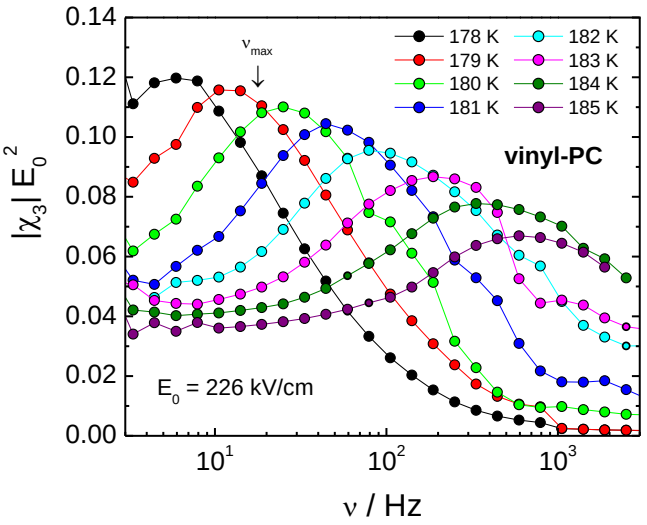


FIG. 6.14 Cubic susceptibility shown as $|\chi_3|E_0^2$ versus fundamental frequency $\nu$ for vinyl PC at temperatures between $T$ = 178 and 185 K. All curves are recorded for an ac field with peak value $E_0$ = 226 kV/cm. The frequency positions of the $|\chi_3(\omega)|$ maxima are about a factor three below the loss peak frequencies, $\nu_{max}$. For the $T$ = 178 K case, the low field loss peak frequency is indicated by the arrow labeled $\nu_{max}$.

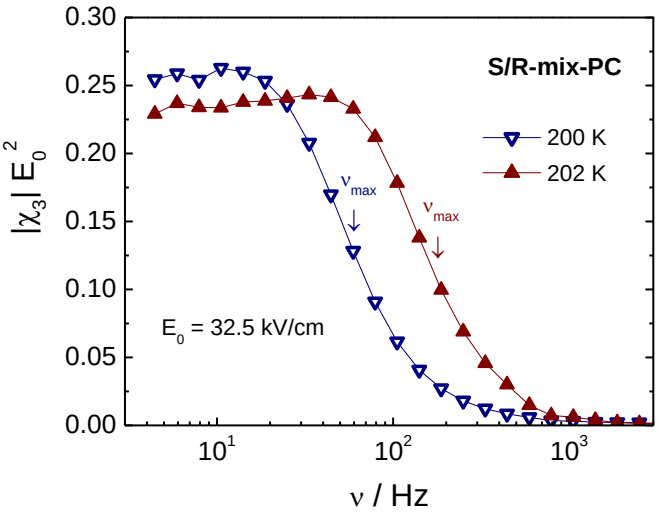


FIG. 6.15. Cubic susceptibility shown as $|\chi_3|E_0^2$ versus fundamental frequency $\nu$ for S/R-mix-PC at two temperatures, $T$ = 200 and 202 K. Both curves are recorded for an ac field with peak value $E_0$ = 32.5 kV/cm. The low field loss peak frequencies are indicated by arrows labeled $\nu_{max}$.

### 6.2.1 Discussion

#### 6.2.1.1 Linear Response Properties

The glass forming liquid propylene carbonate (PC), usually a racemic mixture of (*S*)-(−)-propylene carbonate and (*R*)-(+)-propylene carbonate, is known for its high polarity, $\varepsilon_s > 100$ near $T_g$, high fragility of $m = 99$,[60] and relatively narrow loss peak as quantified by the stretching exponent $\beta = 0.75$.[56] According to Jedrzejowska *et al.*,[56] the PC derivatives addressed in this work reach very high dielectric constants, have similar fragilities, and display narrow loss peaks consistent with values as high as $\beta = 0.84$. High polarities or dielectric constants imply a considerable interaction with external electric fields, which make these liquids prime candidates for nonlinear dielectric experiments. In recent studies on nonlinear dielectric effects of less polar liquids,[39] it was observed that the magnitudes of dielectric saturation and the electro-rheological effect are correlated with the field induced entropy reduction, which can be estimated on the basis of the relation provided by Fröhlich,[35]

$$\Delta_E S = \upsilon \frac{\varepsilon_0}{2} \left( \frac{\partial \varepsilon_s}{\partial T} \right)_V E_B^2 \ . \tag{6.16}$$

where $\upsilon$ is the molar volume. The derivation of this relation assumes constant volume conditions, but the slopes, $\partial\varepsilon_s/\partial T$, evaluated for isochoric conditions are very similar to the isobaric cases,[61] which are the situations realized in typical experiments. According to the data in Table 6.1, the methoxy-PC derivatives (S-MeO-PC, R-MeO-PC, and their mixture S/R-mix-PC) display extraordinarily high values of both slopes, $\partial\varepsilon_s/\partial T$ and

$\partial \ln \Delta\varepsilon / \partial \ln T$, which reflect the sensitivity of $\Delta\varepsilon$ to changes in $T$ on absolute and relative scales, respectively.

The dielectric constant of PC itself can be rationalized on the basis of its dipole density alone using the Onsager equation, or equivalently, the Kirkwood-Fröhlich equation,[53]

$$\frac{(\varepsilon_s - \varepsilon_\infty)(2\varepsilon_s + \varepsilon_\infty)}{\varepsilon_s(\varepsilon_\infty + 2)^2} = \frac{\rho N_A}{9 k_B T \varepsilon_0 M} g_K \mu^2 \ . \tag{6.17}$$

with the Kirkwood correlation factor $g_K$ set to near unity in the very viscous regime.[59] A more detailed analysis of the present data for PC reveals that $g_K$ declines from 1.05 at $T$ = 225 K to 0.90 at $T$ = 165 K, a trend that is consistent with earlier observations.[59,62] Whether orientational correlations of dipoles leading to $g_K > 1$ are relevant for the high $\varepsilon_s$ values of the PC derivative can assessed by the following method. Assuming that $\varepsilon_\infty$, density $\rho$, $g_K$, and dipole moment $\mu$ are practically temperature invariant, the derivative $\partial\varepsilon_s/\partial T$ can be evaluated from Eq. (6.17), which yields

$$\frac{\partial \varepsilon_s}{\partial T} = \frac{\partial \Delta\varepsilon}{\partial T} = -\frac{(2\varepsilon_s + \varepsilon_\infty)}{(2\varepsilon_s + \varepsilon_\infty^2/\varepsilon_s)} \frac{\Delta\varepsilon}{T} \ . \tag{6.18}$$

For any $\varepsilon_s > \varepsilon_\infty$, the inequality $1 \le (2\varepsilon_s + \varepsilon_\infty)/(2\varepsilon_s + \varepsilon_\infty^2/\varepsilon_s) \le (3 + 1.25\sqrt{6})/(3 + \sqrt{6}) \approx 1.11$ holds, so that $\partial \Delta\varepsilon / \partial T \approx -\Delta\varepsilon / T$ , or, equivalently, $\partial \ln \Delta\varepsilon / \partial \ln T \approx -1$. For the very polar systems with $\varepsilon_s > 200$, values of $\partial \ln \Delta\varepsilon / \partial \ln T < -2.5$ in Table 1 reveal that these methoxy-PC liquids have pronounced slopes, $\partial\varepsilon_s/\partial T$, not only because $\varepsilon_s$ is large, but also because

$g_K$ changes considerably with temperature. Analogous features can be found for some monohydric alcohols and other liquids with strong orientational correlations.[54]

#### 6.2.1.2 Nonlinear Effects at the Fundamental Frequency

This section focuses on the nonlinear effects observed at the fundamental frequency $\omega$, while the results derived from higher harmonic signals ($3\omega$) will be discussed in Section 6.2.3.3. Four contributions to nonlinear dielectric effects have been recognized thus far in the literature: saturation,[53] chemical effect,[63] energy absorption,[8,64] and the electro-rheological effect (entropy effect).[55,14,40,13] A considerable chemical effect requires two species with sufficiently different dipole moments to coexist in thermodynamic equilibrium, and this is not expected for simple liquids such as those studied here. Energy absorption leads to considerable changes only in the case of time dependent fields of high amplitudes. The main effect of energy absorption from the field is to enhance the fictive temperatures of relaxation modes, thereby shifting time constants towards faster dynamics, even at a constant temperature.[8,64] The typical signature of energy absorption is to increase the high frequency wing of the loss profile, i.e., $(\varepsilon''_{hi} - \varepsilon''_{lo})/\varepsilon''_{lo}$ reaches a positive plateau for frequencies $\nu > \nu_{max}$ and is practically zero otherwise.[65,30] The model that captures these effects predicts that the changes in $\varepsilon''(\nu > \nu_{max})$ are equivalent to a temperature rise that amounts to $\varepsilon_0 E_0^2 \Delta\varepsilon / \left(2\rho\Delta C_p\right)$, with the impact on $\varepsilon''$ then being a matter of the apparent activation energy, $\partial \ln \tau_\alpha / \partial(1/T)$, and the slope $\partial \lg \varepsilon'' / \partial \lg \nu$.[55,33] The present PC derivatives are similar in all relevant parameters except $\Delta\varepsilon$, so for a given field these $\varepsilon''(\nu > \nu_{max})$ plateau levels should change with the polarity. When applying an ac electric field of $E_0$ = 100 kV/cm, the plateau values for the

increases of $\varepsilon''$ all fall into the range +2.5 ±0.4 %. These values do not differ strongly across this family of PC derivatives, but they are lower than the value of +6.3 % for PC itself.[32] Thus, we find little correlation between the magnitude of the nonlinear effect based upon energy absorption and the level of $\varepsilon_s$ or its derivative $\partial\varepsilon_s/\partial T$, with those numbers taken from Fig. 6.7.

The remainder of the discussion will focus on the nonlinear effects arising from strong dc-fields, where, of the four phenomenological nonlinear effects listed above, saturation and electro-rheological effects are expected to dominate the field induced changes of the permittivity. The leading terms of these effects can be captured as negative values for $\Delta_E \ln\Delta\varepsilon$ and positive values for $\Delta_E \ln\tau$. Experimentally, both values are obtained from steady state spectra such as those depicted in Fig. 6.8 for vinyl-PC. The saturation level, $\Delta_E \ln\Delta\varepsilon$, is derived from the field induced relative reduction of $\varepsilon''$ at the frequency $\nu = \nu_{max}$, where $\partial \lg\varepsilon''/\partial \lg\nu = 0$ and where a small change in $\tau$ does not affect the loss at that frequency. In Fig. 6.8, the average value of saturation, $\Delta_E \ln\Delta\varepsilon$, is indicated by the dashed horizontal line, and because the temperature variation of this quantity is minimal, all curves cross this −1.88 % level at $\nu \approx \nu_{max}$. For temperatures at which $\nu_{max} \approx$ 300 Hz, these saturation percentage values are listed in Table 6.1 for all samples of this study as well as for PC. For the present situation of the sample being in equilibrium with a high dc bias field, no pronounced frequency dependence for saturation is expected, and the same values would be obtained from the low frequency plateau of the real part of permittivity, i.e., from $(\varepsilon'_{hi} - \varepsilon'_{lo})/(\varepsilon'_{lo} - \varepsilon_\infty)$, but with added uncertainty regarding the choice of $\varepsilon_\infty$.

The assessment of the electro-rheological effect, $\Delta_E \ln \tau$, involves analyzing the shape of the $(\varepsilon''_{hi} - \varepsilon''_{lo})/\varepsilon''_{lo}$ spectrum relative to the saturation level. In Fig. 6.8 and Fig. 6.9, the loss values are shifted below the saturation level for $\nu > \nu_{max}$ and remain above $\Delta_E \ln \varepsilon''(\nu = \nu_{max})$ for $\nu < \nu_{max}$. These features clearly indicate a shift of the loss peak to lower frequencies, equivalent to a field induced increase of relaxation times or $T_g$. A robust analysis leading to $\Delta_E \ln \tau$ is to fit $\varepsilon''_{lo}(\nu)$ by a Havriliak-Negami (HN) type permittivity function, and then vary $\Delta\varepsilon$ and $\tau$ to match $\varepsilon''_{hi}(\nu)$ or the $(\varepsilon''_{hi} - \varepsilon''_{lo})/\varepsilon''_{lo}$ spectrum. In the present cases, considerable deviations from the HN power law occur at high frequencies,[6] so that a second smaller process is added which accounts for the excess wing, but that contribution is considered field invariant. The overall fit function then reads

$$\hat{\varepsilon}(\omega) = \varepsilon_\infty + \frac{\Delta\varepsilon_\alpha}{\left[1 + (i\omega\tau_\alpha)^\alpha\right]^\gamma} + \frac{\Delta\varepsilon_\beta}{\left[1 + (i\omega\tau_\beta)^{\alpha'}\right]^{\gamma'}} \quad . \tag{6.19}$$

with only $\Delta\varepsilon_\alpha$ and $\tau_\alpha$ considered to depend on the field. Fits without the secondary process or excess wing contribution ($\Delta\varepsilon_\beta = 0$) are shown for different fields in Fig. 6.9 as dashed lines, while those that account for the excess wing loss are included as solid lines. It is obvious that the addition of the excess wing results in superior fits, and the effects of the high static fields on the loss spectra can be entirely captured by the field induced changes of the two parameters, $\Delta\varepsilon_\alpha$ and $\tau_\alpha$. For temperatures at which $\nu_{max} \approx 300$ Hz, these percentage values for the electro-rheological effect are included in Table 6.1 for all samples

of this study as well as for PC.

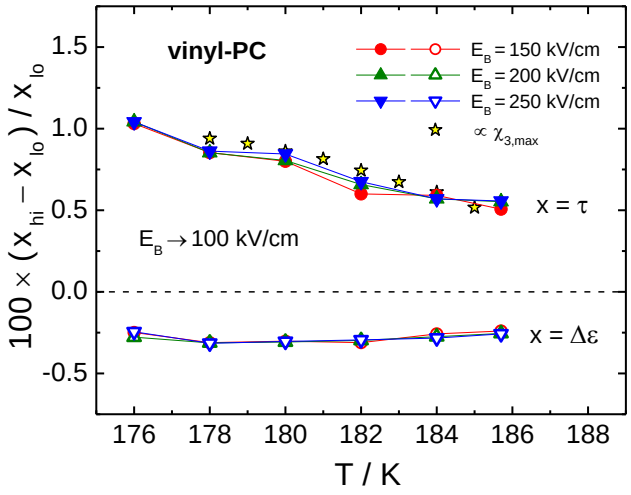


FIG. 6.16. Field induced relative changes of the dielectric relaxation time constant, $\Delta_E \ln \tau \approx (\tau_{hi} - \tau_{lo})/\tau_{lo}$ (solid symbols), and of the relaxation amplitude, $\Delta_E \ln \Delta\varepsilon \approx (\Delta\varepsilon_{hi} - \Delta\varepsilon_{lo})/\Delta\varepsilon_{lo}$ (open symbols), for vinyl-PC versus temperature for values between $T$ = 176 and 186 K. Data (circles and triangles) are recorded at different fields as indicated in the legend ($E_B$ =150, 200, and 250 kV/cm), but shown after rescaling to $E_B \rightarrow$ 100 kV/cm. The stars represent the peak values (scaled arbitrarily) of the cubic susceptibilities, $\chi_{3,max}$, from Fig. 6.14, which track the temperature dependence of $\Delta_E \ln \tau$.

For vinyl-PC, the temperature dependence of both the saturation in terms of $\Delta_E \ln \Delta\varepsilon$ and the electro-rheological effect quantified by $\Delta_E \ln \tau$ have been evaluated, and the results are compiled graphically in Fig. 6.16. Data obtained for different fields were normalized to $E_B \rightarrow$ 100 kV/cm and are available for the temperature range from 176 to 186 K, in which the loss peak position changes from $\nu_{max}$ = 2 Hz to 2 kHz. While the saturation level remains relatively constant at $\Delta_E \ln \Delta\varepsilon \approx$ –0.3 %, the magnitude of the electro-rheological effect changes by a factor of two, from $\Delta_E \ln \tau \approx$ 1.0 % at $T$ = 176 K to ≈ 0.5 % at $T$ = 186 K. Further below, this trend of $\Delta_E \ln \tau(T)$ will be compared with results from the cubic susceptibility.

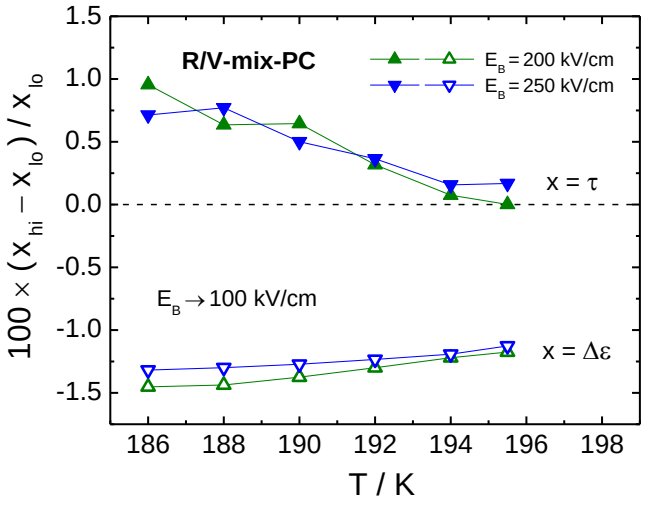


FIG. 6.17. Field induced relative changes of the dielectric relaxation time constant, $\Delta_E \ln \tau \approx (\tau_{hi} - \tau_{lo})/\tau_{lo}$ (solid symbols), and of the relaxation amplitude, $\Delta_E \ln \Delta\varepsilon \approx (\Delta\varepsilon_{hi} - \Delta\varepsilon_{lo})/\Delta\varepsilon_{lo}$ (open symbols), for R/V-mix-PC versus temperature for values between $T$ = 186 and 195.5 K. Data (triangles) are recorded at different fields as indicated in the legend ($E_B$ =200 and 250 kV/cm), but shown after rescaling to $E_B \rightarrow$ 100 kV/cm.

Surprisingly, the nonlinear behavior of the methoxy-PC's (S-MeO-PC and S/R-mix-PC) and hydroxy-PC differs qualitatively from what is shown for vinyl-PC in Fig. 6.8 and Fig. 6.9. While the very high values of both $\varepsilon_s$ and $\partial\varepsilon_s/\partial T$ lead to expecting very pronounced electro-rheological effects for the methoxy-PC's, the results depicted in Fig. 6.10 reveal that there is no signature of the loss peak being shifted to lower frequencies as a result of applying a high dc electric field. The vinyl-PC curve included in Fig. 6.10 is scaled for twice the dc field level $E_B$, and thus effectively magnified a factor of four relative to the methoxy-PC curves. This shows that the saturation effects for S-MeO-PC and S/R-mix-PC exceed the value for vinyl-PC, as judged from the levels of $(\varepsilon''_{hi} - \varepsilon''_{lo})/\varepsilon''_{lo}$ at $\nu = \nu_{max}$ (5.5 % for S-MeO-PC, 4.5 % for S/R-mix-PC, and 0.4 % for vinyl-

PC if scaled to $E_B \rightarrow 100$ kV/cm in each case). Recalling that the signature of an electro-rheological shift of the loss peak appears as increased values of $(\varepsilon''_{hi} - \varepsilon''_{lo})/\varepsilon''_{lo}$ for $\nu < \nu_{max}$ and decreased values for $\nu > \nu_{max}$ relative to the saturation level, no such signature is observed for the two methoxy-PC's nor for hydroxy-PC, see Table 6.1. The overall frequency dependence for these three cases is moderate, but amounts to a slightly narrower peak at high fields.

An interesting intermediate case is observed for R/V-mix-PC, the mixture of (*R*)-(+)-methoxy- and vinyl-PC. An analysis of the data in Fig. 6.11 yields the temperature dependent quantities $\Delta_E \ln \Delta\varepsilon$ and $\Delta_E \ln \tau$, which are presented in Fig. 6.18. At $T$ = 186 K, R/V-mix-PC shows a saturation effect that amounts to $\Delta_E \ln \Delta\varepsilon = -1.4$ % after rescaling to $E_B \rightarrow 100$ KV/cm, almost five times the value found for pure vinyl-PC. The variation of $\Delta_E \ln \Delta\varepsilon$ with temperature is mild, dropping to about −1.2 % at $T$ = 196 K. Although the dielectric constant of R/V-mix-PC is 50 % higher than that of vinyl-PC (see Table 6.1), the field induced shifts in relaxation time are almost the same at the lower temperatures, $\Delta_E \ln \tau \approx 1$ % for R/V-mix-PC at $T$ = 186 K and for vinyl-PC at $T$ = 179 K. Unlike the vinyl-PC case of Fig. 6.17, the mixture shows a pronounced decline of the electro-rheological effect, which vanishes already at $T$ = 196 K, see Fig. 6.18. In comparing R/V-mix-PC with pure vinyl-PC, it appears that the enhanced values of both $\varepsilon_s$ and $\partial\varepsilon_s/\partial T$ do amplify the saturation effects as reflected in $\Delta_E \ln \Delta\varepsilon$, but not the sensitivity of the dynamics to a field as gauged by $\Delta_E \ln \tau$.

A recent prediction of this electro-rheological effect was based upon the field induced entropy change of Eq. (6.16) modifying the dynamics via the Adam-Gibbs (AG)

model, $\lg \tau_\alpha = A + C/(TS_{cfg})$,[37] that connects the structural relaxation time or viscosity with the configurational entropy. While initial experimental results on glycerol supported this picture,[14,40] subsequent studies on five other materials concluded that the AG relation did not provide a quantitative link between field induced change of entropy and the electro-rheological effect.[39,61,41] Still, a survey of eight glass-forming liquids revealed that some correlation between $\Delta_E S$ and $\Delta_E \ln \tau$ exists, where the value of $\Delta_E S$ is largely a matter of the slope $\partial \varepsilon_s / \partial T$, see Eq. (6.16).[55,61] Several observations of the present study challenge a connection between $\Delta_E \ln \tau$ and $\Delta_E S$: The present result that $\Delta_E S$ for S-MeO-PC is extraordinarily high (≈ 100 mJ $K^{-1}$ $mol^{-1}$ at $E_B$ = 100 kV/cm) but its $\Delta_E \ln \tau$ value practically zero suggests that entropy is not always a relevant factor regarding the extent of the electro-rheological effect. A similar argument can be derived from the hydroxy-PC results. Moreover, the increased values of $\varepsilon_s$ and $\partial \varepsilon_s / \partial T$ for the R/V-mix-PC sample relative to pure vinyl-PC does not enhance the field induced change in relaxation times, nor can a correlation between $\Delta_E \ln \tau$ and $\Delta_E S$ explain that $\Delta_E \ln \tau$ approaches zero for R/V-mix-PC at somewhat elevated temperatures. While it has been shown previously that $\Delta_E S$ combined with the AG relation is in many cases not capable of rationalizing the field induced change in dynamics in a quantitative fashion,[39,61] the present observations involving methoxy- and hydroxy- derivatives of PC points more towards a qualitative issue with linking $\Delta_E \ln \tau$ to $\Delta_E S$, at least for the present class of liquids.

The spectra of the field induced changes of the dielectric loss shown as $(\varepsilon''_{hi} - \varepsilon''_{lo})/\varepsilon''_{lo}$ vs $\nu$ in Fig. 6.8, Fig. 6.9, Fig. 6.10, and Fig. 6.11 are meant to reflect steady state behavior, i.e., the situations in which the sample is in equilibrium with the high field. The

ensure that this is the case, numerous time-resolved curves of $(\varepsilon''_{hi} - \varepsilon''_{lo})/\varepsilon''_{lo}$ at a fixed frequency have been recorded, tracking the temporal evolution of the nonlinear effect until steady state had been reached. The long time plateau values of such curves confirm that the above spectra reflect steady state situations, and two representative examples are illustrated in Fig. 6.12 (vinyl-PC) and Fig. 6.13 (S-MeO-PC). In the vinyl-PC case, Fig. 6.12, about half of the 3.9 % reduction in $\varepsilon''$ stems from saturation ($\Delta_E \ln \Delta\varepsilon$), the other half is due to the electro-rheological effect ($\Delta_E \ln \tau$). By contrast, practically the entire 4.5 % depression of the loss is a matter of the saturation effect in the S-MeO-PC case of Fig. 6.14. Both examples of the time resolved rise and decay of the nonlinear effect display the rise/decay asymmetry seen in all time curves of nonlinear effects that depend quadratically on the field,[55,40,39] including the optically detected analogues of the present features, namely the electro-optical Kerr effect studies on similar viscous liquids.[66,67,68,69] The basic idea of the explanation of this effect is that these patterns do not follow the symmetric rise and decay of polarization $P(t)$, but rather the rise and decay of $P^2(t)$, for which the symmetry is lost.[40,55] The S-MeO-PC example of Fig. 6.15 is the first case where this is observed for saturation being practically the sole nonlinear effect.

#### 6.2.1.3 Cubic Susceptibilities

We now turn to the cubic susceptibilities of these highly polar liquids, i.e., the measures of the third harmonic component of polarizability for a given ac field of high amplitude. In the context of supercooled liquids, this quantity has gained notoriety on the basis of a model that links the temperature dependence of the peak height, $\chi_{3,max}$, of the cubic susceptibility, $|\chi_3(\omega)|$, to that of the number of dynamically correlated particles,

$N_{corr}$, for systems close to a critical point.[16] Motivated by this model, data for $|\chi_3(\omega)|$ has been collected for numerous materials and analyzed regarding the change of $N_{corr}$ with temperature.[15,17,70,71] The main interest in $N_{corr}(T)$ is its potential explanation of the significant increase in the apparent activation energy as the temperature is reduced towards the glass transition at $T_g$. Bauer *et al.* have argued that $N_{corr}(T)$ may explain this super-Arrhenius temperature dependence of the structural relaxation times.[18]

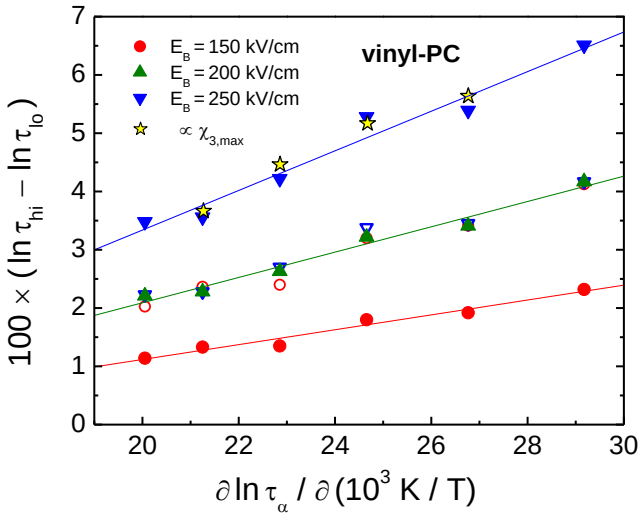


FIG. 6.18. Field induced relative changes of the dielectric relaxation time constant, $\Delta_E \ln \tau \approx (\tau_{hi} - \tau_{lo})/\tau_{lo}$ (solid symbols), for vinyl-PC versus apparent activation energy in terms of $\partial \ln \tau / \partial (1/T)$. Data are for temperatures between $T$ = 176 and 186 K from Fig. 6.16, and recorded at different fields as indicated in the legend ($E_B$ =150, 200, and 250 kV/cm). Open symbols (partly hidden behind the solid triangles for $E_B$ = 200 kV/cm) represent the $E_B$ = 150 and 250 kV/cm after rescaling to $E_B \rightarrow$ 200 kV/cm, demonstrating the quadratic field dependence of the nonlinear effects. The stars represent the peak values (scaled arbitrarily) of the cubic susceptibilities, $\chi_{3,max}$, from Fig. 6.14, which depend linearly on the apparent activation energy.

The present $|\chi_3(\omega)|$ curves of Fig. 6.14 are reminiscent of the cubic susceptibilities observed for various other liquids in their highly supercooled state:[15,17,18,57,70,71] a plateau

emerges at low frequencies, a so-called 'hump' in $|\chi_3(\omega)|$ appears that reaches about twice the amplitude of the low frequency plateau level, $\chi_{3,lf}$, and the peak of the cubic susceptibility is positioned at about $\nu_{max}/3$, where $\nu_{max}$ refers to the low field loss peak frequency. Another feature that is observed repeatedly is that the 'hump' amplitude, $\chi_{3,max}$, decreases as the temperature is increased. In Fig. 6.17, this temperature variation of $\chi_{3,max}(T)$ is compared (after arbitrary scaling) with that of the electro-rheological effect, $\Delta_E \ln \tau(T)$, and the two trends are strikingly similar. By comparison, the level of $\chi_{3,lf}$ plateau is nearly temperature invariant, consistent with its assignment to dielectric saturation and the nearly constant $\Delta_E \ln \Delta\varepsilon(T)$ in Fig. 6.17. These features underline the previous notion that the 'hump' of $|\chi_3(\omega)|$ and the electro-rheological effect are coupled phenomena, while the low frequency plateau reflects the level of saturation.[45,57] Moreover, both the magnitude of the electro-rheological effect, $\Delta_E \ln \tau$, as extracted from nonlinear effects at the fundamental frequency ($\omega$) and the 'hump' amplitude, $\chi_{3,max}$, taken from the cubic susceptibility ($3\omega$) vary linearly with the apparent activation energy quantified in terms of $\partial \ln \tau_\alpha / \partial(1/T)$. This is demonstrated for vinyl-PC in Fig. 6.19, which may be understood as indicating that the sensitivity of $\tau_\alpha$ to changes in temperature is correlated with the variation of $\tau_\alpha$ with the squared electric field, $E_B^2$. Interestingly, all quantities in Fig. 6.19 extrapolate to zero nonlinear effect for an apparent activation parameter of $\partial \ln \tau_\alpha / \partial(10^3 \mathrm{K}/T) \approx 10.6$, equivalent to $T = 211$ K or $\tau_\alpha \approx 20$ ns. This could indicate that dynamics are not expected to be sensitive to an external electric field for

temperatures in excess of about $T_c$, the critical temperature of the idealized mode coupling theory.

Once again, the methoxy-PC's, represented in Fig. 6.16 by the S/R-mix-PC case, differ qualitatively from the usual appearance of the cubic susceptibility spectra. While S/R-mix-PC displays a high level of saturation ($\Delta_E \ln \Delta\varepsilon(T)$) and accordingly a high plateau value ($\chi_{3,lf}$) at low frequencies, the $|\chi_3(\omega)|$ curves of Fig. 6.16 fail to rise significantly above $\chi_{3,lf}$ at higher frequencies. Recalling that the methoxy-PC's did not display any discernable electro-rheological effect, this is considered a clear and model-free indication that the $|\chi_3(\omega)|$ 'hump' is intimately linked to the electro-rheological effect.

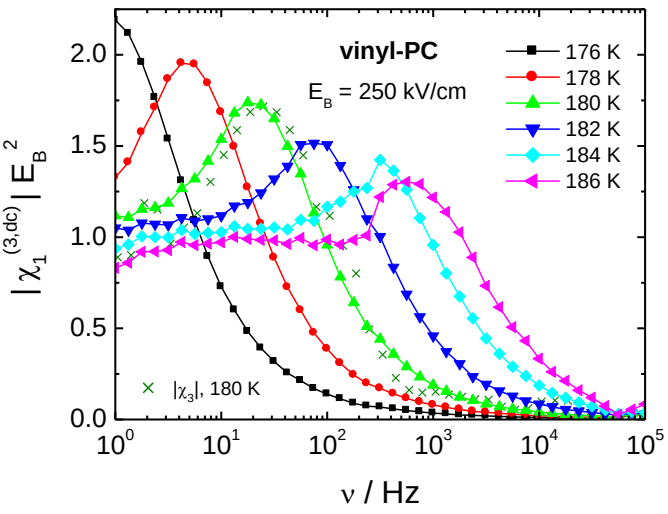


FIG. 6.19. Field induced susceptibility change at the fundamental frequency, shown as $|\chi_1^{(3,dc)}|E_B^2$ versus fundamental frequency $\nu$ for vinyl-PC at temperatures in the range from $T$ = 176 to 186 K. All curves are recorded for a small ac field with peak value $E_0$ = 35 kV/cm superimposed onto a dc bias field of $E_B$ = 250 kV/cm. Values are derived from the same permittivity data that are shown as $(\varepsilon''_{hi} - \varepsilon''_{lo})/\varepsilon''_{lo}$ in Fig. 6.8. The $|\chi_3|$ spectrum for vinyl-PC at $T$ = 180 K is reproduced as crosses from Fig. 6.14, after rescaling the amplitude to match that of $|\chi_1^{(3,dc)}|E_B^2$.

The above notion implies a link between $\chi_1^{(3,dc)}(\omega)$ and $\chi_3^{(3)}(\omega)$ in Eq. (6.13), i.e., between the changes in permittivity (at the fundamental frequency) that arise from a high dc field and the cubic susceptibility $\chi_3(\omega)$ originating from a large amplitude ac field. The modulus of the susceptibility $\chi_1^{(3,dc)}(\omega)$ can be derived from permittivity values via

$$\left|\hat{\chi}_1^{(3,dc)}(\omega)\right| E_B^2 = \sqrt{\left(\varepsilon'_{hi}(\omega) - \varepsilon'_{lo}(\omega)\right)^2 + \left(\varepsilon''_{hi}(\omega) - \varepsilon''_{lo}(\omega)\right)^2} \quad , \tag{6.20}$$

which follows from Eq. (6.13). Experimental spectra of $|\chi_1^{(3,dc)}|$ are shown for vinyl-PC and SR-mix-PC in Fig. 6.20 and Fig. 6.21, respectively. Clearly, these spectral profiles are very similar to the respective $|\chi_3(\omega)|$ curves of Fig. 6.15 and Fig. 6.16, see especially the crosses in Fig. 6.20 representing $|\chi_3(\omega)|$ for a direct comparison with $|\chi_1^{(3,dc)}|$ at $T$ = 180 K. Also, the qualitatively different $|\chi_3(\omega)|$ behavior of vinyl-PC and SR-mix-PC is reiterated in the $|\chi_1^{(3,dc)}|$ spectra of the two liquids, and the very high values of $|\chi_1^{(3,dc)}|$ for the SR-mix-PC case are a reflection of the high dielectric constant and saturation levels of that compound. Overall, the similarity of $\chi_1^{(3,dc)}(\omega)$ and $\chi_3(\omega)$ supports a recent model which calculated $|\chi_3(\omega)|$ spectra on the basis of $\chi_1$ susceptibilities leading to semi-quantitative agreement with experiments.[57]

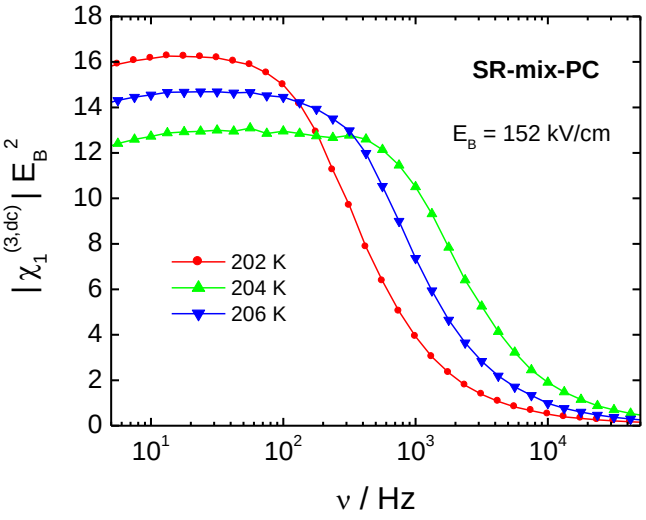


FIG. 6.20. Field induced susceptibility change at the fundamental frequency, shown as $|\chi_1^{(3,dc)}|E_B^2$ versus fundamental frequency $\nu$ for S/R-mix-PC at temperatures in the range from $T$ = 202 to 206 K. All curves are recorded for a small ac field with peak value $E_0$ = 21.5 kV/cm superimposed onto a dc bias field of $E_B$ = 152 kV/cm. Values are derived from the same permittivity data that are shown as $(\varepsilon''_{hi} - \varepsilon''_{lo})/\varepsilon''_{lo}$ in Fig. 6.10.

### 6.2.2 Conclusions

Derivatives of propylene carbonates are highly polar glass-forming liquids reaching static dielectric constants $\varepsilon_s$ as high as 250 for S-MeO-PC. Expectedly, the magnitudes of dielectric saturation, $\Delta_E \ln\Delta\varepsilon$, increase systematically with the polarity of the liquid, with S-MeO-PC reducing its static dielectric constant by 5 % when subject to a dc bias field of $E_B$ = 100 kV/cm. For vinyl-PC and its mixture with R-MeO-PC, a static field also modifies the dynamics by shifting the dielectric loss profile to lower frequencies, equivalent to increasing the dielectric relaxation times or shifting $T_g$ to higher temperatures. It turns out that this electro-rheological effect for vinyl-PC is of similar magnitude compared with PC itself. Based on the extraordinarily high values of $\varepsilon_s$ and $\partial\varepsilon_s/\partial T$ for the methoxy-PC's, even more pronounced electro-rheological effects are

readily expected for S-MeO-PC, R-MeO-PC, and S/R-mix-PC. However, no sensitivity of the loss peak position to a static field could be detected for these methoxy derivatives of PC. This material specific absence or presence of a significant electro-rheological effect in terms of $\Delta_E \ln \tau$ correlates strongly with the occurrence of a peak in the cubic susceptibility, $|\chi_3(\omega)|$, that rises well above the low frequency plateau level, $|\chi_3(\omega \rightarrow 0)|$. This is seen as a clear indication of the $|\chi_3(\omega)|$ 'hump' being linked to the nonlinear dielectric effect that originates from the electro-rheological behavior. Further support of this notion stems from the observation that both the magnitude of the electro-rheological effect and the peak height of the cubic susceptibility vary linearly with the apparent activation energy, but extrapolating to zero effect when $\partial \ln \tau_\alpha / \partial(1/T)$ has dropped to about one third of its value at $T_g$.

The finding that a simple molecular liquid with high values of $\varepsilon_s$ and $\partial \varepsilon_s / \partial T$ displays no field induced increase of dielectric relaxation times and no clear maximum in the cubic susceptibility implies that, at present, there is no clear understanding of which properties of a liquid determine the sensitivity of liquid dynamics to a static field. Apart from the high dielectric constants of those cases that do not display electro-rheological behavior, another common feature is the correspondingly low width of the loss profiles ($\beta_{KWW} > 0.8$), but there is no obvious connection between stretching exponent and magnitude of a nonlinear dielectric effect. The earlier idea that the field induced entropy change controls the magnitude of the electro-rheological features via the Adam-Gibbs relation is challenged on a qualitative level by the results of this study. Further research is required to be able to elucidate the mechanism of how dynamics change as a result of

applying a static field and to predict the electro-rheological effect for molecular materials on a quantitative level.

### 6.3 References


[1] F. Kremer and A. Schönhals (Eds.), *Broadband Dielectric Spectroscopy* (Springer, Berlin, 2002).

[2] R. Richert, Adv. Chem. Phys. **156**, 101 (2014).

[3] J. Małecki, J. Chem. Phys. **36**, 2144 (1962).

[4] L. P. Singh and R. Richert, Phys. Rev. Lett. **109**, 167802 (2012).

[5] J. Herweg, Z. Physik **3**, 36 (1920).

[6] K. De Smet, L. Hellemans, J. F. Rouleau, R. Corteau, and T. K. Bose, Phys. Rev. E **57**, 1384 (1998).

[7] D. V. Matyushov, J. Chem. Phys. **142**, 244502 (2015).

[8] B. Schiener, R. Böhmer, A. Loidl, and R. V. Chamberlin, Science **274**, 752 (1996).

[9] T. Matsuo, H. Suga, and S. Seki, Bull. Chem. Soc. Jpn. **39**, 1827 (1966).

[10] A. Khalife, U. Pathak, and R. Richert, Eur. Phys. J. B **83**, 429 (2011).

[11] T. Bauer, P. Lunkenheimer, S. Kastner, and A. Loidl, Phys. Rev. Lett. **110**, 107603 (2013).

[12] G. P. Johari, J. Chem. Phys. **138**, 154503 (2013).

[13] D. L'Hôte, R. Tourbot, F. Ladieu, and P. Gadige, Phys. Rev. B **90**, 104202 (2014).

[14] S. Samanta and R. Richert, J. Chem. Phys. **142**, 044504 (2015).

[15] C. Crauste-Thibierge, C. Brun, F. Ladieu, D. L'Hôte, G. Biroli, and J.-P. Bouchaud, Phys. Rev. Lett. **104**, 165703 (2010).

[16] J.-P. Bouchaud and G. Biroli, Phys. Rev. B **72**, 064204 (2005).

[17] C. Brun, F. Ladieu, D. L'Hôte, M. Tarzia, G. Biroli, and J.-P. Bouchaud, Phys. Rev. B **84**, 104204 (2011).

[18] Th. Bauer, P. Lunkenheimer, and A. Loidl, Phys. Rev. Lett. **111**, 225702 (2013).

[19] M. Michl, Th. Bauer, P. Lunkenheimer, and A. Loidl, Phys. Rev. Lett. **114**, 067601 (2015).

[20] M. Michl, Th. Bauer, P. Lunkenheimer, and A. Loidl, J. Chem. Phys. **144**, 114506 (2016).

[21] R. Richert, J. Chem. Phys. **133**, 074502 (2010).

[22] R. Richert and S. Weinstein, Phys. Rev. Lett. **97**, 095703 (2006).

[23] S. Havriliak and S. Negami, Polymer **8**, 161 (1967).

[24] D. V. Matyushov and R. Richert, J. Chem. Phys. **144**, 041102 (2016).

[25] A. J. Kovacs, J. J. Aklonis, J. M. Hutchinson, and A. R. Ramos, J. Polym. Sci. B: Polym. Phys. **17**, 1097 (1979).

[26] I. M. Hodge, J. Non-Cryst. Solids **169**, 211 (1994).

[27] R. V. Chamberlin, B. Schiener, and R. Böhmer, Mat. Res. Soc. Symp. Proc. **455**, 117 (1997).

[28] B. Schiener, R. V. Chamberlin, G. Diezemann, and R. Böhmer, J. Chem. Phys. **107**, 7746 (1997).

[29] K. R. Jeffrey, R. Richert, and K. Duvvuri, J. Chem. Phys. **119**, 6150 (2003).

[30] S. Weinstein and R. Richert, Phys. Rev. B **75**, 064302 (2007).

[31] T. Blochowicz and E. A. Rössler, J. Chem. Phys. **122**, 224511 (2005).

[32] W. Huang and R. Richert, J. Chem. Phys. **130**, 194509 (2009).

[33] R. Richert, Thermochim. Acta **522**, 28 (2011).

[34] L.-M. Wang and R. Richert, Phys. Rev. Lett. **99**, 185701 (2007).

[35] H. Fröhlich, *Theory of Dielectrics* (Clarendon, Oxford, 1958).

[36] I. V. Blazhnov, N. P. Malomuzh, and S. V. Lishchuk, J. Chem. Phys. **121**, 6435 (2004).

[37] G. Adam and J. H. Gibbs, J. Chem. Phys. **43**, 139 (1965).

[38] M. Goldstein, J. Chem. Phys. **123**, 244511 (2005).

[39] S. Samanta and R. Richert, J. Phys. Chem. B (in press).

[40] A. R. Young-Gonzales, S. Samanta, and R. Richert, J. Chem. Phys. **143**, 104504 (2015).

[41] S. Samanta, O. Yamamuro, and R. Richert, Thermochim. Acta **636**, 57 (2016).

[42] R. Richert, J. Chem. Phys. **134**, 144501 (2011).

[43] S. Samanta and R. Richert, J. Chem. Phys. **140**, 054503 (2014).

[44] R. Richert, J. Non-Cryst. Solids **357**, 726 (2011).

[45] R. Richert, J. Chem. Phys. **144**, 114501 (2016).

[46] W. T. Coffey and B. V. Paranjape, Proc. R. Ir. Acad. **78**, 17 (1978).

[47] J. L. Déjardin and Yu. P. Kalmykov, Phys. Rev. E **61**, 1211 (2000).

[48] R. Richert, Phys. Rev. E **88**, 062313 (2013).

[49] S. Albert, Th. Bauer, M. Michl, G. Biroli, J.-P. Bouchaud, A. Loidl, P. Lunkenheimer, R. Tourbot, C. Wiertel-Gasquet, and F. Ladieu, Science **352**, 1308 (2016).

[50] B. Riechers, K. Samwer, and R. Richert, J. Chem. Phys. **142**, 154504 (2015).

[51] C. Brun, C. Crauste-Thibierge, F. Ladieu, D. L'Hôte, J. Chem. Phys. **134**, 194507 (2011).

[52] G. Diezemann, Phys. Rev. E **85**, 051502 (2012).

[53] P. Debye, *Polar Molecules* (Chemical Catalog Company, New York, 1929).

[54] C. J. F. Böttcher, *Theory of Electric Polarization*, Vol.1 (Elsevier, Amsterdam, 1973).

[55] R. Richert, J. Phys.: Condens. Matter **29**, 363001 (2017).

[56] A. Jedrzejowska, K. L. Ngai, and M. Paluch, J. Phys. Chem. A **120**, 8781 (2016).

[57] P. Kim, A. R. Young-Gonzales, and R. Richert, J. Chem. Phys. **145**, 064510 (2016).

[58] H. Wagner and R. Richert, J. Phys. Chem. B **103**, 4071 (1999).

[59] L. Simeral and R. L. Amey, J. Phys. Chem. **74**, 1443 (1970).

[60] L.-M. Wang, V. Velikov, and C. A. Angell, J. Chem. Phys. **117**, 10184 (2002).

[61] R. Richert, J. Chem. Phys. **146**, 064501 (2017).

[62] R. Payne and I. E. Theodorou, J. Phys. Chem. **76**, 2891 (1972).

[63] J. Małecki, J. Mol. Struct. **436-437**, 595 (1997).

[64] W. Huang and R. Richert, J. Phys. Chem. B **112**, 9909 (2008).

[65] R. Richert and S. Weinstein, Phys. Rev. Lett. **97**, 095703 (2006).

[66] R. Coelho and D. Khac Manh, C. R. Acad. Sc. Paris - Serie C **264**, 641 (1967).

[67] M. S. Beevers, J. Crossley , D. C. Garrington, and G. Williams, Faraday Symp. Chem. Soc. **11**, 38 (1977).

[68] M. S. Beevers, D. A. Elliott, and G. Williams, J. Chem. Soc. Faraday Trans. 2 **76**, 112 (1980).

[69] J. L. Déjardin, Y. P. Kalmykov, and P. M. Déjardin, Adv. Chem. Phys. **117**, 275 (2001).

[70] C. Crauste-Thibierge, C. Brun, F. Ladieu, D. L'Hôte, G. Biroli, and J.-P. Bouchaud, J. Non-Cryst. Solids **357**, 279 (2011).

[71] R. Casalini, D. Fragiadakis, and C. M. Roland, J. Chem. Phys. **142**, 064504 (2015).

COPMPREHENSIVE LIST OF REFERENCES

## CHAPTER 1


[1] P. Debije, Verh. Dtsch. Phys. Ges. **15** 777 (1913).

[2] P. Debye, *Polar Molecules*, Chemical Catalog Company, New York, 1929.

[3] D.W. Davidson, R.H. Cole, J. Chem Phys. **19**, 1484 (1951).

[4] W. Dannhauser, A. F. Flueckinger, Phys. Chem. Liq. **2**, 37 (1970).

[5] W. Dannhauser, J. Chem. Phys. **48**, 1911 (1968).

[6] G. P. Johari, W. Dannhauser, J. Chem. Phys. **48**, 3407 (1968) .

[7] G. P. Johari, W. Dannhauser, J. Phys. Chem. **72**, 3273 (1968).

[8] J.K. Vij, W.G. Scaife, J.H. Calderwood, J. Phys. D: Appl. Phys. **11**, 545 (1978).

[9] J.K. Vij, W.G. Scaife, J.H. Calderwood, J. Phys. D: Appl. Phys. **14**, 733 (1981).

[10] W. Kauzmann, Chem. Rev. **43**, 219 (1948).

[11] T. Lyon, T. A. Litovitz, J. Appl. Phys. **27**, 179 (1956).

[12] T. A. Litovitz, G. E. McDuffie, J. Chem. Phys. **39**, 729 (1963).

[13] B.M. Fung, T.W. McGaughy, J. Chem. Phys. **65**, 2970 (1976).

[14] H. Versmold, Ber. Bunsenges. Phys.Chem. **78**, 1318 (1974).

[15] C. Hansen, F. Stickel, T. Berger, R. Richert, E.W. Fischer, J. Chem. Phys. **107**, 1086 (1997).

[16] P. G. Debenedetti, F. H. Stillinger; *Nature* **410**, 259 (2001).

[17] R. Kohlrausch, Ann. Phys. **167**, 179 (1854); G. Williams and D.C. Watts, Trans. Faraday Soc. **66**, 80 (1970).

[18] H. Vogel, Phys. Z. 22, 645 (1921); G.S. Fulcher, J. Am. Ceram. Soc. **8**, 339 (1925); G. Tammann, W. Hesse, Z. Anorg. Allgem. Chem. **156**, 245 (1926)

[19] H. Huth, L.-M. Wang, C. Schick, and R. Richert, J. Chem. Phys. **126**, 104503 (2007).

[20] S. S. N. Murthy and M. Tyagi, J. Chem. Phys. **117**, 3837 (2002).

[21] L.-M. Wang, Y. Tian, R. Liu, and R. Richert, J. Chem. Phys. **128**, 084503 (2008).

[22] G. P. Johari, O. E. Kalinovskaya, and J. K. Vij, J. Chem. Phys. **114**, 4634 (2001).

[23] O. E. Kalinovskaya, J. K. Vij, and G. P. Johari, J. Phys. Chem. A **105**, 5061 (2001).

[24] L. P. Singh, C. Alba-Simionesco, and R. Richert, J. Chem. Phys. **139**, 144503 (2013).

[25] J. G. Kirkwood, J. Chem. Phys. **7**, 911 (1939)

[26] C. J. F. Bötcher, *Theory of Electric Polarization* (Elsevier, Amsterdam, 1973), Vol. 1.

[27] L. P. Singh and R. Richert, Phys. Rev. Lett. **109**, 167802 (2012).

[28] V. V. Levin and Y. D. Feldman, Chem. Phys. Lett. 87, 162 (1982

[29] C. Gainaru, R. Meier, S. Schildmann, C. Lederle, W. Hiller, E. A. Rössler, and R. Böhmer, Phys. Rev. Lett. 105, 258303 (2010).).

[30] R. Brand, P. Lunkenheimer, U. Schneider, and A. Loidl, J. Phys. Rev. B **62**, 8878 (2000).

[31] Y. Z. Chua, A. R. Young-Gonzales, R. Richert, M. D. Ediger, C. Schick, J. Chem. Phys. **147**, 014502.1 (2017).

[32] J. Malecki, J. Chem. Phys. **36,** 2144 (1962).

[33] J. Malecki, J.Chem. Phys. **43**, 1351 (1965).

[34] A. Piekara, J. Chem. Phys. **36**, 2145 (1962)

[35] J. Malecki, J. Mol. Struct. **436,** 595 (1997).

[36] T. Matsuo, H. Suga, and S. Seki, Bull. Chem. Soc. Japan, **39**, 1827 (1996)

[37] A. Khalife, U. Pathak, and R. Richert, Eur. Phys. J. B **83**, 429 (2011).

[38] S. Galema, Chem. Soc. Rev. **26**, 233 (1997)

[39] R. Richert, J. Phys.: Condens. Matter **29**, 363001 (2017).

## CHAPTER 2


1 F. Kremer, A. Schönhals (Eds.), Broadband Dielectric Spectroscopy ( Springer, 2003)

2 W. Huang and R. Richert, J. Chem. Phys.130, 194509 (2009).

3 P. Horowitz, The Art of Electronics 2nd ed. (Winfield Hill, 1989)

4 L. Yang, A. Guiseppi-Wilson, and A. Guiseppi-Elie, Biomed. Microdevices **13**, 279 (2011).

5 M. Tylinski, M. S. Beasley, Y. Z. Chua, C. Schick, and M. D. Ediger, J. Chem. Phys. **146**, 203317 (2017).

6 M. Tylinski, Y. Z. Chua, M. S. Beasley, C. Schick, and M. D. Ediger, J. Chem. Phys. **145**, 174506 (2016).

7 S. Capponi, S. Napolitano, and M. Wübbenhorst, Nat. Commun. **3**, 1233 (2012)

8 A. Kasina, T. Putzeys, and M. Wübbenhorst, J. Chem. Phys. **143**, 244504 (2015)

9 B. Reichers, A. Guiseppi-Ellie, M.D. Ediger, and R. Richert, J. Chem. Phys. (Submitted)


## CHAPTER 3


1 R. Richert, Adv. Chem. Phys. **156**, 101 (2014).

2 J. Herweg, Z. Physik **3**, 36 (1920).

3 K. De Smet, L. Hellemans, J. F. Rouleau, R. Corteau, and T. K. Bose, Phys. Rev. E **57**, 1384 (1998).

4 D. V. Matyushov, J. Chem. Phys. **142**, 244502 (2015).

5 J. Małecki, J. Chem. Phys. **36**, 2144 (1962).

6 L. P. Singh and R. Richert, Phys. Rev. Lett. **109**, 167802 (2012).

7 B. Roling, J. Chem. Phys. **117**, 1320 (2002).

8 B. Roling, S. Murugavel, A. Heuer, L. Lühning, R. Friedrich, and S. Röthel, Phys. Chem. Chem. Phys. **10**, 4211 (2008).

9 J. Zioło and S. J. Rzoska, Phys. Rev. E **60**, 4983 (1999).

[10] A. Drozd-Rzoska, S. J. Rzoska, J. Zioło, Phys. Rev. E **77**, 041501 (2008).

[11] G. P. Johari, J. Chem. Phys. **138**, 154503 (2013).

[12] S. Samanta and R. Richert, J. Chem. Phys. **142**, 044504 (2015).

[13] J. K. Park, J. C. Ryu, W. K. Kim, and K. H. Kang, J. Phys. Chem. B **113**, 12271 (2009).

[14] V. Kaiser, S. T. Bramwell, P. C. W. Holdsworth, and R. Moessner, Nature Materials **12**, 1033 (2013).

[15] J. F. Scott, Annu. Rev. Mater. Res. **41**, 229 (2011).

[16] B. Schiener, R. Böhmer, A. Loidl, and R. V. Chamberlin, Science **274**, 752 (1996).

[17] T. Matsuo, H. Suga, and S. Seki, Bull. Chem. Soc. Jpn. **39**, 1827 (1966).

[18] A. Khalife, U. Pathak, and R. Richert, Eur. Phys. J. B **83**, 429 (2011).

[19] T. Bauer, P. Lunkenheimer, S. Kastner, and A. Loidl, Phys. Rev. Lett. **110**, 107603 (2013).

[20] W. Huang and R. Richert, J. Phys. Chem. B **112**, 9909 (2008).

[21] J.-P. Bouchaud and G. Biroli, Phys. Rev. B **72**, 064204 (2005).

[22] C. Crauste-Thibierge, C. Brun, F. Ladieu, D. L'Hôte, G. Biroli, and J.-P. Bouchaud, Phys. Rev. Lett. **104**, 165703 (2010).

[23] C. Brun, F. Ladieu, D. L'Hôte, M. Tarzia, G. Biroli, and J.-P. Bouchaud, Phys. Rev. B **84**, 104204 (2011).

[24] J. L. Déjardin. Y. P. Kalmykov, and P. M. Déjardin, Adv. Chem. Phys. **117**, 275 (2001).

[25] S. Havriliak and S. Negami, Polymer **8**, 161 (1967).

[26] H. Fröhlich, *Theory of Dielectrics* (Clarendon, Oxford, 1958).

[27] R. Richert, Thermochim. Acta **522**, 28 (2011).

[28] M. D. Ediger, Ann. Rev. Phys. Chem. **51**, 99 (2000).

[29] R. Richert, J. Phys.: Condens. Matter **14**, R703 (2002).

[30] R. Richert, Physica A **322**, 143 (2003).

[31] M. Goldstein, J. Chem. Phys. **123**, 244511 (2005).

[32] C. Hansen, F. Stickel, T. Berger, R. Richert, and E. W. Fischer, J. Chem. Phys. **107**, 1086 (1997).

[33] T. Blochowicz and E. A. Rössler, J. Chem. Phys. **122**, 224511 (2005).

[34] S. Weinstein and R. Richert, Phys. Rev. B **75**, 064302 (2007).

[35] W. Huang and R. Richert, J. Chem. Phys. **130**, 194509 (2009).

[36] G. Adam and J. H. Gibbs, J. Chem. Phys. **43**, 139 (1965).

[37] R. Richert and C. A. Angell, J. Chem. Phys. **108**, 9016 (1998).

[38] R. Böhmer, C. Gainaru, and R. Richert, Physics Reports **545**, 125 (2014).

[39] C. T. Moynihan and A. V. Lesikar, Ann. New York Acad. Sci. **371**, 151 (1981).

[40] D. L'Hôte, R. Tourbot, F. Ladieu, and P. Gadige, Phys. Rev. B **90**, 104202 (2014).

[41] L.-M. Wang and R. Richert, Phys. Rev. Lett. **99**, 185701 (2007).

[42] R. Kohlrausch, Pogg. Ann. Phys. **91**, 179 (1854).

[43] G. Williams and D. C. Watts, Trans. Faraday Soc. **66**, 80 (1970).

[44] I. M. Hodge, J. Non-Cryst. Solids **169**, 211 (1994).

[45] L.-M. Wang and R. Richert, J. Chem. Phys. **121**, 11170 (2004).

[46] C. J. F. Böttcher, *Theory of Electric Polarization, Vol 1* (Elsevier, Amsterdam, 1973).

[47] L. P. Singh, C. Alba-Simionesco, and R. Richert, J. Chem. Phys. **139**, 144503 (2013).

[48] H. Huth, L.-M. Wang, C. Schick, and R. Richert, J. Chem. Phys. **126**, 104503 (2007).

[49] M. S. Beevers, D. A. Elliott, and G. Williams, J. Chem. Soc. Faraday Trans. 2 **76**, 112 (1980).

[50] R. Coelho and D. Khac Manh, C. R. Acad. Sc. Paris - Serie C **264**, 641 (1967).

[51] J. Crossley and G. Williams, J. Chem. Soc. Faraday Trans. 2 **73**, 1906 (1977).

[52] M. S. Beevers, J. Crossley, D. C. Garrington, and G. Williams, Faraday Symp. Chem. Soc. **11**, 38 (1977).

[53] J. Crossley and G. Williams, J. Chem. Soc. Faraday Trans. 2 **73**, 1651 (1977).

[54] V. Rosato and G. Williams, J. Chem. Soc. Faraday Trans. 2 **77**, 1767 (1981).

[55] M. Michl, Th. Bauer, P. Lunkenheimer, and A. Loidl, Phys. Rev. Lett. **114**, 067601 (2015).

[56] B. Riechers, K. Samwer, R. Richert, J. Chem. Phys. **142**, 154504 (2015).

## CHAPTER 4

[1] R. Böhmer, C. Gainaru, and R. Richert, Physics Reports **545**, 125 (2014).

[2] S. S. N. Murthy, J. Phys. Chem. **100**, 8508 (1996).

[3] L.-M. Wang and R. Richert, J. Phys. Chem. B **109**, 11091 (2005).

[4] L.-M. Wang and R. Richert, J. Chem. Phys. **123**, 054516 (2005).

[5] C. Gainaru, T. Hecksher, N. B. Olsen, R. Böhmer, and J. C. Dyre, J. Chem. Phys. **137**, 064508 (2012).

[6] C. Gainaru, S. Bauer, E. Vynokur, H. Wittkamp, W. Hiller, R. Richert, and R. Böhmer, J. Phys. Chem. B **119**, 15769 (2015).

[7] W. Huang and R. Richert, J. Phys. Chem. B **112**, 9909 (2008).

[8] J. S. Hansen, A. Kisliuk, A. P. Sokolov, and C. Gainaru, Phys. Rev. Lett. **116**, 237601 (2016).

[9] H. Huth, L.-M. Wang, C. Schick, and R. Richert, J. Chem. Phys. **126**, 104503 (2007).

[10] S. S. N. Murthy and M. Tyagi, J. Chem. Phys. **117**, 3837 (2002).

[11] L.-M. Wang, Y. Tian, R. Liu, and R. Richert, J. Chem. Phys. **128**, 084503 (2008).

[12] T. A. Litovitz and G. E. McDuffie, J. Chem. Phys. **39**, 729 (1963).

[13] B. Jakobsen, C. Maggi, T. Christensen, and J. C. Dyre, J. Chem. Phys. **129**, 184502 (2008).

[14] C. Hansen, F. Stickel, T. Berger, R. Richert, and E. W. Fischer, J. Chem. Phys. **107**, 1086 (1997).

[15] C. J. F. Böttcher, *Theory of Electric Polarization, Vol 1* (Elsevier, Amsterdam, 1973).

[16] P. Bordewijk, F. Gransch, and C. J. F. Böttcher, J. Phys. Chem. **73**, 3255 (1969).

[17] G. P. Johari, O. E. Kalinovskaya, and J. K. Vij, J. Chem. Phys. **114**, 4634 (2001).

[18] W. Dannhauser, J. Chem. Phys. **48**, 1911 (1968).

[19] H. Fröhlich, *Theory of Dielectrics* (Clarendon, Oxford, 1958).

[20] L. P. Singh and R. Richert, Phys. Rev. Lett. **109**, 167802 (2012).

[21] L. P. Singh, C. Alba-Simionesco, and R. Richert, J. Chem. Phys. **139**, 144503 (2013).

[22] S. Samanta and R. Richert, J. Chem. Phys. **142**, 044504 (2015).

[23] S. Havriliak and S. Negami, Polymer **8**, 161 (1967).

[24] A. R. Young-Gonzales, S. Samanta, and R. Richert, J. Chem. Phys. **143**, 104504 (2015).

[25] S. Samanta, O. Yamamuro, and R. Richert, Thermochim. Acta **636**, 57 (2016).

[26] M. S. Beevers, D. A. Elliott, and G. Williams, J. Chem. Soc. Faraday Trans. 2 **76**, 112 (1980).

[27] R. Coelho and D. Khac Manh, C. R. Acad. Sc. Paris - Serie C **264**, 641 (1967).

[28] J. Crossley and G. Williams, J. Chem. Soc. Faraday Trans. 2 **73**, 1906 (1977).

[29] M. S. Beevers, J. Crossley, D. C. Garrington, and G. Williams, Faraday Symp. Chem. Soc. **11**, 38 (1977).

[30] J. Crossley and G. Williams, J. Chem. Soc. Faraday Trans. 2 **73**, 1651 (1977).

[31] C. Gainaru, R. Meier, S. Schildmann, C. Lederle, W. Hiller, E. A. Rössler, and R. Böhmer, Phys. Rev. Lett. **105**, 258303 (2010).

[32] W. Huang and R. Richert, J. Chem. Phys. **130**, 194509 (2009).

[33] R. Richert, Adv. Chem. Phys. **156**, 101 (2014).

[34] G. P. Johari, J. Chem. Phys. **138**, 154503 (2013).

## CHAPTER 5

[1] C. J. F. Böttcher, *Theory of Electric Polarization, Vol 1* (Elsevier, Amsterdam, 1973).

[2] R. Böhmer, C. Gainaru, and R. Richert, Physics Reports **545**, 125 (2014).

[3] C. Hansen, F. Stickel, T. Berger, R. Richert, and E. W. Fischer, J. Chem. Phys. **107**, 1086 (1997).

[4] T. A. Litovitz and G. E. McDuffie, J. Chem. Phys. **39**, 729 (1963).

[5] L.-M. Wang and R. Richert, J. Chem. Phys. **123**, 054516 (2005).

[6] L.-M. Wang, Y. Tian, R. Liu, and R. Richert, J. Chem. Phys. **128**, 084503 (2008).

[7] B. Jakobsen, C. Maggi, T. Christensen, and J. C. Dyre, J. Chem. Phys. **129**, 184502 (2008).

[8] H. Huth, L.-M. Wang, C. Schick, and R. Richert, J. Chem. Phys. **126**, 104503 (2007).

[9] Y. Z. Chua, A. R. Young-Gonzales, R. Richert, M. D. Ediger, and C. Schick, J. Chem. Phys. **147**, 014502 (2017).

[10] H. Fröhlich, *Theory of Dielectrics* (Clarendon, Oxford, 1958).

[11] W. Dannhauser, J. Chem. Phys. **48**, 1911 (1968).

[12] L. P. Singh, C. Alba-Simionesco, and R. Richert, J. Chem. Phys. **139**, 144503 (2013).

[13] S. S. N. Murthy, J. Phys. Chem. **100**, 8508 (1996).

[14] S. F. Swallen, K. L. Kearns, M. K. Mapes, Y. S. Kim, R. J. McMahon, M. D. Ediger, T. Wu, L. Yu, and S. Satija, Science **315**, 353 (2007).

[15] M. Tylinski, M. S. Beasley, Y. Z. Chua, C. Schick, and M. D. Ediger, J. Chem. Phys. **146**, 203317 (2017).

[16] M. Tylinski, Y. Z. Chua, M. S. Beasley, C. Schick, and M. D. Ediger, J. Chem. Phys. **145**, 174506 (2016).

[17] Y. Chen, W. Zhang, and L. Yu, J. Phys. Chem. B **120**, 8007 (2016).

[18] Y. Chen, M. Zhu, A. Laventure, O. Lebel, M. D. Ediger, and L. Yu, J. Phys. Chem. B **121**, 7221 (2017).

[19] S. Capponi, S. Napolitano, and M. Wübbenhorst, Nat. Commun. **3**, 1233 (2012).

[20] A. Kasina, T. Putzeys, and M. Wübbenhorst, J. Chem. Phys. **143**, 244504 (2015).

[21] L. Yang, A. Guiseppi-Wilson, and A. Guiseppi-Elie, Biomed. Microdevices **13**, 279 (2011).

[22] H.-B. Yu, M. Tylinski, A. Guiseppi-Elie, M. D. Ediger, and R. Richert, Phys. Rev. Lett. **115**, 185501 (2015).

[23] M. C. Zaretsky, L. Mouyad, and J. R. Melcher, IEEE Trans. Electr. Insul. **23**, 897 (1988).

[24] W. Dannhauser, J. Chem. Phys. **48**, 1918 (1968).

[25] S. S. N. Murthy and M. Tyagi, J. Chem. Phys. **117**, 3837 (2002).

[26] S. Bauer, K. Burlafinger, C. Gainaru, P. Lunkenheimer, W. Hiller, A. Loidl, and R. Böhmer, J. Chem. Phys. **138**, 094505 (2013).

[27] S. Bauer, H. Wittkamp, S. Schildmann, M. Frey, W. Hiller, T. Hecksher, N. B. Olsen, C. Gainaru, and R. Böhmer, J. Chem. Phys. **139**, 134503 (2013).

[28] S. Pawlus, M. Wikarek, C. Gainaru, M. Paluch, and R. Böhmer, J. Chem. Phys. **139**, 064501 (2013).

[29] A. R. Young-Gonzales and R. Richert, J. Chem. Phys. **145**, 074503 (2016).

[30] A. L. Agapov, A. I. Kolesnikov, V. N. Novikov, R. Richert, and A. P. Sokolov, Phys. Rev. E **91**, 022312 (2015).

## CHAPTER 6

[1] F. Kremer and A. Schönhals (Eds.), *Broadband Dielectric Spectroscopy* (Springer, Berlin, 2002).

[2] R. Richert, Adv. Chem. Phys. **156**, 101 (2014).

[3] J. Małecki, J. Chem. Phys. **36**, 2144 (1962).

[4] L. P. Singh and R. Richert, Phys. Rev. Lett. **109**, 167802 (2012).

[5] J. Herweg, Z. Physik **3**, 36 (1920).

[6] K. De Smet, L. Hellemans, J. F. Rouleau, R. Corteau, and T. K. Bose, Phys. Rev. E **57**, 1384 (1998).

[7] D. V. Matyushov, J. Chem. Phys. **142**, 244502 (2015).

[8] B. Schiener, R. Böhmer, A. Loidl, and R. V. Chamberlin, Science **274**, 752 (1996).

[9] T. Matsuo, H. Suga, and S. Seki, Bull. Chem. Soc. Jpn. **39**, 1827 (1966).

[10] A. Khalife, U. Pathak, and R. Richert, Eur. Phys. J. B **83**, 429 (2011).

[11] T. Bauer, P. Lunkenheimer, S. Kastner, and A. Loidl, Phys. Rev. Lett. **110**, 107603 (2013).

[12] G. P. Johari, J. Chem. Phys. **138**, 154503 (2013).

[13] D. L'Hôte, R. Tourbot, F. Ladieu, and P. Gadige, Phys. Rev. B **90**, 104202 (2014).

[14] S. Samanta and R. Richert, J. Chem. Phys. **142**, 044504 (2015).

[15] C. Crauste-Thibierge, C. Brun, F. Ladieu, D. L'Hôte, G. Biroli, and J.-P. Bouchaud, Phys. Rev. Lett. **104**, 165703 (2010).

[16] J.-P. Bouchaud and G. Biroli, Phys. Rev. B **72**, 064204 (2005).

[17] C. Brun, F. Ladieu, D. L'Hôte, M. Tarzia, G. Biroli, and J.-P. Bouchaud, Phys. Rev. B **84**, 104204 (2011).

[18] Th. Bauer, P. Lunkenheimer, and A. Loidl, Phys. Rev. Lett. **111**, 225702 (2013).

[19] M. Michl, Th. Bauer, P. Lunkenheimer, and A. Loidl, Phys. Rev. Lett. **114**, 067601 (2015).

[20] M. Michl, Th. Bauer, P. Lunkenheimer, and A. Loidl, J. Chem. Phys. **144**, 114506 (2016).

[21] R. Richert, J. Chem. Phys. **133**, 074502 (2010).

[22] R. Richert and S. Weinstein, Phys. Rev. Lett. **97**, 095703 (2006).

[23] S. Havriliak and S. Negami, Polymer **8**, 161 (1967).

[24] D. V. Matyushov and R. Richert, J. Chem. Phys. **144**, 041102 (2016).

[25] A. J. Kovacs, J. J. Aklonis, J. M. Hutchinson, and A. R. Ramos, J. Polym. Sci. B: Polym. Phys. **17**, 1097 (1979).

[26] I. M. Hodge, J. Non-Cryst. Solids **169**, 211 (1994).

[27] R. V. Chamberlin, B. Schiener, and R. Böhmer, Mat. Res. Soc. Symp. Proc. **455**, 117 (1997).

[28] B. Schiener, R. V. Chamberlin, G. Diezemann, and R. Böhmer, J. Chem. Phys. **107**, 7746 (1997).

[29] K. R. Jeffrey, R. Richert, and K. Duvvuri, J. Chem. Phys. **119**, 6150 (2003).

[30] S. Weinstein and R. Richert, Phys. Rev. B **75**, 064302 (2007).

[31] T. Blochowicz and E. A. Rössler, J. Chem. Phys. **122**, 224511 (2005).

[32] W. Huang and R. Richert, J. Chem. Phys. **130**, 194509 (2009).

[33] R. Richert, Thermochim. Acta **522**, 28 (2011).

[34] L.-M. Wang and R. Richert, Phys. Rev. Lett. **99**, 185701 (2007).

[35] H. Fröhlich, *Theory of Dielectrics* (Clarendon, Oxford, 1958).

[36] I. V. Blazhnov, N. P. Malomuzh, and S. V. Lishchuk, J. Chem. Phys. **121**, 6435 (2004).

[37] G. Adam and J. H. Gibbs, J. Chem. Phys. **43**, 139 (1965).

[38] M. Goldstein, J. Chem. Phys. **123**, 244511 (2005).

[39] S. Samanta and R. Richert, J. Phys. Chem. B (in press).

[40] A. R. Young-Gonzales, S. Samanta, and R. Richert, J. Chem. Phys. **143**, 104504 (2015).

[41] S. Samanta, O. Yamamuro, and R. Richert, Thermochim. Acta **636**, 57 (2016).

[42] R. Richert, J. Chem. Phys. **134**, 144501 (2011).

[43] S. Samanta and R. Richert, J. Chem. Phys. **140**, 054503 (2014).

[44] R. Richert, J. Non-Cryst. Solids **357**, 726 (2011).

[45] R. Richert, J. Chem. Phys. **144**, 114501 (2016).

[46] W. T. Coffey and B. V. Paranjape, Proc. R. Ir. Acad. **78**, 17 (1978).

[47] J. L. Déjardin and Yu. P. Kalmykov, Phys. Rev. E **61**, 1211 (2000).

[48] R. Richert, Phys. Rev. E **88**, 062313 (2013).

[49] S. Albert, Th. Bauer, M. Michl, G. Biroli, J.-P. Bouchaud, A. Loidl, P. Lunkenheimer, R. Tourbot, C. Wiertel-Gasquet, and F. Ladieu, Science **352**, 1308 (2016).

[50] B. Riechers, K. Samwer, and R. Richert, J. Chem. Phys. **142**, 154504 (2015).

[51] C. Brun, C. Crauste-Thibierge, F. Ladieu, D. L'Hôte, J. Chem. Phys. **134**, 194507 (2011).

[52] G. Diezemann, Phys. Rev. E **85**, 051502 (2012).

[53] P. Debye, *Polar Molecules* (Chemical Catalog Company, New York, 1929).

[54] C. J. F. Böttcher, *Theory of Electric Polarization*, Vol.1 (Elsevier, Amsterdam, 1973).

[55] R. Richert, J. Phys.: Condens. Matter **29**, 363001 (2017).

[56] A. Jedrzejowska, K. L. Ngai, and M. Paluch, J. Phys. Chem. A **120**, 8781 (2016).

[57] P. Kim, A. R. Young-Gonzales, and R. Richert, J. Chem. Phys. **145**, 064510 (2016).

[58] H. Wagner and R. Richert, J. Phys. Chem. B **103**, 4071 (1999).

[59] L. Simeral and R. L. Amey, J. Phys. Chem. **74**, 1443 (1970).

[60] L.-M. Wang, V. Velikov, and C. A. Angell, J. Chem. Phys. **117**, 10184 (2002).

[61] R. Richert, J. Chem. Phys. **146**, 064501 (2017).

[62] R. Payne and I. E. Theodorou, J. Phys. Chem. **76**, 2891 (1972).

[63] J. Małecki, J. Mol. Struct. **436-437**, 595 (1997).

[64] W. Huang and R. Richert, J. Phys. Chem. B **112**, 9909 (2008).

[65] R. Richert and S. Weinstein, Phys. Rev. Lett. **97**, 095703 (2006).

[66] R. Coelho and D. Khac Manh, C. R. Acad. Sc. Paris - Serie C **264**, 641 (1967).

[67] M. S. Beevers, J. Crossley , D. C. Garrington, and G. Williams, Faraday Symp. Chem. Soc. **11**, 38 (1977).

[68] M. S. Beevers, D. A. Elliott, and G. Williams, J. Chem. Soc. Faraday Trans. 2 **76**, 112 (1980).

[69] J. L. Déjardin, Y. P. Kalmykov, and P. M. Déjardin, Adv. Chem. Phys. **117**, 275 (2001).

[70] C. Crauste-Thibierge, C. Brun, F. Ladieu, D. L'Hôte, G. Biroli, and J.-P. Bouchaud, J. Non-Cryst. Solids **357**, 279 (2011).

[71] R. Casalini, D. Fragiadakis, and C. M. Roland, J. Chem. Phys. **142**, 064504 (2015).

# APPENDIX A

# SUPPLEMENTAL MATERIAL FOR CHAPTER 3

The sensitivity of $\Delta_E S$ to $E_B^2$ depends on the slope $\partial\varepsilon_s/\partial T$, which can be positive or negative, depending on the material. Many organic molecular liquids follow the Kirkwood-Fröhlich relation,[45]

$$f(\varepsilon_s,\varepsilon_\infty)=\frac{(\varepsilon_s-\varepsilon_\infty)(2\varepsilon_s+\varepsilon_\infty)}{\varepsilon_s(\varepsilon_\infty+2)^2}=\frac{\rho N_A}{9k_BT\varepsilon_0 M}g_K\mu^2\ , \qquad \text{(A1)}$$

which is equivalent to the Onsager relation in the special case given by $g_K \equiv 1$. The derivative of $f(\varepsilon_s, \varepsilon_\infty)$ with respect to $\Delta\varepsilon(T) = \varepsilon_s(T) - \varepsilon_\infty$ amounts to $(2 + \varepsilon_\infty^2/\varepsilon_s^2)/(\varepsilon_\infty + 2)^2$ and is thus practically constant for a polar liquid with $\varepsilon_\infty << \varepsilon_s\sqrt{2}$. Therefore, unless $g_K$ is strongly temperature dependent, $T\Delta\varepsilon(T)$ is constant and $\Delta\varepsilon/T \approx -\partial\varepsilon_s/\partial T$. In this case, i.e., when $g_K$ is temperature invariant, the slope $\partial\varepsilon_s/\partial T$ and thus $\Delta_E S$ is negative. Accordingly, field induced increases of entropy are confined to systems with considerable changes of $g_K$ with temperature, e.g., some monohydroxy alcohols.[11]

# APPENDIX B

## MEASUREMENTS OF 2-FLUOROPYRIDINE:METHANE SULFONIC ACID

I measured the ionic compound 2FPy:HOMs in an NMR tube, in order to determine if it had unique spectral properties. The set up used was previously described by Huang *et al.* [W. Huang, C.A. Angell, J.L. Yarger, R. Richert, Rev. Sci. Instrum. **84**, 073906 (2013)] Based on dielectric measurements we observed an interesting feature at 190 K that looks as if the material goes through a phase transition. (Fig. A1.)

Samples were prepared and put into an NMR tube, which was flame sealed or capped. Since 2FPy:HOMs is solid at room temperature, they were heated to 60 C and melted. After melting, the sample was cooled to 180 K and subsequently measured from 180 K – 200 K, in 2 K steps upon heating. There was a 15 minute wait time between each temperature, in order for the material to equilibrate at each temperature.

Pure 2-fluoropyridine was measured in a flame sealed NMR tube from 150 K – 230 K in 10 K steps upon heating (Fig A2). Pure HOMs was measured from 180 K- 230 K upon heating (Fig. A3).

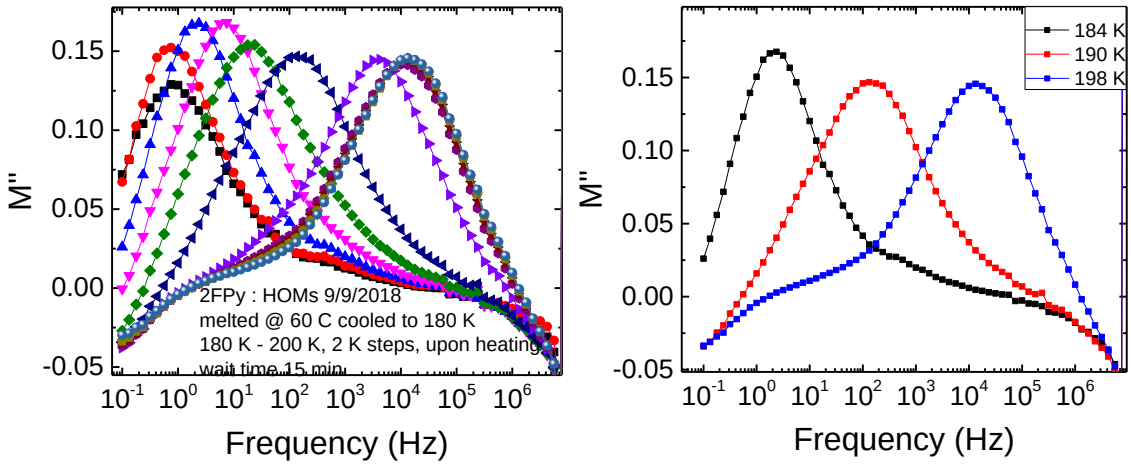


FIG A1: (Left) 2FPY:HOMs represented as M" vs. Frequency for temperatures 180 K – 200 K in 2K steps. (Right) M" vs Frequency of 2FPy :HOMs for T = 184 K, 190 K, and 198 K. from the measurement on the right. These temperatures were selected to look at the material to the high and low frequency side of the change that occurs at 190 K

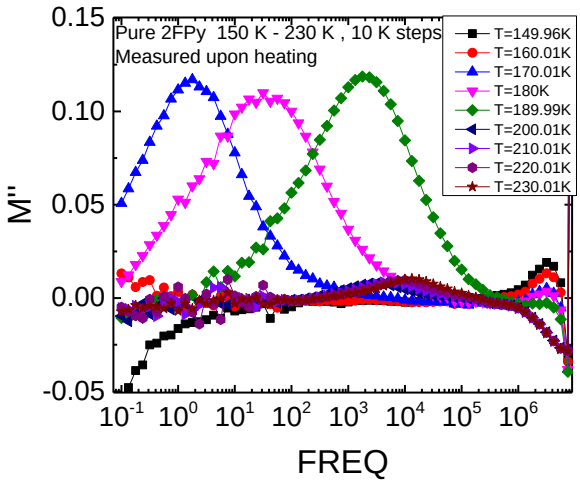


Fig.A2: Pure 2FPy represented as M" vs. Frequency for T = 150 K – 230 K, measured in 10 K steps.

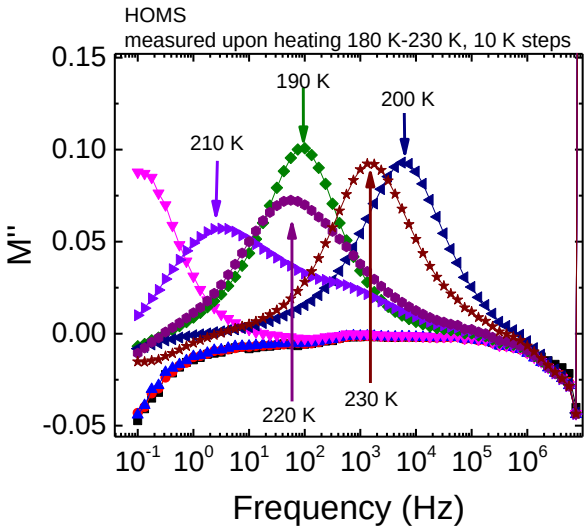


Fig A3: Pure HOMs represented as M" vs Frequency for T = 180 K to 230 K , measured upon heating in 10 K steps. The arrows point to the temperatures listed above each arrow.

# APPENDIX C

## PUBLISHED PORTIONS

Portions of this dissertation have been previously published partially or in full. The published materials were included with permission from all co-authors.

Chapter 3

*Dynamics of Glass-Forming Liquids. XIX. Rise and Decay of Field Induced Anisotropy in the Non-linear Regime*

A. R. Young-Gonzales, S. Samanta, R. Richert, J. Chem. Phys. 143, 104504 (2015)

Chapter 4

*Field induced changes in the ring/chain equilibrium of hydrogen bonded structures: 5-methyl-3-heptanol*

A. R. Young-Gonzales, R. Richert, J. Chem. Phys. 145. 074503 (2016)

Chapter 5

*Modifying hydrogen-bonded structures by physical vapor deposition: 4-methyl-3-heptanol*

A. R. Young-Gonzales, A. Guiseppi-Elie, M. D. Ediger, R. Richert, J. Chem. Phys. 147, 194504 (2017)

Chapter 6

*Dynamics of glass-forming liquids. XX. Third harmonic experiments of non-linear dielectric effects versus a phenomenological model*

P. Kim, A. R. Young-Gonzales, R. Richert, J. Chem. Phys. 145, 064510 (2016)

*Nonlinear dielectric features of highly polar glass formers: Derivatives of propylene carbonate*

A. R. Young-Gonzales, K. Adrjanowicz, M. Paluch, R. Richert, J. Chem. Phys. 147, 224501 (2017)